

DIMETHYL FUMARATE ALTERS INTRACELLULAR CALCIUM HANDLING BY REDOX-MEDIATED PLEIOTROPIC EFFECTS

DISSERTATION

**ZUR ERLANGUNG DES GRADES
„DOKTOR DER NATURWISSENSCHAFTEN“**

**AM FACHBEREICH BIOLOGIE
DER JOHANNES GUTENBERG-UNIVERSITÄT MAINZ**

ANN-KATHRIN HERRMANN

GEBOREN AM 18.05.1985 IN KIRN

MAINZ, 2019

This work was supported by short-term EMBO and NENS fellowships and performed in the Institute for Molecular Medicine, University Medical Center of Johannes Gutenberg-University Mainz, Germany. Some experiments were conducted in the Department of Cellular and Molecular Medicine, KU Leuven, Belgium (02/2016 & 11/2016), in the Department of Medicine, Vascular Biology, Boston University School of Medicine, United States (01/2017 – 04/2017) or in the Wolfson Centre for Age-Related Diseases, King's College London, United Kingdom (02/2018 – 04/2018).

Partial results of my Master's thesis "Die Rolle von oxidativem Stress in der Regulation von SOCE (Store-operated Ca²⁺ entry)" presented in 2014 at Johannes Gutenberg-University Mainz have been included in this work.

First Supervisor:

Second Supervisor:

Date of oral examination:

CONTENTS

1	ABSTRACT	1
2	ZUSAMMENFASSUNG	2
3	INTRODUCTION	3
3.1	Multiple sclerosis	3
3.2	Dimethyl fumarate	3
3.2.1	<i>DMF interferes with the cellular redox system</i>	4
3.2.2	<i>DMF inhibits NF-κB translocation</i>	5
3.2.3	<i>DMF changes innate and adaptive immune cells and cytokine production</i>	5
3.2.4	<i>Newest insights in DMFs mechanism of action</i>	6
3.3	Calcium and calcium signaling	7
3.3.1	<i>Stromal interaction molecule 1</i>	9
3.3.2	<i>Sarco/endoplasmic reticulum Ca²⁺ - ATPase</i>	10
3.3.3	<i>Transient receptor potential anykrin 1</i>	11
3.3.4	<i>Transcription factors</i>	13
3.3.4.1	<i>Nuclear factor of activated T cells</i>	13
3.3.4.2	<i>Nuclear factor kappa light chain enhancer of activated B cells</i>	14
3.4	Oxidative stress	16
3.4.1	<i>Ca²⁺ signaling and oxidative stress</i>	17
3.4.2	<i>Endoplasmic reticulum and stress</i>	18
3.4.3	<i>The mitochondrial respiratory system and stress</i>	19
3.5	Aim of this work	20
4	MATERIALS	21
4.1	Consumables	21
4.2	Chemicals, buffers, markers and media for molecular biology	22
4.3	Media, supplements and chemicals for cell culture	22
4.4	Cell culture media composition	23
4.5	Chemicals, buffers and solutions for protein biochemistry	24
4.6	Buffer composition	26
4.7	Chemicals for high-resolution respirometry	26
4.8	Chemicals and solutions for electrophysiology	26
4.9	Chemicals, solutions and media for flow cytometry	27
4.10	Chemicals, solutions, dyes and media for microscopy	28
4.11	Antibodies and marker for immunoblotting	28
4.12	Antibodies and dyes for flow cytometry	29

4.13	Antibodies and dyes for immunocytochemistry	30
4.14	Kits	30
4.15	Restriction enzymes	30
4.16	Transfection reagents	31
4.17	Primer for mutagenesis PCR and sequencing	31
4.18	Primer and probes for qPCR	31
4.19	Plasmid DNA	32
4.20	Bacteria	32
4.21	Cell lines	33
4.21.1	<i>MEF cells</i>	33
4.21.2	<i>CHO cells</i>	33
4.21.3	<i>COS1 cells</i>	33
4.22	Mice	33
4.23	Devices	34
4.24	Softwares	36
5	METHODS	37
5.1	Molecular biology	37
5.1.1	<i>Polymerase chain reaction</i>	37
5.1.2	<i>Agarose gel electrophoresis</i>	38
5.1.3	<i>DNA gel extraction</i>	38
5.1.4	<i>Kinase-Ligase-DpnI reaction</i>	38
5.1.5	<i>Preparation of chemically competent DH5 α bacteria</i>	39
5.1.6	<i>Heat shock transformation</i>	39
5.1.7	<i>Overnight cultures and glycerol stock preparation</i>	39
5.1.8	<i>Plasmid DNA isolation</i>	40
5.1.9	<i>Restriction enzyme digest</i>	40
5.1.10	<i>Plasmid DNA sequencing</i>	40
5.1.11	<i>RNA isolation</i>	40
5.1.12	<i>Reverse transcription</i>	40
5.1.13	<i>Quantitative real-time polymerase chain reaction</i>	41
5.2	Cell culture – Immortalized cell lines	42
5.2.1	<i>Culturing and passaging</i>	42
5.2.2	<i>Living cell count</i>	42
5.2.3	<i>Cryopreservation</i>	42
5.2.4	<i>Thawing of cells</i>	42
5.2.5	<i>Transient transfection</i>	43
5.2.6	<i>DMF treatment</i>	43
5.3	Cell culture – Splenocytes	44

5.3.1	<i>Cell isolation</i>	44
5.3.2	<i>Living cell count</i>	44
5.3.3	<i>Culturing of splenocytes and activation of T cells</i>	44
5.3.4	<i>DMF treatment in vivo and ex vivo</i>	45
5.4	Cell culture – Primary MEF cells	45
5.4.1	<i>MEF cell isolation</i>	45
5.5	Protein biochemistry	45
5.5.1	<i>Protein isolation</i>	45
5.5.2	<i>BCA protein assay</i>	46
5.5.3	<i>Bradford protein assay</i>	46
5.5.4	<i>Nuclear and cytosolic fractionation</i>	47
5.5.5	<i>SDS-PAGE</i>	47
5.5.6	<i>Coomassie staining</i>	48
5.5.7	<i>Immunoblotting</i>	48
5.5.8	<i>Antibody stripping</i>	49
5.5.9	<i>Blue Native PAGE</i>	49
5.5.10	<i>GFP-Trap</i>	50
5.5.11	<i>BIOGEE assay</i>	51
5.5.12	<i>Total cellular glutathione assay</i>	51
5.5.13	<i>OxyBlot</i>	52
5.5.14	<i>Glutathione fusion assay</i>	52
5.5.15	<i>Dual-Glo® Luciferase assay</i>	53
5.5.16	<i>Immunocytochemistry</i>	53
5.5.17	<i>Microsomal preparation</i>	54
5.5.18	<i>ATPase activity assay</i>	55
5.6	High-resolution respirometry	55
5.6.1	<i>Coupling control protocol</i>	55
5.7	Electrophysiology	56
5.7.1	<i>Whole-cell patch clamping</i>	56
5.8	Flow cytometry	57
5.8.1	<i>Ca²⁺ and reactive oxygen species</i>	58
5.8.2	<i>Ca²⁺ store depletion and SOCE</i>	59
5.8.3	<i>STIM1 expression</i>	59
5.8.4	<i>Glucose uptake</i>	60
5.8.5	<i>NFAT translocation</i>	61
5.9	Microscopy	61
5.9.1	<i>Confocal laser scanning microscopy</i>	61
5.9.2	<i>High content screening microscopy</i>	62

5.9.2.1	Live cell imaging.....	62
5.9.2.2	Fixed cell imaging.....	62
5.9.3	<i>Ca²⁺ imaging microscopy</i>	63
5.9.3.1	<i>Ca²⁺ store depletion</i>	64
5.9.3.2	SOCE.....	64
5.9.3.3	Oxidative stress-induced <i>Ca²⁺ entry through H₂O₂</i>	64
5.10	Statistical analysis	64
6	RESULTS	65
6.1	DMF causes short-term oxidative stress and activates the antioxidant response leading to increased glutathione levels	65
6.2	Cytosolic <i>Ca²⁺</i> increases as an immediate response to DMF	66
6.3	During patch clamping of splenocytes, DMF creates a current with characteristics of a TRP channel	67
6.4	TRPA1 inhibitors abolish DMF-evoked cytosolic <i>Ca²⁺</i> increase	69
6.5	Patch clamping of splenocytes with TRP inhibitors is inconclusive	70
6.6	mRNA expression of TRP channels is not changed by DMF	71
6.7	Cytosolic <i>Ca²⁺</i> increases as a long-term effect of DMF	72
6.8	In vivo treatment with DMF shows increased <i>Ca²⁺</i> levels, balanced glutathione levels, but still increased ROS levels in B cells	73
6.9	DMF reduces <i>Ca²⁺</i> store content in splenocytes after 24 h of incubation	75
6.10	SERCA2b expression is reduced while its activity is increased because of S-glutathionylation of its C674	76
6.11	DMF decreases SOCE in MEF cells after 24 h of incubation	78
6.12	DMF reduces STIM1 expression in MEF cells and splenocytes	80
6.13	GSH decreases STIM1 oligomerization	82
6.14	Punctae formation is reduced in STIM1 mutants	83
6.15	SOCE is increased in STIM1 mutants	85
6.16	DMF does not alter glucose-uptake, but mitochondrial respiration and superoxide levels	86
6.17	DMF does not cause ER stress	89
6.18	NFAT expression is not altered by DMF, but its translocation into the nucleus is increased	91
6.19	DMF does not change NF-κB expression and translocation	93
7	DISCUSSION	96
8	LITERATURE	103

9 APPENDIX.....	125
ABBREVIATIONS	125
ACKNOWLEDGMENT.....	128
DECLARATION	129
CURRICULUM VITAE.....	130

LIST of FIGURES

Figure 1: Ca ²⁺ signaling.	8
Figure 2: STIM1 structure.	9
Figure 3: SERCA2b structure.	11
Figure 4: TRPA1 structure.	12
Figure 5: NFAT activation and translocation.	14
Figure 6: NF-κB activation and translocation.	15
Figure 7: Ca ²⁺ signaling and oxidative stress.	18
Figure 8: The mitochondrial respiratory system.	20
Figure 9: DMF causes short-term oxidative stress and activates the antioxidant response leading to increased glutathione levels.	65
Figure 10: Cytosolic Ca ²⁺ increases as an immediate response to DMF.	67
Figure 11: During patch clamping of splenocytes, DMF creates a current with characteristics of a TRP channel.	68
Figure 12: TRPA1 inhibitors abolish DMF-evoked cytosolic Ca ²⁺ increase.	69
Figure 13: Patch clamping of splenocytes with TRP inhibitors is inconclusive.	71
Figure 14: mRNA expression of TRP channels is not changed by DMF.	72
Figure 15: Cytosolic Ca ²⁺ increases as a long-term effect of DMF.	73
Figure 16: In vivo treatment with DMF shows increased Ca ²⁺ levels, balanced glutathione levels, but still increased ROS levels in B cells.	74
Figure 17: DMF reduces Ca ²⁺ store content in splenocytes after 24 h of incubation.	75
Figure 18: SERCA2b expression is reduced while its activity is increased because of S- glutathionylation of its C674.	77
Figure 19: DMF decreases SOCE in MEF cells after 24 h of incubation.	79
Figure 20: DMF reduces STIM1 expression in MEF cells and splenocytes.	81
Figure 21: GSH decreases STIM1 oligomerization.	82
Figure 22: Punctae formation is reduced in STIM1 mutants.	84
Figure 23: SOCE is increased in STIM1 mutants.	85
Figure 24: DMF does not alter glucose-uptake, but mitochondrial respiration and superoxide levels.	88
Figure 25: DMF does not cause ER stress.	90
Figure 26: NFAT expression is not altered by DMF, but its translocation into the nucleus is increased.	91
Figure 27: DMF does not change NF-κB expression.	93
Figure 28: DMF does not change NF-κB translocation.	94

LIST OF TABLES

Table 1: Consumables.....	21
Table 2: Chemicals, buffers, markers and media for molecular biology.....	22
Table 3: Media, supplements and chemicals for cell culture.....	22
Table 4: Cell culture media composition.....	23
Table 5: Chemicals, buffers and solutions for protein biochemistry.....	24
Table 6: Buffer composition.....	26
Table 7: Chemicals for high-resolution respirometry.....	26
Table 8: Chemicals and solutions for electrophysiology.....	26
Table 9: Chemicals, solutions and media for flow cytometry.....	27
Table 10: Chemicals, solutions, dyes and media for microscopy.....	28
Table 11: Antibodies and marker for immunoblotting.....	28
Table 12: Antibodies and dyes for flow cytometry.....	29
Table 13: Antibodies and dyes for immunocytochemistry.....	30
Table 14: Kits.....	30
Table 15: Restriction enzymes.....	30
Table 16: Transfection reagents.....	31
Table 17: Primer for mutagenesis PCR and sequencing.....	31
Table 18: Primer and probes for qPCR.....	31
Table 19: Plasmid DNA.....	32
Table 20: Bacteria.....	32
Table 21: Devices.....	34
Table 22: Softwares.....	36
Table 23: Q5 [®] Site-Directed Mutagenesis PCR.....	37
Table 24: Antibodies used for immunoblots.....	49
Table 25: Antibodies used in ICC.....	54

1 ABSTRACT

Dimethyl fumarate (DMF) is a treatment option for the autoimmune diseases multiple sclerosis and psoriasis. It causes short-term oxidative stress and induces the antioxidant response via the transcription factor nuclear factor erythroid 2-related factor 2 (Nrf2). Its immunosuppressive effect, however, is poorly understood. As calcium signaling plays a crucial role in the correct functioning of the immune system, this work focuses on understanding how DMF influences the calcium homeostasis in immune cells and if the DMF-induced changes in cellular redox state are responsible for such changes.

I confirmed that DMF evoked short-term oxidative stress in immune cells, which was resolved after 24 h through increased glutathione levels. The major finding of this work was an increase of cytosolic calcium levels in splenocytes immediately after DMF application that remained elevated as a long-term effect. The assumption that the immediate increase of cytosolic calcium was caused by calcium influx through the transient receptor potential ankyrin 1 (TRPA1) channel could not entirely be confirmed. I detected a DMF-caused reduced calcium store content, which could be explained by a reduced expression of the calcium store refilling sarco/endoplasmic reticulum Ca^{2+} -ATPase 2b (SERCA2b). However, SERCA activity was increased due to S-glutathionylation of the redox-regulated cysteine 674. A reduced stromal interaction molecule 1 (STIM1) abundance fits the results that store-operated calcium entry (SOCE) was significantly reduced after DMF treatment. Additionally, oligomerization of STIM1 was found to be modified by reduced glutathione, a hallmark of oxidative stress. STIM1 mutants of the highly conserved cysteines 49 and 56 showed less punctae formation compared to STIM1 wildtype cells when triggered with store depletion. Surprisingly, in contrast to published literature, SOCE was increased in all STIM1 mutants and I did not find any increase in oxidative-stress induced calcium entry. No signs of endoplasmic reticulum (ER) stress were detected, nor changes in glucose uptake, but mitochondrial respiration was altered. The expression of the transcription factors nuclear factor of activated T cells (NFAT) and nuclear factor kappa-light-chain-enhancer of activated B cells (NF- κ B) was not altered, but NFAT translocation was increased.

In summary, DMF causes pleiotropic changes at different levels of the cellular calcium homeostasis, probably due to its ability to redox-modify protein thiols.

2 ZUSAMMENFASSUNG

Dimethylfumarat (DMF) ist eine Behandlungsoption für die Autoimmunkrankheiten Multiple Sklerose und Psoriasis. Es verursacht kurzfristigen oxidativen Stress und induziert die antioxidative Antwort über den Transkriptionsfaktor *Nuclear Factor Erythroid 2-Related Factor 2* (Nrf2). Der Mechanismus seiner immunsuppressiven Wirkung ist jedoch kaum bekannt. Da Kalziumsignalwege eine sehr wichtige Rolle für das korrekte Funktionieren des Immunsystems spielen, konzentrierte sich diese Arbeit darauf, zu verstehen, wie DMF die Kalziumhomöostase in Immunzellen beeinflusst und ob die durch DMF induzierten Veränderungen des zellulären Redoxzustandes dafür verantwortlich sind.

Ich konnte bestätigen, dass der durch DMF verursachte kurzzeitige oxidative Stress in Immunzellen nach 24 h durch einen erhöhten Glutathionspiegel kompensiert wird. Die wichtigste Beobachtung dieser Arbeit war, dass zytosolische Kalziumlevel in Splenozyten sofort nach DMF-Gabe und auch als Langzeiteffekt erhöht sind. Ein vermehrter Kalziumeinstrom durch den *Transient Receptor Potential Ankyrin 1* (TRPA1)-Kanal als Ursache für den sofortigen Kalziumanstieg konnte nicht eindeutig bewiesen werden. DMF reduzierte die Kalziumspiegel der intrazellulären Kalziumspeicher, was durch eine geringere Proteinexpression der Sarco/endoplasmatischen Retikulum Ca^{2+} -ATPase 2b (SERCA2b) erklärbar wäre. Die SERCA2b-Aktivität war jedoch aufgrund vermehrter S-Glutathionylierung des redoxregulierten Cysteins 674 erhöht. Der *Store-Operated Calcium Entry* (SOCE), der Kalziumeinstrom in die Zelle, war nach DMF-Behandlung ebenso signifikant reduziert wie die Expression von *Stromal Interaction Molecule 1* (STIM1). STIM1-Mutanten der hochkonservierten Cysteine 49 und 56 zeigten im Vergleich zu STIM1-Wildtyp-Zellen eine geringere Punctaebildung, wenn sie durch Speicherentleerung getriggert wurden. Im Gegensatz zu veröffentlichter Literatur war der SOCE überraschenderweise bei allen STIM1-Mutanten erhöht. Es konnten weder Anzeichen von Stress im Endoplasmatischen Retikulum (ER) noch Veränderungen der Glukoseaufnahme festgestellt werden, aber die mitochondriale Respiration der Zellen war modifiziert. Die Expression der Transkriptionsfaktoren *Nuclear Factor of Activated T cells* (NFAT) und *Nuclear Factor Kappa-Light-Chain-Enhancer of Activated B cells* (NF- κ B) war nicht verändert, aber die NFAT-Translokation erhöht.

Zusammengefasst verursacht DMF pleiotrope Veränderungen in verschiedenen Level der zellulären Kalziumhomöostase wahrscheinlich aufgrund seiner Fähigkeit, Proteinthiole redox-modifizieren zu können.

3 INTRODUCTION

3.1 MULTIPLE SCLEROSIS

Multiple sclerosis (MS) is a chronic immune-mediated inflammatory disease of the central nervous system (CNS) that causes demyelination and damages axons (Compston and Coles, 2008). The inflammatory reaction causes lesions in the brain and spinal cord, resulting in the characteristic symptoms of MS, which include among others loss of vision, cognitive impairments and motoric deficits (Compston and Coles, 2008). Most patients are diagnosed as young adults and women are more affected than men (Confavreux et al., 1980). A genetic disposition (Moutsianas et al., 2015), environmental factors (Belbasis et al., 2015) and oxidative stress (Ohl et al., 2016) increase the risk of MS. The autoimmune disease can occur in exacerbations or as a progressive disease. During the primary progressive MS, the disease severity continuously increases (Lublin and Reingold, 1996). The relapsing-remitting MS is characterized by acute exacerbations followed by recovery and can turn into secondary progressive MS (Lublin and Reingold, 1996). The animal model of MS, experimental autoimmune encephalomyelitis (EAE), is used to study the disease (Croxford et al., 2011). Relapsing-remitting EAE in Swiss Jim Lambert (SJL) mice, for example, is induced by the subcutaneous injection of proteolipid protein to stimulate autoreactive immune cells (McRae et al., 1992). Activated immune cells such as macrophages, B cells, CD8+ T cells and CD4+ T helper 1 (Th1) and Th17 cells infiltrate the CNS during MS and EAE (Dendrou et al., 2015). Some of the treatment options for MS target inflammation by trying to shift the T cell type from Th1 and Th17 towards the anti-inflammatory Th2 (Miller et al., 1998; Kozovska et al., 1999; Wu et al., 2017).

3.2 DIMETHYL FUMARATE

The dicarboxylic acid ester dimethyl fumarate (DMF) is a lipophilic, α,β -unsaturated electrophilic compound that is rapidly metabolized to its active metabolite, monomethyl fumarate (MMF) (Litjens et al., 2004). First discovered for the treatment of psoriasis in the 1950s (Schweckendiek, 1959), DMF is approved as a treatment option for a second autoimmune disease, multiple sclerosis, since 2013 (Xu et al., 2015). In keratinocytes, the antiproliferative and thus antipsoriatic potential of a complex mixture of fumaric acid

3 INTRODUCTION

derivatives was found to be due to DMF (Seböck et al., 1994). Because of its antiproliferative effects on lymphocytes, as shown by an increased apoptosis in activated T cells (Treumer et al., 2003) and the fact that DMF suppresses chemokine production in peripheral blood mononuclear cells (PBMCs) (Stoof et al., 2001) and reduces inflammatory T cell cytokine expression (Ockenfels et al., 1998), there was an increased interest in using DMF not only in psoriasis but also in other autoimmune or inflammatory diseases, including MS. Tecfidera®, the registered name of the drug for MS, reduces disease activity and progression in patients with relapsing-remitting MS (Kappos et al., 2008). Similar effects were shown in EAE, the animal model for MS. In myelin oligodendrocyte glycoprotein-induced EAE in C57BL/6 mice (Linker et al., 2011) or myelin proteolipid protein-induced EAE in SJL mice (Al-Jaderi and Maghazachi, 2015) DMF and MMF attenuated the disease. Its immunosuppressive effect, however, is still poorly understood.

3.2.1 DMF interferes with the cellular redox system

Held et al. already found in 1988 that DMF depletes intracellular glutathione (GSH) (Held et al., 1988). Further studies of Schmidt et al. revealed a spontaneous reaction of DMF with thiols, such as GSH, due to its α,β -unsaturated electrophilic nature (Schmidt et al., 2007) and showed that GSH is rapidly deprived by DMF in cultured primary astrocytes (Schmidt and Dringen, 2010), thus leading to oxidative stress. Nelson et al. revealed that a transient GSH decrease was followed by an increase of intracellular GSH (Nelson et al., 1999) and this effect of DMF on GSH led to further research on the involvement of the nuclear factor erythroid 2-related factor 2 (Nrf2) pathway. As a result of oxidative stress, the transcription factor Nrf2 dissociates from kelch like-ECH-associated protein 1 (KEAP1) and translocates into the nucleus to activate the antioxidative response (Itoh et al., 1999). Activation of the Nrf2 pathway prevents oxidative stress-induced neuronal cell death in human neural stem cells (Li et al., 2005). Several studies revealed that DMF induces the Nrf2 pathway, hence, having neuroprotective effects (Lin et al., 2011; Linker et al., 2011; Albrecht et al., 2012). Albrecht et al. showed in neuronal cells that DMF first caused short-term oxidative stress and then induced the antioxidant response and increased GSH levels via activation of the transcription factor Nrf2 (Albrecht et al., 2012). Whereas Lin et al. published the anti-inflammatory effects of DMF in astrocytes involve GSH and heme oxygenase-1 (Lin et al., 2011), Linker et al. found an accumulation of

3 INTRODUCTION

reduced nicotinamide adenine dinucleotide (phosphate) (NAD(P)H) quinone oxidoreductase-1 (NQO1) after DMF treatment (Linker et al., 2011). NQO1 catalyzes the two-electron reduction of quinones and prevents the one-electron reduction that results in the production of radical species (Vasiliou et al., 2006). NQO1 is upregulated in oxidative stress and electrophile stress, thus, DMF is protective against both. DMF was reported to induce glutathione transferases and NQO1 in rodent cells and tissues (Spencer et al., 1990) as well as NQO1 in human peripheral blood lymphocytes (Gordon et al., 1991) to protect cells against the toxicity of electrophiles.

As the balance between GSH and oxidative stress is critical for cell survival, DMF also induces glutathione recycling by the upregulation of glutathione reductase (GSR) (Hoffmann et al., 2017). Nevertheless, DMF not only affects the oxidative balance of the cell but also the Ca^{2+} homeostasis. Thio et al. described an immediate elevation of intracellular calcium (Ca^{2+}) concentration in human keratinocytes (Thio et al., 1994).

3.2.2 DMF inhibits NF- κ B translocation

DMF was reported to inhibit tumor necrosis factor-alpha (TNF- α) induced nuclear translocation of nuclear factor kappa light chain enhancers of activated B cells (NF- κ B) protein Rel A (p65) in human endothelial cells (Loewe et al., 2002) and rat heart endothelial cells (Meili-Butz et al., 2008). DMF-induced inhibition of NF- κ B1 in human T cells (Gerdes et al., 2007) or NF- κ B1 (p50) in human dermal fibroblast cells (Vandermeeren et al., 2001) was demonstrated as well. Others showed DMF suppressing extracellular signal-regulated kinase 1 and 2 and mitogen and stress-activated kinases 1 and 2 and therefore indirectly inhibiting Rel A (p65) (Gesser et al., 2007; Peng et al., 2012). DMF blocked TNF- α -induced NF- κ B DNA binding in a different study (Seidel et al., 2010). Kastrati et al. revealed that DMF inhibits the NF- κ B pathway by covalent modification of p65 in breast cancer cells (Kastrati et al., 2016). Previously, the NF- κ B signaling pathway was shown to be affected by DMF in an Nrf2-dependent (Campolo et al., 2017) and independent manner (Gillard et al., 2015).

3.2.3 DMF changes innate and adaptive immune cells and cytokine production

Treumer et al. reported DMF-induced increased apoptosis in activated T cells (Treumer et al., 2003). The reduction of CD8⁺ T cells was more pronounced than the reduction of the CD4⁺

3 INTRODUCTION

subset (Spencer et al., 2015). Furthermore, DMF reduced inflammatory T cell cytokine expression, such as interleukin-6 (IL-6) and interferon-gamma (IFN- γ), but stimulated IL-10 secretion (Ockenfels et al., 1998). Others studies described the downregulation of type 1 T cell cytokines like IFN- γ in circulating blood cells (Litjens et al., 2003) and the upregulation of the type 2 T cell cytokines IL-4 and IL-5 in PBMCs (Jong et al., 1996). Another study revealed that DMF reduced memory T cells and confirmed that DMF shifted the expression from Th1 and Th17 cells in the direction to anti-inflammatory Th2 cells (Wu et al., 2017).

In MS patients DMF diminished mature B cell survival by inducing apoptosis (Li et al., 2017). Moreover, DMF significantly reduced the expression of IL-6 and TNF- α , resulting in a robust anti-inflammatory shift of B cell response cytokines (Li et al., 2017). DMF also down-regulated TNF- α -induced secretion of IL-6 in human lung fibroblasts (Seidel et al., 2010) and suppresses synthesis of proinflammatory TNF- α , IL-1 β , and IL-6 cytokines at the RNA level in activated microglia and astrocytes (Wilms et al., 2010).

DMF suppressed chemokine production in PBMCs (Stoof et al., 2001), strongly reduced macrophage infiltration and increased IL-10 production in EAE in C57BL/6 mice (Schilling et al., 2006). Additionally, DMF induced apoptotic cell death in human mast cells (Förster et al., 2013), impaired neutrophil function by inhibiting its activation (Müller et al., 2016) and increased the number of immunoregulatory natural killer cells (Smith et al., 2018).

3.2.4 Newest insights in DMFs mechanism of action

Until the evidence that DMF protected Nrf2 wildtype (WT) and Nrf2 knockout (-/-) mice equally well from the development of EAE (Schulze-Topphoff et al., 2016), everything pointed to Nrf2-mediated effects. Ever since different mechanism of actions of DMF are proposed. One of them is the downregulation of aerobic glycolysis through succination and inactivation of the catalytic cysteine of the glycolytic enzyme glyceraldehyde 3-phosphate dehydrogenase (GAPDH) (Kornberg et al., 2018). Another mechanism of action of DMF involves alterations of redox-sensitive thiols in proteins. Blewett et al. tested >2400 cysteine residues in human T cells with the help of a site-specific chemical proteomic approach to find DMF sensitive proteins. They identified proteins important for the immune response as DMF targets (Blewett et al., 2016).

3.3 CALCIUM AND CALCIUM SIGNALING

Redox-mediated alterations can also influence intracellular calcium (Ca^{2+}) signaling and Ca^{2+} homeostasis. Ca^{2+} is a universal second messenger which is important for numerous cellular functions that range from short-term responses in muscle contraction or the secretion of substances like neurotransmitters to the long-term regulation of gene expression for cell proliferation as well as cell death (Berridge et al., 2003). Therefore, its intracellular concentration is tightly regulated by Ca^{2+} binding proteins, channels, pumps, and exchangers (Lam and Galione, 2013). Most of the Ca^{2+} is stored in the endoplasmic reticulum (ER), Golgi apparatus and mitochondria (Pozzan et al., 1994). Disturbances in Ca^{2+} homeostasis are associated with neurodegeneration and inflammatory processes in diseases like Alzheimer's disease, Huntington's disease, Parkinson's disease and multiple sclerosis (Zündorf and Reiser, 2011). Elevations in cytosolic Ca^{2+} concentration, caused by Ca^{2+} influx from the extracellular space or release from internal Ca^{2+} stores, have a signaling effect. In immune cells, this signal transmission is crucial for their activation, differentiation, cytokine production, and survival (Feske, 2007; Vig and Kinet, 2009). Direct or indirect ways to mediate Ca^{2+} influx from extracellular space include activation of transient receptor potential (TRP) channels, G-protein-coupled receptors (GPCR) or receptors interacting with tyrosine kinases (Berridge et al., 2003). Receptors interacting with tyrosine kinases include B or T cell receptors (BCR or TCR) (Sefton and Taddie, 1994). B and T cell receptor activation results in the induction of phospholipase C (PLC), which cleaves phosphatidylinositol-4,5-bisphosphate (PIP₂) into inositol 1,4,5-trisphosphate (IP₃) and diacylglycerol (DAG). IP₃ is able to bind and open IP₃ receptors (IP₃R) localized in the ER membrane, thus releasing Ca^{2+} from the ER lumen (Decrock et al., 2013). The subsequent increase in cytosolic Ca^{2+} concentration induces another way to deplete intracellular Ca^{2+} stores by opening the Ca^{2+} -sensitive ryanodine receptors (RyR) (Meissner, 1994). Store-operated Ca^{2+} entry (SOCE) from the extracellular space is triggered by Ca^{2+} store depletion to replenish the ER Ca^{2+} stores (Takemura et al., 1989). Stromal interaction molecule 1 (STIM1) is a protein that detects ER Ca^{2+} levels and initiates SOCE (Liou et al., 2005; Roos et al., 2005). Upon Ca^{2+} store depletion, STIM1 undergoes conformational changes (Yu et al., 2013), oligomerizes and forms punctae near the plasma membrane (Wu et al., 2006; Luik et al., 2008). STIM1 binds to the N- and C-termini of Orai1, the pore forming unit of the Ca^{2+}

3 INTRODUCTION

release-activated Ca^{2+} (CRAC) channel in the plasma membrane, via its CRAC activation domain (Prakriya et al., 2006; Zhang et al., 2006; Park et al., 2009). The binding and activation of CRAC channels allows Ca^{2+} influx into the cell, the refilling of ER Ca^{2+} stores, and activation of the transcription factors nuclear factor of activated T cells (NFAT) and nuclear factor kappa light chain enhancers of activated B cells (NF- κ B) (Dolmetsch et al., 1997). As sustained levels of increased cytosolic Ca^{2+} can be pathogenic, the Ca^{2+} is redistributed to restore physiological levels through a variety of mechanisms such as refilling of ER Ca^{2+} stores by sarco/endoplasmic reticulum Ca^{2+} -ATPases (SERCAs), importing Ca^{2+} to the mitochondria through mitochondrial Ca^{2+} uniporter, and Ca^{2+} transport into the extracellular space via plasma membrane Ca^{2+} -ATPases (PMCA) or $\text{Na}^+/\text{Ca}^{2+}$ -exchanger (Berridge et al., 2003).

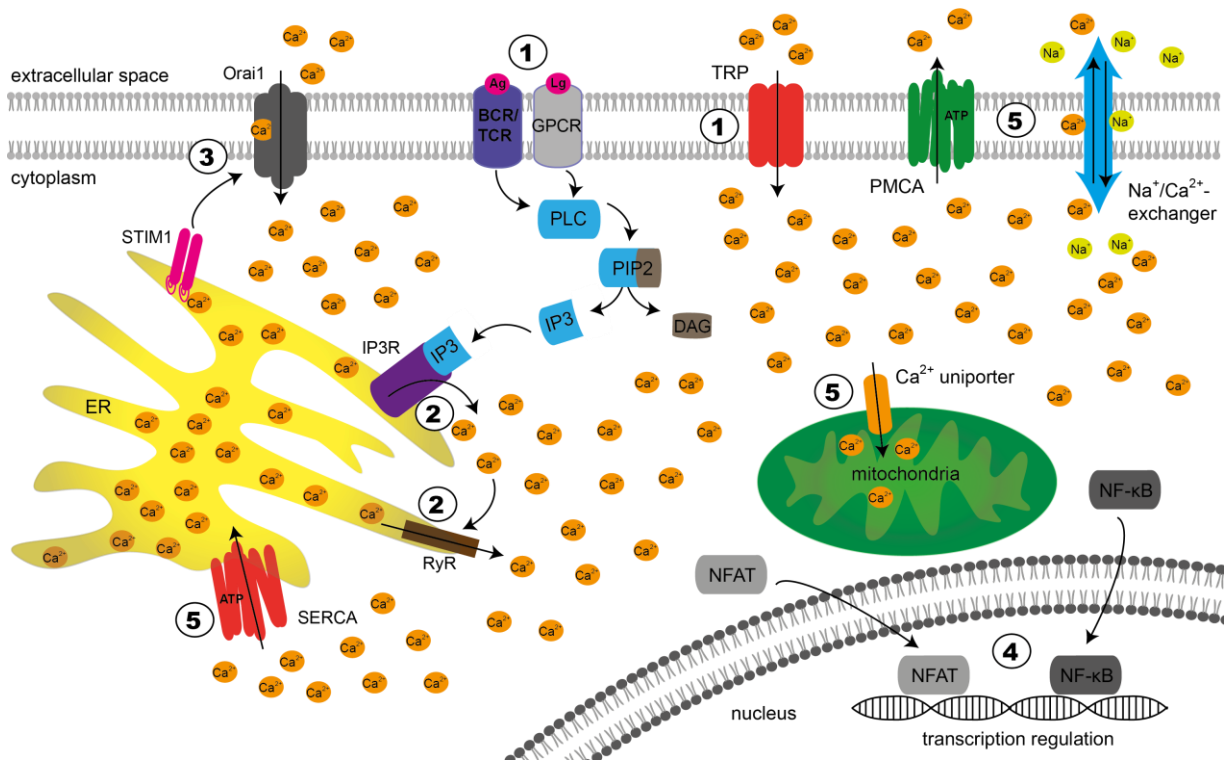


Figure 1: Ca^{2+} signaling.

1) The Ca^{2+} influx from extracellular space can be mediated through transient receptor potential (TRP) channels. Activation of G-protein-coupled receptors (GPCR) by a ligand (Lg) or activation of B or T cell receptors (BCR or TCR) by an antigen (Ag) induces phospholipase C (PLC), which cleaves phosphatidylinositol-4,5-bisphosphate (PIP₂) into inositol 1,4,5-trisphosphate (IP₃) and diacylglycerol (DAG). 2) IP₃ is able to bind and open IP₃ receptors (IP₃R), thus releasing Ca^{2+} from the ER. The subsequent increase in cytosolic Ca^{2+} concentration induces the opening of the Ca^{2+} -sensitive ryanodine receptors (RyR) and releases even more Ca^{2+} from the Ca^{2+} store. 3) Store-operated Ca^{2+} entry (SOCE) from the extracellular space is triggered by Ca^{2+} store depletion. Stromal interaction molecule 1 (STIM1) senses a decrease in ER Ca^{2+} levels, undergoes conformational changes, oligomerizes and binds and opens Orai1, the pore forming unit of the Ca^{2+} release-activated Ca^{2+} (CRAC) channel in the plasma membrane, which allows Ca^{2+} influx into the cell. 4) The transcription factors nuclear factor of activated

3 INTRODUCTION

T cells (NFAT) and nuclear factor kappa light chain enhancers of activated B cells (NF- κ B) are activated as a downstream reaction of increased cytosolic Ca^{2+} . 5) Mechanisms to restore the normal intracellular Ca^{2+} concentration include refilling of ER Ca^{2+} stores by sarco/endoplasmic reticulum Ca^{2+} -ATPases (SERCAs), importing Ca^{2+} to the mitochondria through mitochondrial Ca^{2+} uniporter and Ca^{2+} transport into the extracellular space via plasma membrane Ca^{2+} -ATPases (PMCAs) or $\text{Na}^+ / \text{Ca}^{2+}$ - exchanger.

3.3.1 Stromal interaction molecule 1

The sensor that detects ER Ca^{2+} levels and initiates SOCE is the ubiquitously expressed stromal interaction molecule 1 (STIM1) (Liou et al., 2005; Roos et al., 2005). STIM1 belongs together with the co-expressed STIM2 to the stromal interaction molecule family (Williams et al., 2001). STIM1 is a highly conserved protein with a single transmembrane domain (TM) that is mainly located in the ER membrane but can also be found in the plasma membrane (Soboloff et al., 2012). Under basal ER Ca^{2+} levels, STIM1 is a dimer (Covington et al., 2010), but undergoes conformational changes upon Ca^{2+} store depletion (Yu et al., 2013), oligomerizes and forms punctae in ER-plasma membrane junctions (Wu et al., 2006; Luik et al., 2008). The cytoplasmic part of the protein consists of three coiled-coil (CC) domains, a proline and serine-rich region (PS) and a lysine-rich region (K) (Soboloff et al., 2012). The CRAC activation domain (CAD) that binds to the N- and C-termini of Orai1 is located here as well (Park et al., 2009). The luminal N-terminus of STIM1 consists of a signal peptide (SP), two highly conserved cysteines (C49 and C56), a canonical and a hidden EF-hand (cEF and hEF) domain and a sterile α -motif (SAM) domain (Soboloff et al., 2012). The canonical EF-hand domain binds calcium ions and senses changes in ER Ca^{2+} concentration with the help of three negatively charged amino acids (D76, D78, and E87) (Feske, 2007). The two highly conserved cysteines C49 and C56 are crucial for SOCE because mutations of these cysteines were found to inhibit STIM1 punctae formation and SOCE (Prins et al., 2011). Additionally, oxidative-stress induced S-glutathionylation of C56 or mutation of C49 and C56 were described to induce constitutive Ca^{2+} entry independent of Ca^{2+} concentration of intracellular stores (Hawkins et al., 2010).

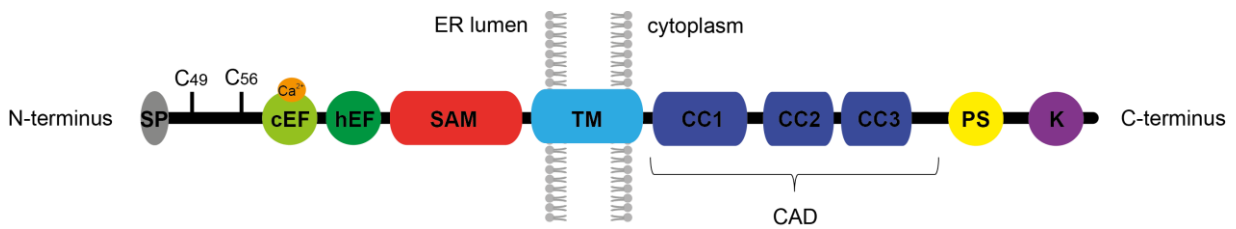


Figure 2: STIM1 structure.

STIM1 is a highly conserved protein located in the ER membrane with a single transmembrane domain (TM). The luminal N-terminus consists of a signal peptide (SP), two highly conserved cysteines C49 and

3 INTRODUCTION

C56, a canonical and a hidden EF-hand domain (cEF and hEF) and a sterile α -motif (SAM) domain. The cytoplasmic part of the protein consists of three coiled-coil (CC) domains, a proline and serine-rich region (PS) and a lysine-rich region (K). The canonical EF-hand domain binds calcium ions and senses changes in ER Ca^{2+} concentration. Via its CRAC activation domain (CAD) STIM1 binds to the N and C termini of Orai1, the pore forming unit of the Ca^{2+} release-activated Ca^{2+} (CRAC) channel to induce SOCE (based on Prins et al., 2011 and Soboloff et al., 2012).

3.3.2 Sarco/endoplasmic reticulum Ca^{2+} - ATPase

Sarco/endoplasmic reticulum Ca^{2+} -ATPases are P-type Ca^{2+} - ATPases and responsible for the transport of Ca^{2+} from the cytosol into the ER lumen to maintain filled Ca^{2+} stores. Using the energy released from hydrolysis of one adenosine triphosphate (ATP) these enzymes transport two Ca^{2+} ions across the membrane (Inesi et al., 1980), thereby existing in two states, E1 and E2. Scarborough reviewed that SERCAs affinity for Ca^{2+} is very high and the calcium binding sites point to the cytoplasm in the E1 state, whereas in the E2 state the calcium binding sites face the ER lumen and have a low affinity for Ca^{2+} (Scarborough, 1999). During the transport of Ca^{2+} ions, SERCA proteins become temporarily autophosphorylated by transferring the γ -phosphate of one ATP to a single aspartyl residue, which is a common feature of P-type Ca^{2+} -ATPases (Pedersen and Carafoli, 1987). Several SERCA isoforms exist by alternative splicing of the proteins that are encoded by three genes, SERCA1, SERCA2, and SERCA3 (Wu et al., 1995). Important for this work is SERCA2b, the ATPase isoform which is expressed in various tissues (Wu et al., 1995). One common feature of the SERCA variants is that their activity is repressed by the lactone thapsigargin (Thastrup et al., 1990). Additionally, the different SERCA isoforms can be inhibited by diverse micropeptides, like another-regulin for SERCA2b, that reduce their affinity for Ca^{2+} (Anderson et al., 2016). SERCA2b consists of eleven transmembrane helices (TM) (Gunteski-Hamblin et al., 1988; Bayle et al., 1995), luminal linkers between those and three cytoplasmic domains: the actuator domain (A), the nucleotide binding domain (N) and the phosphorylation domain (P) (Toyoshima et al., 2000). The N-terminus is located in the cytoplasm (Toyoshima et al., 2000), whereas the C-terminus is situated in the ER lumen (Gunteski-Hamblin et al., 1988; Bayle et al., 1995). The transmembrane region possesses two Ca^{2+} binding sites, the actuator domain is located near the N-terminal end of the protein and regulates Ca^{2+} ion binding and release, the nucleotide binding domain binds the adenosine of the ATP, and the phosphorylation domain holds the aspartyl residue D351, which is phosphorylated during ATP hydrolysis (Toyoshima et al., 2000; Rossi and Dirksen, 2006). SERCA

3 INTRODUCTION

activity is susceptible to stimulatory and inhibitory oxidative posttranslational modifications, especially at the highly conserved cysteine 674 (C674) (Grover et al., 2003; Adachi et al., 2004). Additionally, mutation of C674 to serine (C674S), its irreversible oxidation during atherosclerosis or because of high glucose was shown to abolish the increased SERCA activity gained by S-glutathionylation of the cysteine (Adachi et al., 2004; Tong et al., 2008).

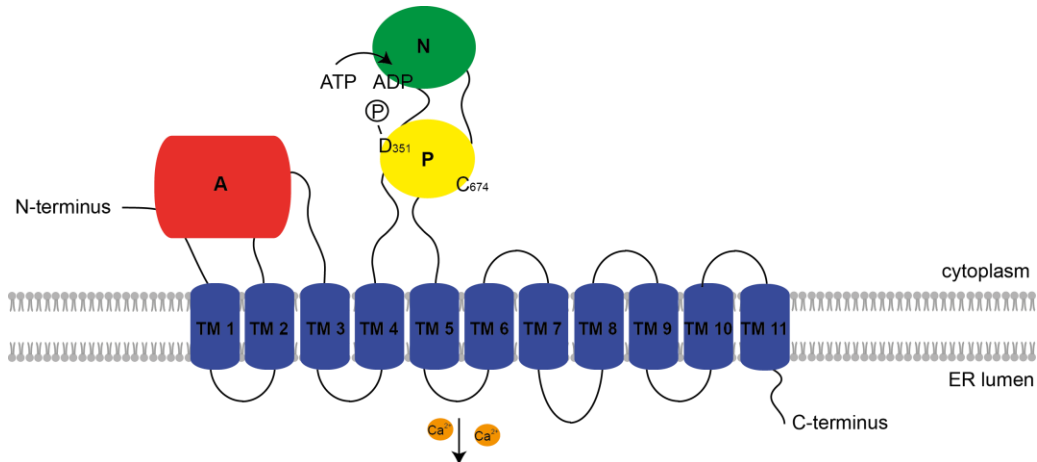


Figure 3: SERCA2b structure.

SERCA2b consists of eleven transmembrane helices (TM1-11), luminal linkers between those and three cytoplasmic domains: the actuator (A) domain, the nucleotide binding (N) domain, and the phosphorylation (P) domain. The N-terminus is located in the cytoplasm whereas the C-terminus is situated in the ER lumen. The transmembrane region possesses two Ca²⁺ binding sites, the actuator domain regulates Ca²⁺ ion binding and release, the nucleotide binding domain binds the adenosine of the ATP, and the phosphorylation domain holds the highly conserved cysteine 674 (C674) and the aspartyl residue D351, which is phosphorylated during ATP hydrolysis (based on Dode et al., 2003 and Palmgren and Nissen, 2011).

3.3.3 Transient receptor potential ankyrin 1

Transient receptor potential ankyrin 1 (TRPA1) is a calcium-permeable non-selective cation channel in the cell membrane that was first described in 1999 (Jaquemar et al., 1999). TRPA1 belongs to the transient receptor potential (TRP) family of ion channels, which is divided into two broad subgroups based on sequence homologies. The first group includes the transient receptor potential canonical (TRPC), transient receptor potential vanilloid (TRPV), transient receptor potential melastatin (TRPM), transient receptor potential ankyrin (TRPA) and transient receptor potential no mechanoreceptor potential C (TRPN), whereas TRPN is not expressed in mammals. The second group consists of transient receptor potential mucolipin (TRPML) and transient receptor potential polycystin (TRPP) (Venkatachalam and Montell, 2007). In contrast to the other ion channels of subgroup one, the TRPA subfamily has only one

3 INTRODUCTION

mammalian member (Chen and Hackos, 2015). TRPA1 is a tetramer with six transmembrane helices (TM) in each monomer, while the pore-forming unit is positioned between TM 5 and 6. N- and C-termini are both located intracellularly (Chen and Hackos, 2015). The protein part with ankyrin repeats (14 for mouse TRPA1 (Story et al., 2003), 16 for human TRPA1 (Bautista et al., 2013)) at the N-terminus, was eponymous for the TRPA subfamily and contains a Ca^{2+} -binding site (Hinman et al., 2006). TRPA1 is expressed in a subgroup of neurons in the dorsal root ganglia together with TRPV1 (Story et al., 2003), but can also be found in several other tissues like the spleen (Stokes et al., 2006) or the skin (Atoyan et al., 2009). Its activation not only depolarizes the membrane but also induces a Ca^{2+} influx into the cell, which can be monitored via calcium imaging. The ion channel can be activated by electrophiles such as allicin, an unstable component of fresh garlic (Macpherson et al., 2005), acrolein, an environmental irritant (Bautista et al., 2006) or formalin (McNamara et al., 2007). Other ways to stimulate TRPA1 include bacterial endotoxins (Meseguer et al., 2014), fenamate non-steroidal anti-inflammatory drugs (Hu et al., 2010) or thiol-reactive molecules (Andersson et al., 2008). Electrophilic or oxidative TRPA1 activation occurs through covalent modification of specific cysteine residues in the N-terminal domain (Macpherson et al., 2007; Takahashi et al., 2008). Macpherson et al. even showed, that C415, C422, and C622 are necessarily required for channel activation (Macpherson et al., 2007). Because of its ability to sense various environmental changes, the specific TRPA1 antagonists A967079 (Chen et al., 2011) and HC030031 (McNamara et al., 2007) were developed to block its channel activity and to allow further research.

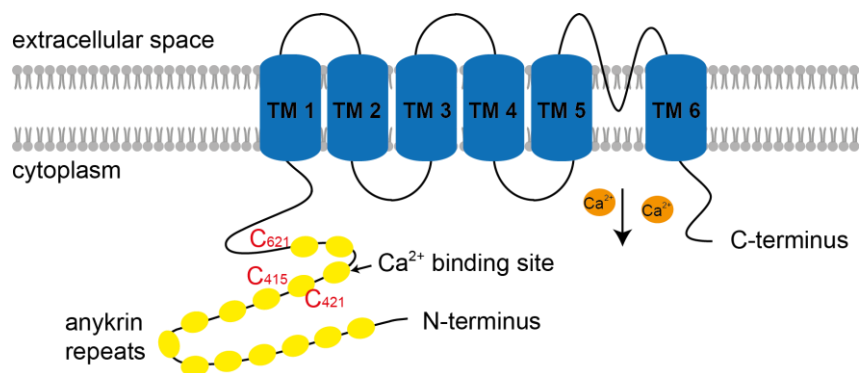


Figure 4: TRPA1 structure.

TRPA1 is a tetramer with six transmembrane helices (TM) in each monomer, while the pore-forming unit is positioned between TM 5 and 6. N- and C-termini are both located intracellularly. The protein part with ankyrin repeats (14 for mouse TRPA1 as displayed here) at the N-terminus, was eponymous

3 INTRODUCTION

for the TRPA subfamily. Reactive cysteines residues (C415, C421 and C621) that are required for TRPA1 activation are located in the N-terminal domain of the protein as well as the Ca²⁺ binding site (adapted from Bautista et al., 2013 and Chen and Hackos, 2015).

3.3.4 Transcription factors

Nuclear factor of activated T cells (NFAT) and nuclear factor kappa light chain enhancers of activated B cells (NF-κB) seem to have a common evolutionary origin, translocate to the nucleus upon cell activation and an increase in cytosolic Ca²⁺ levels and have essential roles in the activation, proliferation and apoptosis of lymphocytes and thus in inflammation (Serfling et al., 2004).

3.3.4.1 Nuclear factor of activated T cells

Nuclear factor of activated T cells (NFAT) was discovered as a regulator of the early T cell activation genes in 1988 (Shaw et al., 1988), but is also expressed in many other immune cells or non-immune cells (Horsley and Pavlath, 2002). The NFAT family encompasses five members (NFATc1-4 and NFAT5) (Vaeth and Feske, 2018), from which NFATc1 (NFAT2 or NFATc) and NFATc2 (NFAT1 or NFATp) are the predominant forms in the peripheral immune system (Zhou et al., 2002). While NFATc2 is abundantly present in the cytoplasm, NFATc1 is induced upon T cell activation (Lyakh et al., 1997). In resting cells, phosphorylated and inactivated NFAT is located in the cytoplasm (Zhou et al., 2002). Upon activation of T or B cell receptors, cytosolic Ca²⁺ levels increase. Consequently, free cytosolic Ca²⁺ can bind to the Ca²⁺ binding protein calmodulin (Means and Dedman, 1980). This Ca²⁺/calmodulin complex activates the phosphatase calcineurin (Stewart et al., 1982). Calcineurin dephosphorylates NFAT, which leads to its translocation into the nucleus (Shaw et al., 1995) where NFAT can bind to specific deoxyribonucleic acid (DNA) sequences and promote transcription of cytokines like IL-2 (Shaw et al., 1988; Chow et al., 1999), IL-4 (Szabo et al., 1993), IL-5 (Stranick et al., 1997), IFN-γ (Kiani et al., 2001) and TNF-α (McCaffrey et al., 1994), which are important for B and T cell differentiation. NFAT kinases re-phosphorylate NFAT in the nucleus, which is followed by its transfer back to the cytoplasm (Müller and Rao, 2010).

3 INTRODUCTION

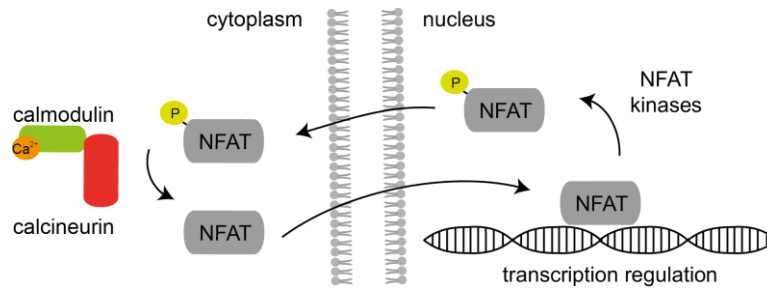


Figure 5: NFAT activation and translocation.

Phosphorylated (P) and inactivated NFAT is located in the cytoplasm. Upon activation of T or B cell receptors, cytosolic Ca^{2+} levels increase and free cytosolic Ca^{2+} can bind to calmodulin. This Ca^{2+} /calmodulin complex activates the phosphatase calcineurin. Calcineurin dephosphorylates NFAT, which leads to its translocation into the nucleus where NFAT can bind to specific DNA sequences and promote transcription of target genes. NFAT kinases re-phosphorylate NFAT in the nucleus, which is followed by its transfer back to the cytoplasm.

3.3.4.2 Nuclear factor kappa light chain enhancers of activated B cells

Nuclear factor kappa light chain enhancers of activated B cells (NF- κ B) is one of the most potent transcription factors in activating proinflammatory genes (Tak and Firestein, 2001). The NF- κ B protein family consists of the five members RelA (p65), RelB, c-Rel, NF- κ B1 (p50 and its precursor p105) and NF- κ B2 (p52 and its precursor p100), which can form homodimers or heterodimers (Perkins, 2007). While the transcription factors p50, p52, and p65 are ubiquitously expressed, RelB and c-rel appear mainly in lymphoid tissues and hematopoietic cells (Ghosh et al., 1998). The precursor proteins p105 and p100 are located solely in the cytoplasm because they mask the nuclear localization signals of p50 and p52 by their C-terminal ankyrin region (Blank et al., 1991; Henkel et al., 1992; Liou et al., 1992; Naumann et al., 1993). All NF- κ B proteins share the Rel homology domain (Ghosh et al., 1998), a conserved region at their N-terminus that is responsible for DNA-binding, dimerization and interaction with inhibitory proteins (Gilmore, 1990; Ganchi et al., 1992). Similar to p105 and p100, NF- κ B inhibitors (I κ B) (Baeuerle and Baltimore, 1988) like I κ B α mask the nuclear localization signal of NF- κ B proteins, thereby inhibiting their transport into the nucleus (Ganchi et al., 1992). NF- κ B activation can be initiated mostly via two signaling ways. The canonical pathway primarily activates p50/p105, p65 and c-Rel, whereas the non-canonical pathway activates p52/p100 and RelB (Sun, 2017). Upon activation of various immune receptors by stimuli like TNF- α (Osborn et al., 1989) or lipopolysaccharides (Parslow and Granner, 1982), I κ B α is phosphorylated by the I κ B kinase (IKK) complex, which results in its ubiquitinylation and

3 INTRODUCTION

degradation (Perkins, 2007; Sun, 2017). This is followed by the release and nuclear translocation of the predominantly existing canonical NF- κ B dimers p50/p65 or p50/c-Rel (Sun, 2017). In the non-canonical pathway, the activation of an IKK α homodimer by the NF- κ B-inducing kinase (NIK) leads to phosphorylation-induced and ubiquitin-mediated degradation of p100 and the production of p52, which can translocate into the nucleus and regulate gene transcription (Perkins, 2007; Sun, 2017). Two typical inducers for this pathway are B cell activating factor (Kayagaki et al., 2002) or cluster of differentiation 40 (CD40) (Coope et al., 2002). In contrast to the rapid activation of the canonical pathway for an innate immune response, the non-canonical pathway is important for the adaptive immune response (Perkins, 2007). Moreover, some studies showed NF- κ B activation via protein kinase C (PKC) and calcineurin, both pathways that require Ca²⁺ signaling. In Jurkat T cells, Frantz et al. described that the Ca²⁺/calmodulin-dependent phosphatase calcineurin together with phorbol 12-myristate 13-acetate (PMA) inactivates I κ B α , thus increasing NF- κ B activation (Frantz et al., 1994). Trushin et al. presented how PKC and calcineurin synergize in T cells to activate NF- κ B through activating the IKK complex (Trushin et al., 1999). Additionally, PKC and intracellular Ca²⁺ were shown to be important for an increased I κ B α degradation and hence an elevated NF- κ B activation (Han and Logsdon, 2000).

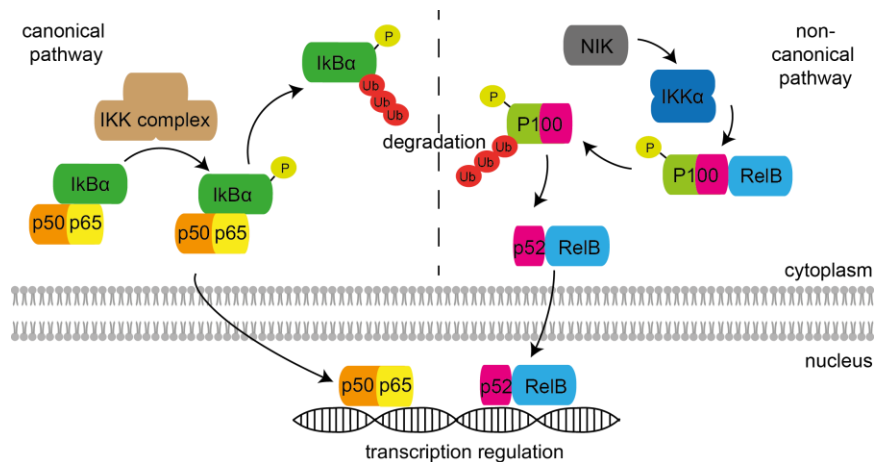


Figure 6: NF- κ B activation and translocation.

NF- κ B activation can be initiated mostly via two signaling ways. Upon activation of the canonical pathway, the NF- κ B inhibitor I κ B α is phosphorylated (P) by the I κ B kinase (IKK) complex, which results in its ubiquitinylation (Ub) and degradation. This is followed by the release and nuclear translocation of the predominantly existing canonical NF- κ B dimers p50/p65 or p50/c-Rel. During the non-canonical pathway, the activation of an IKK α homodimer by the NF- κ B-inducing kinase (NIK) leads to phosphorylation-induced and ubiquitin-mediated degradation of p100 and the production of p52, which can translocate together with RelB into the nucleus and regulate gene transcription.

3.4 OXIDATIVE STRESS

The term oxidative stress was defined in 1985 by Helmut Sies (Sies, 1985) and describes the disturbance in the balance of the production and elimination of oxidants like reactive oxygen species (ROS) or reactive nitrogen species. Physiologically, mitochondria are the main source of ROS because they produce superoxide as an unwanted side-reaction during oxidative phosphorylation (Brand et al., 2004). ROS can also be produced in the ER (Gross et al., 2006) or in peroxisomes (Duve and Baudhuin, 1966). In addition to these endogenous sources, ROS production can be triggered by exogenous stressors such as ultraviolet (UV) radiation, pollution, drugs or pesticides (Phaniendra et al., 2015). The cell opposes the ROS-producing system with the antioxidant defense system, including GSH and enzymes like superoxide dismutase, catalase, and glutathione peroxidase that scavenge ROS (Sies, 1993). The tripeptide GSH, composed of the amino acids γ -glutamate, cysteine and glycine, serves as an important antioxidant and is the most abundant form of a thiol with low molecular weight in cells (Maher, 2005). In the process of detoxifying ROS, two GSH molecules are oxidized to form glutathione disulfide (GSSG), which can be converted back into GSH by the enzyme glutathione reductase (GSR) (Maher, 2005). The transcription of antioxidative response genes is induced by the transcription factor Nrf2 (Itoh et al., 1997). In a balanced oxidant-antioxidant system, Nrf2 is located in the cytoplasm and bound by KEAP1 which interacts with the Cullin3-based E3 ligase to ubiquitinate Nrf2 for its proteasomal degradation (Kobayashi et al., 2004). Upon oxidative stress, KEAP1 dissociates from Nrf2 due to cysteine residue modification, allowing Nrf2 to translocate into the nucleus, where it induces transcription of antioxidative response genes (Itoh et al., 1999; Tebay et al., 2015). If the antioxidant defense system is not able to control oxidative stress, it results in damage and apoptosis of the cell (Kowaltowski and Vercesi, 1999). Besides, atherosclerosis, diabetes, cardiovascular diseases, neurodegenerative diseases or multiple sclerosis are linked to oxidative stress (Valko et al., 2007; Ohl et al., 2016). On the other hand, the reversible oxidation of protein thiols is essential for the correct functioning of various proteins (Brandes et al., 2009).

3.4.1 Ca²⁺ signaling and oxidative stress

Since ROS are chemically very reactive, they are likely to react with thiol groups of important cysteines in proteins and modify their activities (Veal et al., 2007). Thus, redox processes can alter intracellular Ca²⁺ signaling by influencing key players in intracellular Ca²⁺ homeostasis. Under normal cellular ROS levels, SERCA, for example, is activated by nitric oxide-induced S-glutathionylation of the highly conserved cysteine residue C674 (Adachi et al., 2004). Its irreversible oxidation and thus inactivation occurs if the cellular ROS concentration is increased as shown in conditions such as diabetes and atherosclerosis (Adachi et al., 2004; Tong et al., 2008). Short-term treatment of rat ventricular myocytes with hydrogen peroxide (H₂O₂) decreased SERCA activation as well and increased the activity of the Na⁺/Ca²⁺-exchanger (Kuster et al., 2010). H₂O₂ is also known to activate redox-sensitive TRP channels like TRPA1 (Andersson et al., 2008) or inhibit PMCA activity (Zaidi and Michaelis, 1999). ROS modifies a cysteine in the mitochondrial Ca²⁺ uniporter which affects its activity (Dong et al., 2017). Moreover, ROS are able to increase Ca²⁺ release from the ER by activating RyR (Anzai et al., 1998). Oxidative stress augmented PLC-dependent production of IP₃ that is followed by a subsequent release of Ca²⁺ from the ER (Madesh et al., 2005). Oxidants even activate NF-κB translocation in a tyrosine kinase-dependent mechanism (Schieven et al., 1993). ROS was also shown to directly activate Ca²⁺ entry via S-glutathionylation of a highly conserved cysteine in STIM1, thus stimulating store-independent Ca²⁺ entry (Hawkins et al., 2010). Furthermore, Orai1 activity might be influenced by the cellular redox state either directly through H₂O₂-induced oxidation of cysteines (Bogeski et al., 2010) or indirectly through activation of IP₃ receptors and subsequent store depletion (Grupe et al., 2010). Altogether, during profound oxidative stress key players in Ca²⁺ signaling can be mediated, which may be problematic because an intact SOCE machinery is important for the survival of the cell under these conditions (Henke et al., 2012).

3 INTRODUCTION

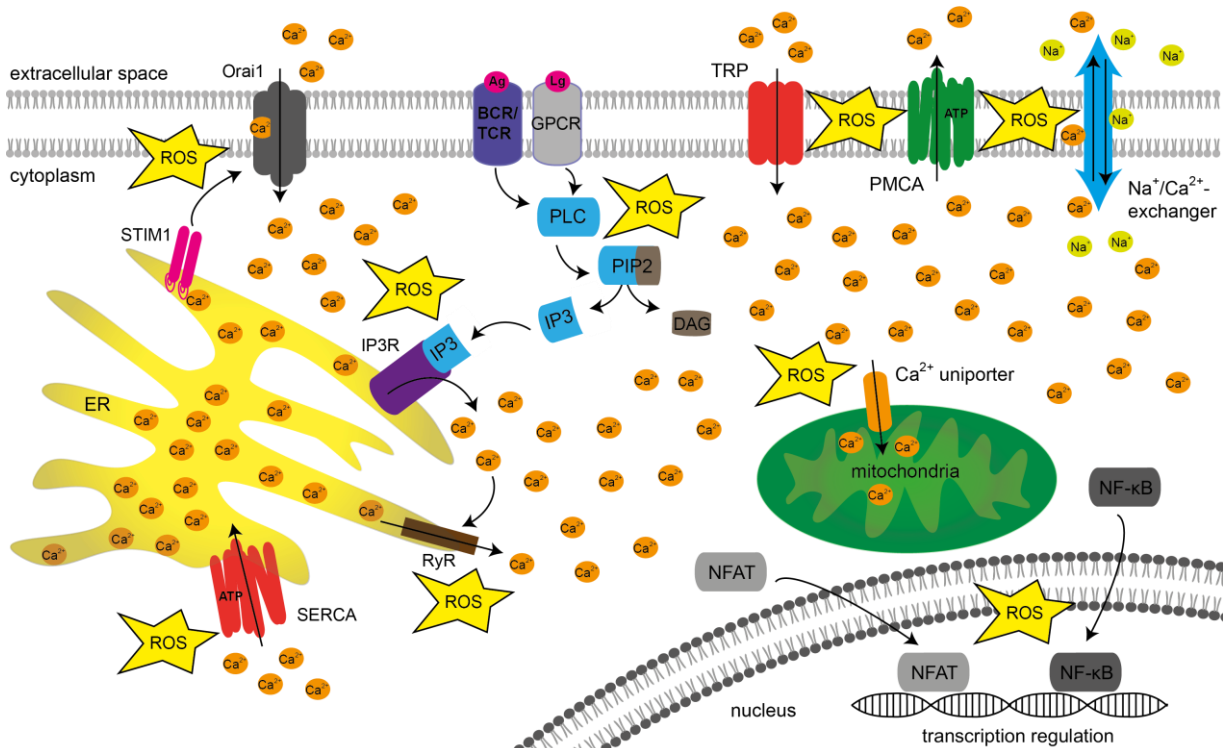


Figure 7: Ca²⁺ signaling and oxidative stress.

Reactive oxygen species (ROS) can influence all key players in Ca²⁺ signaling. Oxidants alter the activities of transient receptor potential (TRP) channels, plasma membrane Ca²⁺-ATPases (PMCA) or Na⁺/Ca²⁺-exchangers. During oxidative stress, ROS can also modify the actions of phospholipase C (PLC), IP3 receptors (IP3R), or ryanodine receptors (RyR). Oxidants can affect stromal interaction molecule 1 (STIM1) and Orai1 as well as the sarco/endoplasmic reticulum Ca²⁺-ATPases (SERCA) or the mitochondrial Ca²⁺ uniporter. Even the nuclear translocation of nuclear factor kappa light chain enhancers of activated B cells (NF-κB) is affected by ROS signaling.

3.4.2 Endoplasmic reticulum and stress

The ER is not only a major Ca²⁺ store but also a place for membrane lipid biosynthesis (Fagone and Jackowski, 2009), posttranslational protein modifications and protein folding (Braakman and Bulleid, 2011). The biological function of a protein depends on its correct folding because misfolded proteins are commonly associated with severe diseases, like α-synuclein with Parkinson's disease (Cooper et al., 2006). To ensure proper protein folding, a group of proteins exists in the ER that assists in protein folding. The lectin calnexin is one of those chaperones, which provides glycosylation-assisted protein folding by binding to membrane-bound and soluble newly synthesized glycoproteins (Ou et al., 1993; Helenius and Aebi, 2004). Another chaperone is the binding immunoglobulin protein (BiP), also known as glucose-regulated protein 78. BiP binds to proteins containing several alternating aromatic and hydrophobic amino acids (Blond-Elguindi et al., 1993). Disturbances in cellular redox-maintenance or Ca²⁺

3 INTRODUCTION

levels can affect the normal ER functions as well as accumulation of unfolded or misfolded proteins in the ER. This triggers a cell stress reaction, the unfolded protein response (UPR) to compensate for damage (Boyce and Yuan, 2006; Hetz, 2012). Upon UPR activation three stress sensors are induced: inositol-requiring enzyme 1 α (IRE1 α), activating transcription factor 6 (ATF6) and protein kinase RNA-like ER kinase (PERK). PERK and IRE1 α are involved in the early UPR, which includes the inhibition of protein translation and the degradation of mRNA for specific ER proteins (Hetz, 2012). The second part of the stress response starts with the induction of transcription factor X box-binding protein 1 (XBP1) mRNA by ATF6 and splicing of the XBP1 mRNA by IRE1 α to produce an active transcription factor (Yoshida et al., 2001; Hetz, 2012). This is followed by an increase in the expression of chaperones like calnexin and BiP (Kozutsumi et al., 1988; Zhao et al., 2019).

3.4.3 The mitochondrial respiratory system and stress

Mitochondria are called "the powerhouse of the cell" (Siekevitz, 1957) because they harbor a variety of enzymes and proteins that help to convert amino acids, fatty acids, and carbohydrates into energy (van der Bliet et al., 2017). The Krebs cycle is used to produce reduced nicotinamide adenine dinucleotide (NADH) and flavin adenine dinucleotide (FADH₂), the electron donors for oxidative phosphorylation (OXPHOS) (van der Bliet et al., 2017). OXPHOS is the process in cells by which mitochondria produce energy in the form of ATP by moving electrons along the electron transport chain or system (ETS) (Saraste, 1999). The ETS consists of four enzyme complexes in the inner mitochondrial membrane called complex I (NADH dehydrogenase or NADH:ubiquinone oxidoreductase), complex II (succinate dehydrogenase or succinate:ubiquinone reductase), complex III (cytochrome bc₁) and complex IV (cytochrome oxidase) (Saraste, 1999). Electrons (e⁻) of NADH and FADH₂ enter the ETS through complex I and II and are then passed along coenzyme Q (ubiquinone), complex III and cytochrome C until they are finally transferred to molecular oxygen by complex IV (Saraste, 1999). Additionally, complex I, III and IV function as proton pumps and generate the electrochemical gradient (Schultz and Chan, 2001) that is used by complex V, the F₁F₀-ATP synthase, to synthesize ATP (Boyer, 1997). Superoxides are normal byproducts of the energy production in OXPHOS (Brand et al., 2004). Because superoxides can damage the cell, mitochondria have a highly developed antioxidative system (Kowaltowski and Vercesi, 1999).

3 INTRODUCTION

Superoxide dismutases convert superoxides into H_2O_2 , which is neutralized and used by peroxidases to produce water (Brand et al., 2004). In stress situations, such as oxidative stress or disturbed Ca^{2+} homeostasis, mitochondrial DNA is damaged, thus leading to a misproduction of proteins of the OXPHOS system and further production of superoxides (Kowaltowski and Vercesi, 1999). Overproduction of superoxides induces lipid peroxidation and uncoupling of the ETS to lower superoxide production (Murphy et al., 2003). Furthermore, Ca^{2+} -induced mitochondrial oxidative stress can be followed by the oxidation of thiols from inner membrane proteins (Kowaltowski and Vercesi, 1999) and mitochondrial permeability transition, which leads to mitochondrial swelling (Halestrap, 2009). If mitochondrial stress situations are not regulated, it results in apoptosis of the cell (Kowaltowski and Vercesi, 1999).

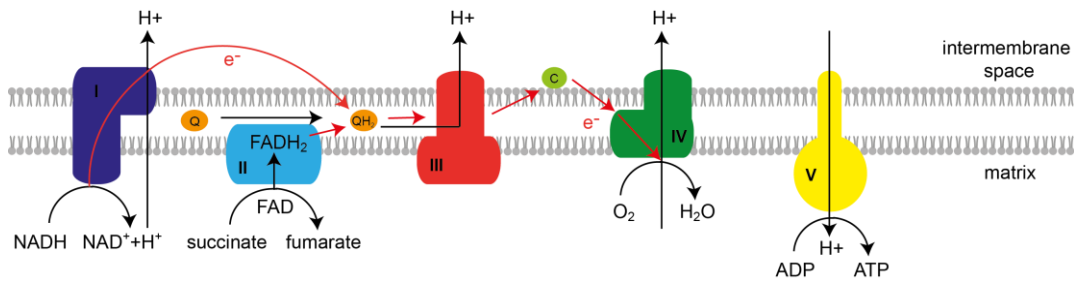


Figure 8: The mitochondrial respiratory system.

The enzyme complexes of the mitochondrial respiratory system are located in the mitochondrial inner membrane and are responsible for the generation of ATP during oxidative phosphorylation. The electron transport system (ETS) consists of four enzyme complexes called complex I (NADH dehydrogenase or NADH : ubiquinone oxidoreductase), complex II (succinate dehydrogenase or succinate : ubiquinone reductase), complex III (cytochrome bc1) and complex IV (cytochrome oxidase). Electrons (e^-) of NADH and FADH_2 enter the ETS through complex I and II and are then passed along coenzyme Q (Q), complex III and cytochrome C (C) until they are finally transferred to molecular oxygen by complex IV. Additionally, complex I, III and IV function as proton (H^+) pumps and generate the electrochemical gradient that is used by complex V, the F_1F_0 -ATP synthase, to synthesize ATP (adapted from Saraste, 1999).

3.5 AIM OF THIS WORK

Oxidative stress and Ca^{2+} signaling are two independent signaling processes but often go hand-in-hand in order to maintain normal cellular physiology. Since Ca^{2+} signaling plays a very important role in the correct functioning of the immune system and DMF is known to induce short-term oxidative stress, this work focuses on the understanding how DMF influences the Ca^{2+} homeostasis in immune cells and if the DMF-induced changes in cellular redox state are responsible for its immunomodulatory effects.

4 MATERIALS

4.1 CONSUMABLES

Table 1: Consumables

Consumable	Supplier
μ -Slide, 8-well, glass bottom	IBIDI
35 mm petri dishes, No.1.0, Coverslip 14 mm glass \emptyset	Mattek
6-, 12-, 24-, 48- and 96-well plates	Greiner bio-one
6-Tube magnetic separation rack	New England Biolabs
96-well plates, black and white	Greiner bio-one
Borosilicate glass capillaries (type GC150F-10)	Harvard Apparatus
Cell culture dishes 100/20 SureGr	Sarstedt
Cell culture dishes 145/20 Cellstar	Greiner bio-one
Cell scraper	Greiner bio-one
Cell strainer, 100 μ m	Greiner bio-one
CoolCell [®] alcohol free cell freezing container	Biocision
Coverslips, \emptyset 12 mm	VWR International
Cryo tubes, 2 ml	Biochrom
Cuvettes, 1.5-3 ml	Brand
FACS tubes, 12 x 75 mm	A. Hartenstein
Falcon tubes, 50 ml and 15 ml	Sarstedt Biozym and Greiner bio-one
Glass Dounce homogenizer	Sigma-Aldrich
Glassware	Schott Duran
Hamilton gastight syringe	Sigma-Aldrich
Luna cell counting chamber slides	Logos Biosystems
Microscope slide	VWR International
Microseal [®] B PCR plate sealing film	Bio-Rad
Mini-PROTEAN TGX Stain-Free Precast Gels, 4-15% or 4-20%	Bio-Rad
Multiplate [™] 96-well PCR plate	Bio-Rad
NativePAGE [™] 4-16% Bis-Tris Protein Gels	Thermo Fisher Scientific
Neubauer counting chamber	Precicolor HBG
Petri dishes, 100x15 mm	Greiner bio-one
Pipette tips	Starlab
Scalpels	Fine Science Tools
Serological pipettes, 5 ml, 10 ml & 25 ml	Greiner bio-one
Syringes, 5 ml	Braun
Trans-Blot Turbo Midi or Mini PVDF or Nitrocellulose Transfer Pack	Bio-Rad
Tubes, 0.2 ml, 0.5 ml, 1.5 ml and 2 ml	Starlab

4 MATERIALS

4.2 CHEMICALS, BUFFERS, MARKERS AND MEDIA FOR MOLECULAR BIOLOGY

Table 2: Chemicals, buffers, markers and media for molecular biology

Chemical/Buffer/Marker/Medium	Supplier
1 kb Plus DNA ladder	Invitrogen
10x Blue Juice Loading buffer	Invitrogen
10x FastDigest buffer	Thermo Fisher Scientific
2-Propanol, 99.95 %	Carl Roth
Acetic acid, 100 %	Carl Roth
Agarose Basic	AppliChem
Ampicillin	Sigma-Aldrich
Calcium chloride (CaCl ₂)	Carl Roth
Ethylenediaminetetraacetic acid (EDTA)	Sigma-Aldrich
Glycerol	Carl Roth
LB Agar	Invitrogen
LB Broth Base	Invitrogen
Magnesium chloride (MgCl ₂)	Carl Roth
Midori Green	Biozym
Nuclease-free water	Life Technologies
S.O.C. medium	Invitrogen
Takyon No ROX Probe Mastermix blue dTTP	Eurogentec
Tris(hydroxymethyl)aminomethane (Tris)	Carl Roth

4.3 MEDIA, SUPPLEMENTS AND CHEMICALS FOR CELL CULTURE

Table 3: Media, supplements and chemicals for cell culture

Medium/Supplement/Chemical	Supplier
0.05% Trypsin-EDTA (1x) and 0.25% Trypsin-EDTA (1x)	Life Technologies
10 000 Units/ml Penicillin and 10 mg/ml Streptomycin	Sigma Aldrich
2-Mercaptoethanol, 50 mM	Life Technologies
5000 Units/ml Penicillin and Streptomycin	Life Technologies
BD Pharm Lyse™ Lysing Buffer (10x)	BD Biosciences
Dimethyl sulfoxide (DMSO)	Sigma-Aldrich
DMEM High Glucose, with 4.5 g Glucose, L-glutamine and pyruvate	Sigma-Aldrich and Gibco
DMEM/F-12 without L-glutamine	Life Technologies
Dulbecco's Phosphate Buffered Saline (PBS), without calcium chloride and magnesium chloride	Sigma-Aldrich
Ethanol, 70%, denatured	AppliChem
Fungizone® (Amphotericin B, 250µg/ml)	Life Technologies

4 MATERIALS

GlutaMAX™ (100x)	Life Technologies
Hamster Anti-mouse CD28, clone 37.51, monoclonal	eBioscience™
Hamster Anti-mouse CD3e, clone 145-2C11, monoclonal	eBioscience™
HEPES, 1 M	Life Technologies
Hyclone Fetal Bovine Serum (FCS)	Thermo Scientific
Ionomycin	Life Technologies
L-glutamine, 200 mM	Life Technologies
MEM NEAA (100x) Non-Essential Amino Acids	Life Technologies
Opti-Mem® I (1x) serumreduced medium	Life Technologies
Phorbol 12-myristate 13-acetate (PMA)	Sigma-Aldrich
RPMI -Medium 1640, without L-glutamine	Sigma-Aldrich
Sodium Phosphate, Dibasic (Na ₂ HPO ₄)	Sigma-Aldrich
Sodium pyruvate, 100 mM (100x)	Life Technologies
Trypan blue, 0.4%	Fluka or Biozym

4.4 CELL CULTURE MEDIA COMPOSITION

Table 4: Cell culture media composition

Medium	Composition
MEF cell growth medium	DMEM High Glucose medium 10% (v/v) FCS 100 U/ml penicillin and 100 µg/ml streptomycin
CHO cell growth medium	DMEM F12 medium 10% (v/v) FCS 100 U/ml penicillin and 100 µg/ml streptomycin 1% (v/v) L-glutamine
COS1 cell growth medium	DMEM High Glucose medium 10% FCS (v/v) 2% (v/v) penicillin/streptomycin (each 5000 U/ml) 2% GlutaMAX™ 1% (v/v) MEM non-essential amino-acids (NEAA) 0.2% (v/v) Fungizone®
Splenocytes isolation medium	DMEM High Glucose medium 100 U/ml penicillin and 100 µg/ml streptomycin)
Splenocytes growth medium	RPMI 1640 medium 12% (v/v) FCS 1.2% (v/v) sodium-pyruvate 1.2% (v/v) HEPES 1.2% (v/v) L-glutamine 1.2% (v/v) MEM NEAA 120 U/ml penicillin and 120 µg/ml streptomycin 0.24% (v/v) 2-mercaptoethanol

4.5 CHEMICALS, BUFFERS AND SOLUTIONS FOR PROTEIN BIOCHEMISTRY

Table 5: Chemicals, buffers and solutions for protein biochemistry

Chemical/Buffer/Solution	Supplier
0.01 % poly-L-lysine	Sigma-Aldrich
1,4-Dithiothreitol (DTT)	Carl Roth
10 x Tris/Glycine/SDS buffer	Biorad
2-Mercaptoethanol, 50 mM	Life Technologies
4% Roti [®] -Histofix (Paraformaldehyde, PFA)	Carl Roth
4x NativePAGE [®] Sample buffer	Thermo Fisher Scientific
5,5'-dithiobis-(2-nitrobenzoic acid) (DTNB)	Sigma-Aldrich
Acetic acid, 100 %	Carl Roth
Adenosine 5'-diphosphate sodium salt	Sigma-Aldrich
Adenosine 5'-triphosphate dipotassium salt hydrate	Sigma-Aldrich
Adenosine 5'-triphosphate disodium salt hydrate	Sigma-Aldrich
Ammonium heptamolybdate tetrahydrate	Sigma-Aldrich
Biotinylated glutathione ethyl ester (BIOGEE)	Thermo Fisher Scientific and VCPBIO
Bovine Serum Albumin (BSA)	Sigma-Aldrich
Bradford Ultra [™] reagent	Expedeon
Bromphenol blue	Sigma-Aldrich
Calcium chloride (CaCl ₂)	Carl Roth
Calcium ionophore A23187	Sigma-Aldrich
Complete Mini Protease Inhibitor Cocktail Tablets	Roche
Coomassie Brilliant Blue G-250	Sigma-Aldrich
Dako Fluorescent Mounting Medium	Dako
Dimethyl fumarate (DMF)	Sigma-Aldrich
Dulbecco's Phosphate Buffered Saline, without calcium chloride and magnesium chloride	Sigma-Aldrich
Ethanol absolute AnalaR NORMAPUR [®]	VWR
Ethanol Rotipuran, 99.8 %	Carl Roth
Ethylene glycol-bis(2-aminoethyl ether)-N,N,N',N'-tetraacetic acid (EGTA)	Bioworld
Ethylenediaminetetraacetic acid (EDTA)	Sigma-Aldrich
Glutathione reductase	Sigma-Aldrich
Glycerol	Carl Roth
Glycine	Sigma-Aldrich
Guanidine hydrochloride	Sigma-Aldrich
Guanosine 5'-triphosphate sodium salt hydrate (GTP)	Sigma-Aldrich
HEPES sodium salt	Sigma-Aldrich
Hydrochloric acid (HCl), 1N	Carl Roth
Ionomycin	Life Technologies
L-ascorbic acid	Sigma-Aldrich

4 MATERIALS

L-glutathione, oxidized	Sigma-Aldrich
L-glutathione, reduced	Sigma-Aldrich
Magnesium acetate tetrahydrate	Carl Roth
Magnesium chloride hexahydrate (MgCl ₂ ·6H ₂ O)	Sigma-Aldrich
Methanol, Rotisol [®] ≥ 99,95%	Carl Roth
Milk powder	Carl Roth
NativePAGE [®] 5% Coomassie Brilliant Blue G-250	Thermo Fisher Scientific
NativePAGE [™] cathode buffer	Thermo Fisher Scientific
NativePAGE [™] running buffer (20x)	Thermo Fisher Scientific
Nicotinamide adenine dinucleotide phosphate, reduced (NADPH)	Sigma-Aldrich
Nonidet-40 (NP-40)	AppliChem
Normal goat serum (NGS)	Vector Laboratories
Nuclease-free water	Life Technologies
Phenylmethylsulphonyl fluoride (PMSF)	Sigma-Aldrich
Phorbol 12-myristate 13-acetate (PMA)	Sigma-Aldrich
PhosSTOP [™] (inhibitor tablets for phosphatase)	Roche
Pierce [®] RIPA buffer	Thermo Scientific
Ponceau S solution	Sigma-Aldrich
Potassium chloride (KCl)	Carl Roth
Potassium dihydrogenphosphate (KH ₂ PO ₄)	Carl Roth
Potassium hydroxide (KOH)	Sigma-Aldrich
Potassium phosphate, dibasic (K ₂ HPO ₄)	Sigma-Aldrich
Recombinant mouse TNF-alpha (aa 80-235) protein	R&D Systems
Roti [®] -ImmunoBlock (10x)	Carl Roth
Sigmafast [™] Protease Inhibitor Cocktail Tablets	Sigma-Aldrich
Sodium chloride (NaCl)	Carl Roth
Sodium citrate	Sigma-Aldrich
Sodium deoxycholate	Sigma-Aldrich
Sodium dodecyl sulfate (SDS)	Sigma-Aldrich
Sodium hydroxide (NaOH)	Applichem
Sodium phosphate, Dibasic (Na ₂ HPO ₄)	Sigma-Aldrich
Sodium succinate dibasic hexahydrate	Sigma-Aldrich
Sodium-(m)-arsenite (NaAsO ₂)	Sigma-Aldrich
Streptavidin magnetic beads (Dynabeads [®] M-280)	New England Biolabs
Sucrose	Sigma-Aldrich
Sulfosalicylic acid	Sigma-Aldrich
TES	Sigma-Aldrich
Triethanolamine	Sigma-Aldrich
Tris (hydroxymethyl) aminomethane (Tris)	Carl Roth
Triton X-100	Carl Roth
Tween [®] 20	Carl Roth

4 MATERIALS

4.6 BUFFER COMPOSITION

Table 6: Buffer composition

Buffer	Composition
1x PBS-T	137 mM NaCl 2.7 mM KCl 6.46 mM Na ₂ HPO ₄ 1.46 mM KH ₂ PO ₄ 0.05% (v/v) Tween®20
1x TBS-T	150 mM NaCl 50 mM Tris-HCl, pH 7.5 0.1% (v/v) Tween®20

4.7 CHEMICALS FOR HIGH-RESOLUTION RESPIROMETRY

Table 7: Chemicals for high-resolution respirometry

Chemical	Supplier
Antimycin A	Sigma-Aldrich
Carbonyl cyanide 4-(trifluoromethoxy) phenylhydrazone (FCCP)	Sigma-Aldrich
Dimethyl fumarate (DMF)	Sigma-Aldrich
Oligomycin	Sigma-Aldrich
Rotenone	Sigma-Aldrich

4.8 CHEMICALS AND SOLUTIONS FOR ELECTROPHYSIOLOGY

Table 8: Chemicals and solutions for electrophysiology

Chemical/Solution	Supplier
0.01 % poly-L-lysine	Sigma-Aldrich
1,2-bis(2-aminophenoxy)ethane-N,N,N',N'-tetraacetic acid (BAPTA)	Sigma-Aldrich
A967079	Tocris
Adenosine 5'-triphosphate disodium salt hydrate (Na ₂ ATP)	Sigma-Aldrich
Adenosine 5'-triphosphate magnesium salt (Mg ₂₊ ATP)	Sigma-Aldrich
Calcium chloride (CaCl ₂)	Carl Roth
D(+)-Glucose	Sigma-Aldrich
Dimethyl fumarate (DMF)	Sigma-Aldrich
Ethylene glycol-bis(2-aminoethyl ether)-N,N,N',N'-tetraacetic acid (EGTA)	Bio Basic Canada Inc.
Flufenamic acid	Sigma-Aldrich
Guanosine 5'-triphosphate sodium salt hydrate (Na ₂ GTP)	Sigma-Aldrich

4 MATERIALS

HC030031	Tocris
HEPES sodium salt	Alfa Aesar
Hydrogen peroxide (H ₂ O ₂), 30%	Merck
Magnesium chloride (MgCl ₂)	Carl Roth
Potassium chloride (KCl)	Carl Roth
Potassium gluconate (K-gluconate)	Sigma-Aldrich
Ruthenium red	Sigma-Aldrich
Sodium chloride (NaCl)	Fluka
Sodium hydrogen carbonate (NaHCO ₃)	Alfa Aesar
Sodium phosphate monobasic monohydrate (NaH ₂ PO ₄)	Sigma-Aldrich

4.9 CHEMICALS, SOLUTIONS AND MEDIA FOR FLOW CYTOMETRY

Table 9: Chemicals, solutions and media for flow cytometry

Chemical/Solution/Medium	Supplier
10 000 Units/ml Penicillin and 10 mg/ml Streptomycin	Sigma Aldrich
4% Roti®-Histofix (Paraformaldehyde, PFA)	Carl Roth
Bovine Serum Albumin (BSA)	Sigma-Aldrich
Calcium chloride (CaCl ₂)	Carl Roth
Dimethyl fumarate (DMF)	Sigma-Aldrich
DMEM High Glucose with 4.5 g Glucose and L-glutamine, without Phenol red	PAA Laboratories
DMEM High Glucose, with 4.5 g Glucose, L-glutamine and pyruvate	Sigma-Aldrich and Gibco
Dulbecco's Phosphate Buffered Saline, without calcium chloride and magnesium chloride	Sigma-Aldrich
Ethylene glycol-bis(2-aminoethyl ether)-N,N',N'-tetraacetic acid (EGTA)	Bio Basic Canada Inc.
Hank's Balanced Salt Solution with calcium and magnesium (HBSS +/+), without Phenol red	Life Technologies
HEPES, 1 M	Life Technologies
Hyclone Fetal Bovine Serum (FCS)	Thermo Scientific
Ionomycin	Life Technologies
Lanthanum(III) chloride heptahydrate (LaCl ₃ x 7H ₂ O)	Sigma-Aldrich
Sterofundin® ISO (Ringer solution)	Braun
Thapsigargin	Life Technologies
Triton X-100	Carl Roth

4 MATERIALS

4.10 CHEMICALS, SOLUTIONS, DYES AND MEDIA FOR MICROSCOPY

Table 10: Chemicals, solutions, dyes and media for microscopy

Chemical/Solution/Dye/Medium	Supplier
CalciFluor Fluo-8, AM	Santa Cruz Biotechnology
Calcium chloride (CaCl ₂)	Carl Roth
D(+)-Glucose	Sigma-Aldrich
Dimethyl fumarate (DMF)	Sigma-Aldrich
DMEM High Glucose, with 4.5 g Glucose, L-glutamine and pyruvate	Sigma-Aldrich and Gibco
Dulbecco's Phosphate Buffered Saline, without calcium chloride and magnesium chloride	Sigma-Aldrich
Ethylene glycol-bis(2-aminoethyl ether)-N,N,N',N'-tetraacetic acid (EGTA)	Bio Basic Canada Inc.
Fibronectin	Sigma-Aldrich
Fura-2-AM (Life Technologies
HEPES sodium salt	Sigma-Aldrich
Hoechst Stain solution	Sigma-Aldrich
Hydrogen peroxide (H ₂ O ₂), 30%	Merck
Ionomycin	Life Technologies
Magnesium chloride hexahydrate (MgCl ₂ .6H ₂ O)	Sigma-Aldrich
Manganese(II) chloride	Sigma-Aldrich
Pluronic™ F-127	Life Technologies
Potassium chloride (KCl)	Carl Roth
Sodium chloride (NaCl)	Carl Roth
Thapsigargin	Life Technologies

4.11 ANTIBODIES AND MARKER FOR IMMUNOBLOTTING

Table 11: Antibodies and marker for immunoblotting

Antibody/Marker	Species	Supplier
Anti-Actin, clone C4, monoclonal	mouse	Merck Chemicals
Anti-BiP, clone C50B12, monoclonal	rabbit	Cell Signaling
Anti-Calnexin, polyclonal	rabbit	Abcam
Anti-c-Rel, polyclona	rabbit	Santa Cruz Biotechnology
Anti-DNP, clone 9H8.1, monoclonal	rabbit	Merck
Anti-GAPDH, clone 14C10, monoclonal	rabbit	New England Biolabs
Anti-GFP, polyclonal	rabbit	Abcam
Anti-GSR, polyclonal	rabbit	Antibodies-online
Anti-HDAC1, polyclonal	rabbit	Cell Signaling
Anti-IκBα, clone 44D4, monoclonal	rabbit	Cell Signaling

4 MATERIALS

Anti-NFATc1, clone 7A6, monoclonal	mouse	Santa Cruz Biotechnology
Anti-NFATc2, clone 4G6-G5, monoclonal	mouse	Santa Cruz Biotechnology
Anti-phospho- $\text{I}\kappa\text{B}\alpha$, clone 14D4, monoclonal	rabbit	Cell Signaling
Anti-RelB, clone C1E4, monoclonal	rabbit	Cell Signaling
Anti-SERCA2b, polyclonal	rabbit	Kind gift from Peter Vangheluwe, Leuven, Belgium
Anti-STIM1/GOK, clone 5A2, monoclonal	mouse	Abnova
Anti- $\alpha\beta$ -Tubulin, polyclonal	rabbit	Cell Signaling
Anti-mouse IgG (H+L) DyLight 680 and 800 Conjugate	goat	New England Biolabs
Anti-rabbit IgG (H+L) DyLight 680 and 800 Conjugate	goat	New England Biolabs
Chameleon Duo Pre-stained Protein Ladder		Licor
MagicMark XP Western Protein Standard		Invitrogen

4.12 ANTIBODIES AND DYES FOR FLOW CYTOMETRY

Table 12: Antibodies and dyes for flow cytometry

Antibody/Dye	Species	Supplier
2-(N-(7-nitrobenz-2-oxa-1,3-diazol-4-yl)amino)-2-deoxyglucose (2-NBDG)		Thermo Fisher Scientific
7-Aminoactinomycin D (7-AAD)		eBioscience™
Alexa Fluor® 488 anti-NFATc1, clone 7A6, monoclonal	mouse	Biolegend
Anti-mouse CD3 APC, clone 17A2, monoclonal	rat	Thermo Fisher Scientific
Anti-mouse/human Alexa Fluor® 700 CD45R/B220, clone RA3-6B2, monoclonal	rat	Biolegend
Anti-mouse/human/rat GOK (STIM1), clone 44, monoclonal	mouse	BD Biosciences
CalciFluor Fluo-8, AM		Santa Cruz Biotechnology
CellROX™ Orange Reagent		Life Technologies
LIVE/DEAD Fixable Dead Cell Stain Kit, violet		Life Technologies
LYNX Rapid Fluorescein Antibody Conjugation Kit		Biorad (AbD Serotec)
MitoSox™ Red Mitochondrial Superoxide Indicator Reagent		Life Technologies

4.13 ANTIBODIES AND DYES FOR IMMUNOCYTOCHEMISTRY

Table 13: Antibodies and dyes for immunocytochemistry

Antibody/Dye	Species	Supplier
4',6-diamidino-2-phenylindole (DAPI)		Life Technologies
Anti-Actin, clone C4, monoclonal	mouse	Merck Chemicals
Anti-mouse Alexa Fluor® 488, polyclonal	goat	Life Technologies
Anti-mouse Alexa Fluor® 568, polyclonal	goat	Life Technologies
Anti-NFATc1, clone 7A6, monoclonal	mouse	DSHB
Anti-NF-κB p65, clone D14E12, monoclonal	rabbit	Cell Signaling
Anti-rabbit Alexa Fluor® 488, polyclonal	goat	Life Technologies
Anti-rabbit Alexa Fluor® 568, polyclonal	goa	Life Technologies
Anti-αβ-Tubulin, polyclonal	rabbit	Cell Signaling

4.14 KITS

Table 14: Kits

Kit	Supplier
BC Assay Protein Quantification Kit	Interchim
Dual-Glo® Luciferase Assay Kit	Promega
GFP-Trap®_M Kit	Chromotek
High Capacity cDNA Reverse Transcription Kit	Applied Biosystems
MEGAquick-spin™ Plus Total Fragment DNA Purification Kit	Intron
Nucleobond®XTRA Plasmid Purification System Kit	Macherey-Nagel
OxyBlot™ Protein Oxidation Detection Kit	Merck
Q5® Site-Directed Mutagenesis Kit	New England Biolabs
Qubit™ Protein Assay Kit	Thermo Fisher Scientific
ZR RNA MiniPrep™ Kit	Zymo Research
Zyppy™ Plasmid Miniprep Kit	Zymo Research

4.15 RESTRICTION ENZYMES

Table 15: Restriction enzymes

Restriction enzyme	Supplier
FastDigest EcoRI	Thermo Fisher Scientific
FastDigest NdeI	Thermo Fisher Scientific

4 MATERIALS

4.16 TRANSFECTION REAGENTS

Table 16: Transfection reagents

Transfection reagent	Supplier
Attractene Transfection Reagent	Qiagen
GeneJuice® Transfection Reagent	Novagen
TurboFectin™ 8.0 Transfection Reagent	Origene

4.17 PRIMER FOR MUTAGENESIS PCR AND SEQUENCING

Table 17: Primer for mutagenesis PCR and sequencing

Primer	Sequence	Supplier
SERCA2b C674S forward	5`-TCG AGT TGA ACC CTC CCA C-3`	Metabion International AG
SERCA2b C674S reverse	5`-GCA AAA GAG CGG GCG TTC AG-3`	Metabion International AG
SERCA2b sequencing	5`-TGA GAC CAA TCT GAC CTT CG-3`	Metabion International AG

4.18 PRIMER AND PROBES FOR QPCR

Table 18: Primer and probes for qPCR

Primer/Probe	Sequence/Catalog number	Supplier
HPRT left	5`-GTT GCA AGC TTG CTG GTG AA -3`	Eurofins Genomics
HPRT right	5`-GAT TCA AAT CCC TGA AGT ACT CA-3`	Eurofins Genomics
Probe #HPRT	5`-CCT CTC GAA GTG TTG GAT ACA GGC CA-3`	Eurofins Genomics
TRPA1 left	5`-CGG CCT GAG TTT ATG CAG AT-3`	Eurofins Genomics
TRPA1 right	5`-TGT GCA TCC GTC ATT GTC TT-3`	Eurofins Genomics
Probe #9	04685075001	Roche
TRPM2 left	5`-CAT TGT CTG CGT GGT GTT G-3`	Eurofins Genomics
TRPM2 right	5`-TGC CAT TGT TGA TGG CAT T-3`	Eurofins Genomics
Probe #81	04689046001	Roche
TRPM7 left	5`-GCA AAG CAG AGT GAC CTG GTA-3`	Eurofins Genomics
TRPM7 right	5`-GCC AGT TGG CCA AAA TCA T-3`	Eurofins Genomics
Probe #6	04685032001	Roche
Unspliced XBP1 left	5`-CTG ACG AGG TTC CAG AGG TG-3`	Eurofins Genomics
Unspliced XBP1 right	5`-GCA GAG GTG CAC ATA GTC TGA G-3`	Eurofins Genomics
XBP1 left	5`-TCT GAC ACT GTT GCC TCT TCA-3`	Eurofins Genomics
XBP1 right	5`-CTC TGG GAG TTC CTC CAG ACT-3`	Eurofins Genomics
Probe #49	04688104001	Roche
Probe #60	04688589001	Roche

4 MATERIALS

4.19 PLASMID DNA

Table 19: Plasmid DNA

Plasmid	Backbone	Insert	Source
NFAT luciferase reporter	pGL2-Basic	Human IL-2 promotor and firefly luciferase	Kind gift from Toren Finkel, Pittsburgh, USA
pRL-TK	pRL-TK	Renilla reniformis luciferase	Promega
pPB CAG HA DEST EV mcherry	pPB CAG HA DEST	mcherry	Generated in the lab
pPB CAG HA DEST STIM1 WT mcherry	pPB CAG HA DEST	Human STIM1 WT and mcherry	Generated in the lab
pPB CAG HA DEST STIM1 C49M mcherry	pPB CAG HA DEST	Human STIM1 C49M and mcherry	Generated in the lab
pPB CAG HA DEST STIM1 C56M mcherry	pPB CAG HA DEST	Human STIM1 C56M and mcherry	Generated in the lab
pPB CAG HA DEST STIM1 C49M C56M mcherry	pPB CAG HA DEST	Human STIM1 C49M C56M and mcherry	Generated in the lab
SERCA2b WT pDEST-N-GFP	pCDNA 6.2-N-GFP-DEST	Human SERCA2b WT	Kind gift from Peter Vangheluwe, Leuven, Belgium
SERCA2b C674S pDEST-N-GFP	pCDNA 6.2-N-GFP-DEST	Human SERCA2b C674S	Generated in this work
SERCA2b WT PMT2	PMT2	Human SERCA2b WT	Kind gift from Peter Vangheluwe, Leuven, Belgium
SERCA2b C674S PMT2	PMT2	Human SERCA2b C674S	Generated in this work

4.20 BACTERIA

Table 20: Bacteria

Strain and Genotype	Supplier
E.coli DH5 α -Bacteria (F- Φ 80lacZ Δ M15 Δ (lacZYA-argF) U169 recA1 endA1 hsdR17 (rK-, mK+) phoA supE44 λ - thi-1 gyrA96 relA1)	Invitrogen

4 MATERIALS

4.21 CELL LINES

4.21.1 MEF cells

In this work, adherent mouse embryonic fibroblast (MEF) cells were used to study STIM1. STIM1 wildtype (WT) cells and STIM1 knockout (-/-) cells were isolated from mouse embryos and immortalized by Masatsugu Oh-Hora and his group (Oh-Hora et al., 2008). In our laboratory the STIM1 -/- cells were transfected with different STIM1 plasmids to create new stable cell lines that express STIM1 WT mcherry, empty vector (EV) mcherry or the mutants STIM1 C49M mcherry, STIM1 C56M mcherry and STIM1 C49M/C56M mcherry.

4.21.2 CHO cells

CHO cells are adherent epithelial cells isolated from Chinese hamster ovaries by Theodore T. Puck (Puck et al., 1958). In this work, CHO cells were used for protein expression.

4.21.3 COS1 cells

CV-1 in Origin Simian-1 (COS1) cells are adherent fibroblast-like cells derived from kidney tissue of the African green monkey. To immortalize the cells, they were transfected with a replication-defective version of the simian virus 40 that can produce the large T antigen (Gluzman, 1981). COS1 cells were used for protein expression in this work.

4.22 MICE

Female, 6-8 weeks old Swiss Jim Lambert (SJL) WT mice were ordered from Janvier Labs and used for all experiments with splenocytes. SJL mice are immunocompetent, show decreased natural killer cell activity and higher levels of circulating T cells. Because SJL mice are sensitive to experimental autoimmune encephalomyelitis (EAE), they are used in multiple sclerosis research. These circumstances and the fact that recent work revealed that splenocytes from SJL mice show an effective response to dimethyl fumarate (DMF) (Albrecht et al., 2012) were the reasons to use SJL mice in this work.

For EAE experiments female, 8-12 weeks old SJL WT mice were purchased from Charles River. All EAE experiments were done by cooperation partners and carried out following the relevant guidelines and regulations for animal welfare by the federal state Rhineland-Palatinate (#G13-1-099). All efforts were made to minimize suffering of the mice. For EAE induction, mice were

4 MATERIALS

immunized subcutaneously at the base of the tail with 250 µg proteolipid protein 139-152 peptide (sequence: ASQKRPSQRS; peptide 2.0) emulsified in Complete Freund's adjuvant (Becton Dickinson), supplemented with additional 10 mg/ml of heat-inactivated *Mycobacterium tuberculosis* H37Ra (Becton Dickinson). Along with immunization and two days post immunization, 100 ng pertussis toxin (List-Biological-Laboratories) in phosphate buffered saline (PBS) was administered by intraperitoneal injection. Daily clinical scoring of EAE symptoms was conducted as follows: 0, no symptoms, normal behavior; 1, tail paralyzed; 2, impaired righting reflex and gait; 3, partial hind limb paralysis; 4, hind legs completely paralyzed; 5, tetraparesis. Mice were analyzed at day 8 or 20 post immunization before disease onset.

For electrophysiological experiments, male and female, 6-12 weeks old C57BL/6 WT mice from Envigo Ltd. Company were used.

To prepare primary MEF cells, 14 days old embryos from in house breeding of WT mice at the animal facility of the Boston University School of Medicine were used. The original C57BL/6 mice were bought from The Jackson Laboratory.

4.23 DEVICES

Table 21: Devices

Device	Supplier
Accu-jet® pro	Brand
Amnis ImageStream X mk II	Merck
ArrayScan® VTI HCS Reader	Thermo Fisher Scientific
BD FACS Canto™ II	BD Biosciences
Centrifuge 5430	Eppendorf
CFX Connect™ Real-Time PCR Detection System	Biorad
CO ₂ -Incubator MCO-20AIC	SANYO
Digidata 1440A digitizer	Molecular Devices
Eclipse Ti-E inverted microscope	Nikon
Electrophoresis Power Supply	Peqlab
End-over-end tumbler	VWR
FlexStation 3 Multi-Mode Microplate Reader	Molecular Devices
Freezer, -80°C	Sanyo
Fresco 21 Centrifuge Heraeus	Thermo Scientific
Heratherm Incubator	Thermo Scientific

4 MATERIALS

High Speed InCyt Im2™ Dual-Wavelength Fluorescence Imaging System	Intracellular Imaging
Ice machine	Ziegra
iXon 897 EM-CCD camera	Andor Technology
Luna Automated Cell Counter	Logos Biosystems
Magnet stirrer and heating plate MR Hei-Standard	Heidolph
Micro Scale CPA 10035	Sartorius
Microscope Motic AE20 Series	Motic
Milli-Q Plus-System	Millipore
Mini PROTEAN Tetra System	Bio-Rad
Mini-Sub® Cell GT Horizontal Electrophoresis System	Bio-Rad
Monochromator FSM150Xe	Bentham Instruments
Monochromator Optoscan	Cairn Research
MSC-Advantage Laminar Flow Hood	Thermo Scientific
Multiclamp 700B amplifier	Axon Instruments
Multifuge 3 L-R Centrifuge Heraeus	Thermo Scientific
Multifuge X1 Centrifuge Heraeus	Thermo Scientific
Multifuge X1R Centrifuge Heraeus	Thermo Scientific
Multitron Standard	Infors HT
Nanodrop 2000c	Peqlab
Odyssey® Infrared Imaging System Sa	LI-COR Biosciences
Opera Phenix™	Perkin Elmer
Optima XPN90 ultracentrifuge	Beckman Coulter
Oxygraph-2k	Oroboros Instruments
P-97 Flaming/Brown micropipette puller	Sutter Instrument Company
pH-Meter Eductaion Line	Mettler Toledo
Pipettes	Eppendorf
PowerPac™ Basic Power Supply	Bio-Rad
Rocking Platform	VWR
Scale ALC-810.2	Acculab – Sartorius Group
SpectraMax® i3 Microplate Detection System	Molecular Devices
TCS SP5 confocal microscope	Leica Microsystems
Tecan Reader, Infinite M200 Pro	Tecan
Thermomixer F 1,5	Eppendorf
Trans-Blot Turbo Transfer System	Bio-Rad
Vacusaft Absaugsystem	Integra Biosciences
Vortex-Genie 2	Scientific Industries
Water bath Aqualine AL 12	LAUDA
XCell SureLock™ Electrophoresis Cell	Novex® Life Technologies

4 MATERIALS

4.24 SOFTWARES

Table 22: Softwares

Software	Supplier
Adobe Illustrator CS6	Adobe
Adobe Photoshop CS6	Adobe
Axoscope 9	Axon Instruments
BD FACSDiva™ Software	BD Biosciences
Cellomics® vHCS:View and Cellomics® Scan software	Thermo Fisher Scientific
Clampex 9	Axon Instruments
Clampfit 9	Axon Instruments
Columbus Software Version 2.7.1	Perkin Elmer
DatLab Software 5.2.1.51	Oroboros Instruments
FlowJo 8.7.3 and V10	Tree Star, Inc
Graph Pad Prism 6	Graph Pad
Ideas Version 6.2	Amnis
Image J (Fiji)	Wayne Rasband, NIH
Image Studio Lite Software Version 3.1 and 5.2	LI-COR Biosciences
InCyt_Im2™	Intracellular Imaging Inc.
Leica Application Suite Advanced Fluorescence (LAS AF) Lite	Leica Microsystems
Microsoft Excel 2010	Microsoft Corporation
Origin 8.6	OriginLab
Serial Cloner 2.5	Serial Basics
Snap Gene® Viewer 3.1.4	Snap Gene®
Winfluor V3.4.0	John Dempster, Strathclyde

5 METHODS

5.1 MOLECULAR BIOLOGY

5.1.1 Polymerase chain reaction

The polymerase chain reaction (PCR) is a procedure to amplify deoxyribonucleic acid (DNA). It requires a thermostable DNA polymerase and synthetically produced oligonucleotides (primers), which are complementary to the DNA sections to be amplified. DNA denaturation is followed by annealing, the binding of primers to the DNA to form the starting point of DNA polymerase elongation. Synthesis of the complementary DNA strand takes place in 5' to 3' direction. The three steps of denaturation, annealing, and elongation are repeatedly cycled, which allows a quick amplification of the target region (Mullis et al., 1986).

In this work, PCR was performed to generate a point mutation in a vector with the help of the Q5® Site-Directed Mutagenesis Kit from New England Biolabs. More precisely, the cysteine 674 (C674) in sarco/endoplasmic reticulum Ca²⁺-ATPase (SERCA) 2b was replaced by a serine (S) creating the SERCA2b C674S mutant in the vectors SERCA2b pDEST-N-GFP and SERCA2b PMT2. In both cases, the desired nucleotide change was included in the forward primer. For one reaction 25 ng DNA, 12.5 µl Q5 Hot Start High-Fidelity 2x Master Mix, 0.5 µM forward and 0.5 µM reverse primer were mixed and filled up to 25 µl with nuclease-free water. The reaction mix was placed in a thermal cycler and the DNA was amplified in a five-step program.

Table 23: Q5® Site-Directed Mutagenesis PCR

Procedure	Temperature	Duration
Initial Denaturation	98°C	30 sec
Denaturation	98°C	10 sec
Annealing	62°C or 70°C	20 sec
Elongation	72°C	4 min 30 sec or 4 min 20 sec
Terminal Elongation	72°C	2 min

} 25 x

5 METHODS

5.1.2 Agarose gel electrophoresis

Agarose gel electrophoresis is a technique used to separate DNA fragments according to their size. An electric current is applied to pull the negatively charged DNA fragments through the gel towards the positive electrode. Small fragments move faster than larger ones because they all have the same ratio of charge per mass. In addition, the migration rate of the nucleic acids depends on their conformation. The fluorescent dye Midori Green intercalates into the DNA and thus serves to visualize the DNA fragments under ultraviolet (UV) light. The light intensity is proportional to the amount of DNA present. The size of the resulting fragments can be identified by means of DNA ladders.

An 1% (w/v) agarose gel was prepared (0.5 g agarose, 50 ml 1x TAE buffer (40 mM Tris, 20 mM acetic acid and 1 mM ethylenediaminetetraacetic acid (EDTA), pH 8) and 1.5 µl Midori Green). DNA samples mixed with 10x Blue Juice Loading buffer were loaded onto the gel. The 1 kb Plus DNA ladder from Invitrogen was used as a DNA marker. The agarose gel electrophoresis was performed in a horizontal running chamber filled with 1x TAE buffer at 100 V for 30 min.

5.1.3 DNA gel extraction

To extract and purify DNA from agarose gels, DNA bands of defined size were excised under UV light before Introns' MEGAquick-spin™ Plus Total Fragment DNA Purification Kit was used according to manufacturers' instructions. The concentration of the extracted DNA was determined photometrically with the Nanodrop 2000c (Thermo Fisher Scientific).

5.1.4 Kinase-Ligase-DpnI reaction

The Q5® Site-Directed Mutagenesis Kit from New England Biolabs provides a Kinase-Ligase-DpnI Mix. After PCR the newly synthesized and purified DNA is phosphorylated by kinase at its 5' end. The ligase forms an ester bond between the 5' phosphate and the deoxyribose at the 3' end and is responsible for recirculation of the vector. The methylation-sensitive restriction enzyme DpnI degrades the template DNA because it only cleaves methylated restriction sites. For one reaction 1 µl gel extracted and purified PCR product, 1 µl 10x KLD Enzyme Mix and 5 µl 2x KLD Reaction Buffer were mixed and filled up to 10 µl with nuclease-free water. The reaction mix was incubated for 5 min at room temperature before a heat shock transformation into bacteria was performed.

5 METHODS

5.1.5 Preparation of chemically competent DH5 α bacteria

The bacterium *Escherichia coli* (*E.coli*) serves as a host organism for the uptake and multiplication of foreign DNA. Already competent DH5 α -*E.coli* cells were grown overnight in 3 ml lysogeny broth (LB) medium at 37°C and 220 rpm on a shaker. The next day, 200 ml LB medium was inoculated with 1 ml bacterial suspension and further incubated at 37°C and 220 rpm. After reaching the desired amount of bacterial growth with an optical density (OD) of 0.5, the suspension was centrifuged (5000 rpm, 4°C) for 15 min. The supernatant was discarded and the bacterial pellet was resuspended in 10 ml ice-cold magnesium chloride (100 mM). Incubation on ice for 15 min followed another centrifugation step (5000 rpm, 4°C) before the pellet was resuspended in 10 ml ice-cold calcium chloride (100 mM, with 15% (v/v) glycerol). After further 15 min on ice, the competent DH5 α -*E.coli* cells were aliquoted at 100 μ l, snap-frozen in liquid nitrogen and stored at -80°C.

5.1.6 Heat shock transformation

During heat shock treatment, chemically competent DH5 α -*E.coli* host cells are capable of accepting foreign DNA (Mandel and Higa, 1970; Cohen et al., 1972). 100 μ l of DH5 α -*E.coli* cells were thawed on ice and mixed with 1-5 μ l DNA (1-100 ng). After 30 min incubation on ice, the heat shock was performed at 42°C for 1 min and the bacteria were immediately cooled down on ice for 2 min. Subsequently, 250 μ l salt-optimized broth medium was added and incubation for 1 h at 37°C and 300 rpm on a shaker followed. Thereafter, the entire bacterial suspension was plated onto a 10 cm LB agar plate containing 50 μ g / ml ampicillin. Then the plate was incubated overnight at 37°C.

5.1.7 Overnight cultures and glycerol stock preparation

The day after the heat shock transformation, a bacteria colony was picked from the agar plate and proliferated in 3 ml or 200 ml LB medium containing 50 μ g / ml ampicillin. After overnight incubation at 37°C and 220 rpm on a shaker, the DNA was isolated as described in 5.1.8. For long-time storage of bacteria 800 μ l bacterial suspension and 200 μ l 80% (v/v) glycerol were mixed and frozen at -80°C.

5 METHODS

5.1.8 Plasmid DNA isolation

Plasmid DNA isolation of small DNA amounts was performed with Zymo Research's Zyppy™ Plasmid Miniprep Kit. To obtain large amounts of plasmid DNA, the Machery-Nagel Nucleobond®XTRA Plasmid Purification System Kit was used. Manufacturers' instructions were followed in both kits. The concentration of the extracted DNA was determined photometrically using Nanodrop 2000c (Thermo Fisher Scientific).

5.1.9 Restriction enzyme digest

To test the success of the Q5® Site-Directed Mutagenesis PCR, a restriction enzyme digest was performed. Restriction enzymes can specifically recognize and cut double-stranded DNA sequences. For one reaction 5 µl DNA obtained from Zymo Research's Zyppy™ Plasmid Miniprep Kit, 1 µl 10x FastDigest Buffer, 0.5 µl FastDigest EcoRI and 0.5 µl FastDigest NdeI were mixed and filled up to 10 µl with nuclease-free water. The reaction mix was incubated for 15 min at 37°C before 10x Blue Juice Loading buffer was added. Then the mixture was loaded onto a 1% agarose gel.

5.1.10 Plasmid DNA sequencing

To verify the correct sequence of the samples, plasmid DNA was sequenced by GATC Biotech AG. The chain termination method according to Sanger was used. Sequencing was performed with primers described in 4.17. Samples were diluted to contain between 30 and 100 ng / µl of DNA in a total of 30 µl.

5.1.11 RNA isolation

Ribonucleic acid (RNA) isolation was performed with Zymo Research's ZR RNA MiniPrep™ Kit according to manufacturers' instructions. The concentration of the extracted RNA was determined photometrically using Nanodrop 2000c (Thermo Fisher Scientific). RNA was stored at -80°C or directly converted to single-stranded complementary DNA (cDNA).

5.1.12 Reverse transcription

Reverse transcription allows the rewriting of RNA into DNA using the enzyme reverse transcriptase (RT), originally derived from viruses. In this work, the conversion of messenger RNA (mRNA) to single-stranded cDNA was performed with the High Capacity cDNA Reverse

5 METHODS

Transcription Kit from Applied Biosystems. The reaction mix contained 2 μl 10x RT Buffer, 0.8 μl dNTP Mix (100 mM), 2 μl 10x RT Random Primers, 1 μl MultiScribe[®] Reverse Transcriptase (50 U/ μl) and 2.4 μl nuclease-free water before 10 μl RNA sample was added. A total volume of 20 μl was incubated in a thermal cycler for 10 min at 25°C, followed by an incubation step for 2 h at 37°C. The reaction was stopped for 5 min at 85°C.

5.1.13 Quantitative real-time polymerase chain reaction

For quantitative real-time PCR (qPCR), the TaqMan method from Roche was used. It is based on TaqMan probes that are complementary to the target sequence and anneal during qPCR. They consist of a fluorophore, covalently attached to its 5'-end, and a quencher at its 3'-end. The quencher molecule quenches fluorescence emitted by the fluorophore when excited, as long as both are in proximity. 5' to 3' exonuclease activity of the Taq polymerase degrades the probe during extension. This degradation releases the fluorophore from the quencher. Hence, fluorescence intensity detected in the qPCR is directly proportional to the fluorophore released and the amount of cDNA template present.

A mixture of 0.2 μl probe (2.5 μM), 0.4 μl primer mix (consisting of 320 μl nuclease-free water and 40 μl of each primer), 10.5 μl Takyon No ROX Probe Mastermix blue dTTP, 2 μl cDNA, and 7.4 μl nuclease-free water was pipetted in triplicates to a 96-well qPCR plate. Plates were sealed with a sticky foil and centrifuged. The qPCR reaction was carried out on a Biorad CFX Connect[™] Real-Time PCR Detection System (95°C for 1 min and 40 cycles of 95°C for 15 sec and 60°C for 1 min). Relative gene expressions were calculated by normalizing to the housekeeping gene hypoxanthine phosphoribosyltransferase (HPRT). The HPRT mixture contained 7.5 μl primer-probe mix (consisting of 1166 μl nuclease-free water, 12 μl of each primer and 10 μl probe), 10.5 μl Takyon No ROX Probe Mastermix blue dTTP and 2 μl cDNA. Data were analyzed with the $\Delta\Delta\text{Ct}$ method.

5.2 CELL CULTURE – IMMORTALIZED CELL LINES

5.2.1 Culturing and passaging

Mouse embryonic fibroblast (MEF) cells and Chinese hamster ovary (CHO) cells were cultured in 10 cm cell culture dishes in a humidified incubator at 37°C and 5% CO₂. CV-1 in Origin Simian-1 (COS1) cells were cultured in 15 cm cell culture dishes in a humidified incubator at 37°C and 10% CO₂. All cell lines were grown in their individual growth media (see chapter 4.4). Cell lines were sub-cultured at a confluence of 80-90% twice a week in a 1:10 to 1:40 ratio under a laminar flow hood. Cells were first washed with phosphate buffered saline (PBS) and then trypsinized with 0.05% Trypsin-EDTA. The reaction was stopped with fresh growth medium. Cells were resuspended and passaged into new cell culture dishes with fresh growth medium.

5.2.2 Living cell count

To determine the cell number of living cells, cells were diluted 1:2 with trypan blue. Trypan blue is a diazo dye that stains dead cells blue whereas living cells remain bright. 10 µl of the mixture was pipetted into the cell counting chamber and counted in the Luna Automated Cell Counter (Logos Biosystems). The device automatically displayed the cell count of living cells.

5.2.3 Cryopreservation

For cryopreservation, cells with a confluence of 80-90% were detached with trypsin, harvested from the cell culture dish and collected by centrifugation (1300 rpm, 3 min). The cell pellet was resuspended in freezing medium (90% (v/v) fetal bovine/calf serum (FCS) and 10% (v/v) dimethyl sulfoxide (DMSO)) and directly pipetted as 1 ml aliquots into cryotubes. They were immediately put in a CoolCell® cell freezing container and frozen at a cooling rate of 1°C per min at -80°C. For long-term storage, the cryotubes were stored in liquid nitrogen.

5.2.4 Thawing of cells

To thaw frozen cells, the cryotube was placed into a 37°C water bath until the cell suspension was liquid. Due to the toxic effect of DMSO in the freezing medium, cells were quickly transferred into a 10 cm cell culture dish with 20 ml of prewarmed growth medium and incubated. The growth medium was changed after 24 h to remove dead cells.

5 METHODS

5.2.5 Transient transfection

For cell transfection, three different transfection reagents were used according to manufacturer's instructions: Attractene Transfection Reagent, GeneJuice® Transfection Reagent, and TurboFectin™ 8.0 Transfection Reagent. Attractene Transfection Reagent was used to transfect CHO cells in a 10 cm cell culture dish. In brief, 1×10^6 cells were seeded and left to adhere overnight. The next day, 4 µg plasmid DNA and 15 µl Attractene Transfection Reagent were mixed in 300 µl plain OptiMEM medium. This transfection mix was vortexed and incubated for 15 min at room temperature to let the positively charged lipid and the negatively charged DNA form a complex (Felgner et al., 1987). Meanwhile, the growth medium was replaced with fresh, prewarmed medium. The transfection mix was added dropwise to the plate. The plate was carefully shaken to provide distribution of the transfection mix and fusion of the DNA lipid complex with the cell membranes of all cells in the plate (Felgner et al., 1987). Then cells were incubated under normal growth conditions. The procedure for the other transfection reagents was similar. GeneJuice® Transfection Reagent was used to transfect COS1 cells in a 15 cm cell culture dish. 4.1×10^6 cells were seeded the day before transfection and 20 µg plasmid DNA and 60 µl GeneJuice® Transfection Reagent were mixed in 2 ml plain DMEM High Glucose medium. TurboFectin™ 8.0 Transfection Reagent was used to transfect MEF cells in a 96-well plate. 2000 cells were seeded the day before transfection and the transfection mixture contained 0.3 µg plasmid DNA and 0.9 µl TurboFectin™ 8.0 Transfection Reagent in 9 µl plain OptiMEM medium.

5.2.6 DMF treatment

For dose response test, 2, 4, 6, 8 or 10 µM DMF (dissolved in deionized water) was added to the growth medium of MEF cells for 24 h. For further experiments in all cell lines 10 µM DMF was used for 1 min, 1 h or 24 h. Deionized water was used as vehicle (Veh) control.

5.3 CELL CULTURE – SPLENOCYTES

5.3.1 Cell isolation

For isolation of splenocytes, mice were sacrificed by cervical dislocation. The fur was disinfected with 70% ethanol. The spleen was removed and transferred to a 1.5 ml tube on ice containing 1 ml splenocytes isolation medium. The next steps were performed under a laminar flow hood. The spleen was meshed through a cell strainer into a 50 ml tube with the riffled end of a syringe to generate a single cell suspension. Cell strainer and syringe were rinsed with 25 ml splenocytes isolation medium. The single cell suspension was centrifuged at 600x g for 5 min at 4°C or at 300x g for 10 min at 4°C. The supernatant was discarded, the pellet resuspended in 2 ml BD Pharm Lyse™ Lysing Buffer and vortexed. After 15 min incubation at room temperature, 23 ml splenocytes isolation medium was added to stop the erythrocyte lysis reaction. The suspension was centrifuged again (600x g, 5 min, 4°C or 300x g, 10 min, 4°C) and the splenocytes were resuspended in splenocytes isolation medium for counting.

5.3.2 Living cell count

To determine the cell number of living cells, cells were diluted 1:2 with trypan blue. Trypan blue is a diazo dye that stains dead cells blue whereas living cells remain bright. 10 µl of the mixture were pipetted into the Neubauer counting chamber and the four corner squares were counted manually under the microscope. In the end, the cell number was determined using this formula:

Concentration (cells/ml)=(Number of counted cells x 10 000)/(Number of squares) x Dilutions

5.3.3 Culturing of splenocytes and activation of T cells

Splenocytes were grown in 24-well plates in splenocytes growth medium in a humidified incubator at 37°C and 5% CO₂.

T cell activation can be mediated by the incubation of cells with anti-CD3 and anti-CD28 or with ionomycin (Iono) in combination with phorbol 12-myristate 13-acetate (PMA). To activate T cells, 5x 10⁶ splenocytes were plated in 24-well plates, coated with 4 µg/ml anti-CD3 and 4 µg/ml anti-CD28 in 500 µl coating buffer (0.1 M Na₂HPO₄, pH 9.2) for 30 min at 37°C. Plates were washed three times with PBS before cells were added in growth medium. After 72 h of stimulation, growth medium was changed and cells were transferred into a new 24-well plate.

5 METHODS

After another 24 h, cells were restimulated with 4 µg/ml anti-CD3 and 4 µg/ml anti-CD28 or with 1 µg/ml Iono in combination with 5 ng/ml PMA for 4 h.

5.3.4 DMF treatment in vivo and ex vivo

For ex vivo experiments, 10 µM DMF (dissolved in deionized water) was added into the growth medium of splenocytes for 1 h or 24 h. Deionized water was used as Veh control. For in vivo experiments, female, 6-8 weeks old SJL mice received DMF administration (0.5 mg/ml DMF in the drinking water = 75 mg DMF/kg mouse/day) freshly prepared every day for 8, 10, 17, 23 or 29 days. In the case of immunized mice, DMF administration started 9 or 15 days before EAE induction.

5.4 CELL CULTURE – PRIMARY MEF CELLS

5.4.1 MEF cell isolation

MEF cells were isolated from 14 days old C57BL/6 embryos under a semi-sterile bench. Placenta, head, arms, legs and all internal organs were removed and discarded. The remaining embryonic tissue was washed a few times in a 10 cm cell culture dish with PBS on ice. The next steps were performed under a laminar flow hood. The embryonic tissue was transferred to a new 10 cm cell culture dish, manually chopped with a scalpel and incubated in 3 ml 0.25% trypsin for 15–30 min at 37°C to generate a single cell suspension. The reaction was stopped by adding MEF cell growth medium and the cell suspension was put through a cell strainer. Cells from each embryo were plated onto a 10 cm cell culture dish in MEF cell growth medium and incubated at 37°C and 5% CO₂. After reaching confluence after 2-4 days of incubation, primary MEF cells were harvested and stored in liquid nitrogen for further use. All experiments were done on passage two or three MEF cells.

5.5 PROTEIN BIOCHEMISTRY

5.5.1 Protein isolation

For protein isolation, cells were harvested and collected by centrifugation (1300 rpm, 3 min for cell lines or 600x g, 5 min or 300x g, 10 min for splenocytes). After washing with PBS, 90-300 µl cold radioimmunoprecipitation assay buffer (RIPA buffer), supplemented with protease inhibitors and phosphatase inhibitors, was added to lyse the cells. The suspension was

5 METHODS

centrifuged at 21 000x g for 30 min at 4°C. The protein containing supernatant was transferred into a new 1.5 ml tube and used immediately for immunoblotting experiments or stored at -80°C.

5.5.2 BCA protein assay

To determine the protein concentration of cell lysates, the bicinchoninic acid (BCA) protein assay was performed using Interchim's BC Assay Protein Quantification Kit according to manufacturers' instructions. In this assay, the Cu^{2+} ions in the solution react with proteins of the sample and are reduced to Cu^+ ions. BCA then forms a purple-blue complex with Cu^+ , which can be detected photometrically (Smith et al., 1985).

In order to determine the protein concentration, a bovine serum albumin (BSA) standard series with known concentrations (0, 6.25, 12.5, 25, 50, 100 and 200 $\mu\text{g}/\text{ml}$) was added as a technical triplicate to a 96-well plate. Cell lysates were diluted 1:10 to 1:50 and pipetted as triplets. 200 μl BCA reagent mixture (reagent A and B 1:50) was added to each well and incubated for 30 min at 37°C. The photometrical analysis at a wavelength (λ) of 562 nm was performed in the Infinite M200 PRO microplate reader (Tecan) before the protein concentrations were calculated with Microsoft Excel.

5.5.3 Bradford protein assay

Unlike the BCA assay, reducing agents at low concentrations do not interfere with this method to determine the protein concentration of cell lysates. The principle of the Bradford assay relies on the binding of proteins to Coomassie Brilliant Blue G-250 under acidic conditions. This reaction directly results in a color change from brown to blue, which can be detected photometrically (Bradford, 1976).

The Bradford assay was performed using Expedeon's Bradford Ultra™ reagent according to manufacturers' instructions. In order to determine the protein concentration, 100 μl of a BSA standard series with known concentrations (0, 2.5, 5, 7.5, 10, 15 and 20 $\mu\text{g}/\text{ml}$) was added as a technical triplicate to a 96-well plate. Cell lysates were diluted 1:1000 and pipetted as triplets (each 100 μl). 100 μl of the Bradford Ultra™ reagent was added to every well and the absorption at 595 nm was measured in the Infinite M200 PRO microplate reader (Tecan) before the protein concentrations were calculated with Microsoft Excel.

5 METHODS

5.5.4 Nuclear and cytosolic fractionation

In order to see expression differences of proteins in the cytoplasm or nucleus, the nuclear and cytosolic fractionation of protein samples was performed. This method is especially applicable for proteins like nuclear factor kappa-light-chain-enhancer of activated B cells (NFκB) and nuclear factor of activated T cells (NFAT), which are translocating to the nucleus after a particular impulse. 40×10^6 splenocytes were harvested and centrifuged at 4000 rpm for 5 min at 4°C. Cells were resuspended in swelling buffer (10 mM HEPES, 10 mM KCl, 0.1 mM EDTA, add 1 mM dithiothreitol (DTT) and protease inhibitors freshly) (100 μl per 10×10^6 cells) and incubated for 15 min on ice. After adding 1 % Nonidet P-40 (NP-40), the suspension was vortexed for 15 sec and incubated for 3 min at room temperature. Another vortexing for 15 sec followed. NP-40 solubilizes membrane proteins in native conformation. The mixture was centrifuged again (5 min, 4000 rpm, 4°C) and the supernatant (= cytosolic fraction) was transferred into a new 1.5 ml tube. The pellet was washed three times with 1 ml swelling buffer before being resuspended in RIPA-buffer, supplemented with protease inhibitors (50 μl per 10×10^6 cells). After 30 min incubation on ice and vortexing, the sample was centrifuged at 13 000 rpm for 10 min at 4°C. The supernatant (= nuclear fraction) was transferred into a new 1.5 ml tube. Nuclear and cytosolic fraction samples were immediately used for immunoblotting experiments or stored at -80°C.

5.5.5 SDS-PAGE

Sodium dodecyl sulfate polyacrylamide gel electrophoresis (SDS-PAGE) is used to separate proteins according to their molecular weight and was first described in 1970 by Laemmli (Laemmli, 1970). The negatively charged sodium dodecyl sulfate (SDS) covers the intrinsic charge of proteins and allows a charge independently separation. Denaturation of the proteins is carried out by heating the samples to 95°C for 5 min. To break the disulfide bridges, DTT was added to the sample buffer.

In brief, 35-85 μg total cellular protein samples, mixed with 5x SDS sample loading buffer (50% (v/v) glycerol, 10% (w/v) SDS, 77 mg/ml DTT, 25% (v/v) 1 M Tris, pH 6.8 and 2 mg/ml bromphenol blue) and nuclease-free water, were denaturated (5 min, 95°C) and separated on 4-15% or 4-20% Mini-PROTEAN® TGX Stain-Free™ gels (Bio-Rad) in a vertical gel electrophoresis chamber filled with 1x SDS buffer. The power supply was adjusted to 300 V for

5 METHODS

14-17 min or to 100-120 V for 50-60 min. As a protein standard ladder, 5 μ l of MagicMark XP Western Protein Standard or Chameleon Duo Pre-stained Protein Ladder was pipetted along with the samples on the gel. Non-reducing gels were performed with the same buffer as used for reducing gels, but lacking the reducing agent DTT.

5.5.6 Coomassie staining

Coomassie Brilliant Blue G-250 is a protein binding dye which can be used to stain proteins in polyacrylamide gels (Diezel et al., 1972). The gels were fixed in fixing solution (50% (v/v) ethanol, 10% (v/v) acetic acid) for at least 1 h and then stained in Coomassie solution (10% (v/v) acetic acid, 0.025% (w/v) Coomassie Brilliant Blue G-250). The gels were destained with warm water until the protein bands were well visible.

5.5.7 Immunoblotting

After SDS-PAGE, proteins in the gel can be transferred onto nitrocellulose or polyvinylidene difluoride (PVDF) membranes using the Trans-Blot® Turbo™ Transfer System (Bio-Rad). Through hydrophobic interactions, proteins adhere to the membranes during the application of an electrical field. Ponceau S solution was poured onto the membranes to quickly proof the protein transfer and had to be removed by washing with TBS-T or PBS-T. To avoid unspecific antibody binding, membranes were blocked either with 3% (w/v) milk powder in TBS-T or PBS-T or with 5% (w/v) BSA in TBS-T or PBS-T for 1 h at room temperature. Primary antibodies were incubated overnight at 4°C on a shaker. The following day, three washing steps with TBS-T or PBS-T followed to remove unbound and unspecifically bound antibodies. For visualization, membranes were incubated for another hour at room temperature in the dark with fluorescence-conjugated secondary antibodies which specifically bind to the species-specific Fc tail of the primary antibodies. After three washing steps with TBS-T or PBS-T, the membranes were detected with the Odyssey® Infrared Imaging System (LI-COR Biosciences) and analyzed with the Image Studio Lite Software (LI-COR Biosciences).

5 METHODS

Table 24: Antibodies used for immunoblots

Primary antibodies	Sekundary antibodies
Anti-STIM1 1:500-1:1000 Anti-Actin 1:4000 Anti-GAPDH 1:4000 in 3% (w/v) milk powder in TBS-T or PBS-T	
Anti-BiP 1:1000 Anti-I κ B α 1:1000 Anti-phospho-I κ B α 1:1000 in 5% (w/v) BSA in TBS-T	
Anti-DNP 1:150 in 1% (w/v) BSA in PBS-T	Anti-mouse IgG (H+L) (DyLight 800 Conjugate) Anti-rabbit IgG (H+L) (DyLight 800 Conjugate)
Anti-NFATc1 1:500 Anti-NFATc2 1:500 in TBS-T	Anti-mouse IgG (H+L) (DyLight 680 Conjugate) Anti-rabbit IgG (H+L) (DyLight 680 Conjugate)
Anti-GSR 1:500 in 3% (w/v) milk powder in PBS-T	Depending on primary antibodies 1:7500 or 1:15 000 in 3% (w/v) milk powder in TBS-T or PBS-T or 5% (w/v) BSA in TBS-T or PBS-T
Anti-Calnexin 1:000 Anti-c-Rel 1:1000 Anti-GFP 1:1000 Anti- $\alpha\beta$ -Tubulin 1:1000 Anti-SERCA2b 1:10 000 Anti-RelB 1:1000 Anti-HDAC1 1:1000 in 3% (w/v) milk powder in TBS-T	

5.5.8 Antibody stripping

Primary and secondary antibodies used for immunoblotting can be removed from the membrane with a stripping buffer (6 M guanidine hydrochloride, 0.2% (v/v) NP-40, 20 mM Tris-HCl, pH 7.5 and 0.1 M 2-mercaptoethanol) (Yeung and Stanley, 2009). The membrane was treated with stripping buffer two times for 5 min before being washed five times with PBS-T or TBS-T for 10 min. The membrane was blocked and treated with new primary and secondary antibodies as described above.

5.5.9 Blue Native PAGE

Blue Native PAGE, initially introduced by Schagger and Jagow (Schagger and Jagow, 1991), was performed to detect native protein complexes without any reducing or denaturing

5 METHODS

components. The electrophoretic mobility of the proteins is achieved by binding to the negatively charged dye Coomassie Brilliant Blue G-250.

2-18 µg total cellular protein samples mixed with 4x NativePAGE® Sample buffer, 0.5 µl NativePAGE® 5% Coomassie Brilliant Blue G-250 and nuclease-free water were separated on NativePAGE™ 4-16% Bis-Tris Protein gels (Thermo Fisher Scientific) in a vertical gel electrophoresis chamber. The outer chamber was filled with anode buffer (40 ml NativePAGE™ running buffer (20x) and 760 ml deionized water), the inner chamber with cathode buffer (200 ml anode buffer supplemented with 1 ml NativePAGE™ cathode buffer). After loading the samples, the Blue Native PAGE was run on ice at 150 V for 1 h, followed by 250 V for 30 minutes. The gel was blotted and the membrane decolorized by washing 1-2 times with 100% (v/v) methanol to avoid the blocking of protein binding sites by the Coomassie Brilliant Blue G-250. Afterwards, the membrane was washed several times with PBS-T to remove the methanol. The membrane was blocked and stained with primary and secondary antibodies.

5.5.10 GFP-Trap

Using Chromotek's green-fluorescent protein (GFP)-Trap® kit with magnetic beads coupled to a GFP-binding protein and a magnetic rack, GFP fusion proteins and their interacting factors can be isolated by immunoprecipitation. The experiment was performed according to manufacturer's instructions. Confluent cells, transfected with SERCA2b WT or C674S pDEST-N-GFP, were harvested, washed with PBS and resuspended in 200 µl ice-cold lysis buffer (supplemented with protease inhibitors and 1 mM phenylmethylsulphonyl fluoride (PMSF)). A 30 min incubation on ice with extensively pipetting every 10 min followed centrifugation at 20 000x g for 10 min at 4°C. The supernatant was mixed with 300 µl dilution buffer (supplemented with protease inhibitors and 1 mM PMSF) before 25-50 µl GFP-Trap®_MA beads were added. After 1 h incubation at 4°C on an end-over-end tumbler, the beads were washed three times with dilution buffer. To elute the immune complexes from the beads, either 0.2 M glycine, pH 2.5 was added and constantly mixed for 30 sec followed by magnetic separation and adding 1 M Tris base, pH 10.4 or 5x SDS sample loading buffer (50% (v/v) glycerol, 10% (w/v) SDS, 77 mg/ml DTT, 25% (v/v) 1 M Tris, pH 6.8 and 2 mg/ml bromphenol blue) was added, the solution boiled for 10 min at 95°C and then magnetically separated.

5 METHODS

5.5.11 BIOGEE assay

To study the glutathionylation status of SERCA2b C674 after DMF treatment, the BIOGEE assay was performed. The strong affinity of streptavidin to biotin was used to isolate glutathionylated proteins. After 24 h incubation with 10 μ M DMF, CHO cells transfected with SERCA2b WT or C674S pDEST-N-GFP were treated with 250 μ M biotinylated glutathione ethyl ester (BIOGEE) for 1 h at 37°C. Cells were harvested and proteins were isolated according to 5.5.1. A 45 min incubation of the whole protein lysate with 25 μ l magnetic streptavidin beads (Dynabeads® M-280) on an end-over-end tumbler was followed by three times washing with self-made 0.5% SDS-RIPA-buffer (25 mM Tris-HCl, pH 7.6, 150 mM NaCl, 1% (v/v) NP-40, 1% (w/v) sodium deoxycholate, 0.5% (w/v) SDS and protease inhibitors). Glutathionylated proteins were eluted by adding 10 μ l 5 x sample loading buffer and 40 μ l deionized water, heating the samples for 5 min to 95°C and magnetic separation.

5.5.12 Total cellular glutathione assay

Total cellular glutathione content was analyzed using an enzymatic assay. 5×10^6 splenocytes were washed with ice-cold PBS and harvested in 200 μ l PBS with 2 mM EDTA before adding 100 μ l of 10% (w/v) sulfosalicylic acid to precipitate proteins. Samples were incubated on ice for 10 min and centrifuged (10 min, 14 000x g, 4°C). 280 μ l of the supernatants were neutralized by transferring into 24 μ l 50% (v/v) triethanolamine in deionized water and vortexing. In order to normalize the total cellular glutathione content in the end, pellets were solubilized in 100 μ l 0.2 N NaOH overnight at 37°C and protein concentration was quantified using the BC Assay Protein Quantification Kit (Interchim). Total cellular glutathione was detected in triplicates by diluting samples in glutathione assay buffer (100 mM Na_2HPO_4 , 1 mM EDTA, pH 7.5) supplemented with 0.8 mM reduced nicotinamide adenine dinucleotide phosphate (NADPH), 0.6 mM 5,5'-dithiobis-(2-nitrobenzoic acid) (DTNB) and 1 U/ml glutathione reductase (GSR). DTNB oxidizes GSH to GSSG and forms the yellow 5'-thio-2-nitrobenzoic acid (TNB). GSSG can be recycled to GSH by GSR under NADPH consumption (Rahman et al., 2006). In sum, TNB is produced using NADPH at a rate proportional to the amount of glutathione. The formation of TNB in the samples was measured kinetically in parallel to the formation of TNB in a standard with known glutathione concentration (0, 0.3125, 0.625, 1.25, 2.5, 5, 10 and 20 μ M) at 412 nm for 20 min using the Infinite M200 PRO

5 METHODS

microplate reader (Tecan). By means of the glutathione standard concentrations and the corresponding amount of protein in the samples, the respective glutathione concentration was finally calculated with Microsoft Excel.

5.5.13 OxyBlot

Proteins modified by oxygen free radicals or other reactive species can be detected in immunoblots with the OxyBlot™ Protein Oxidation Detection Kit (Merck) because carbonyl groups are introduced into these proteins. By adding 2,4-dinitrophenylhydrazine (DNPH) to the protein sample, the carbonyl groups are derivatized to 2,4-dinitrophenyl (DNP) hydrazone and can be detected in immunoblotting with an anti-DNP antibody. Cells, transfected with SERCA2b WT or C674S pDEST-N-GFP, were harvested and lysed with 200 µl RIPA buffer, supplemented with 50 mM DTT. DTT prevents further oxidation of proteins after cell lysis. Lysed cells were centrifuged at 14 000x g for 15 min at 4°C. The supernatant was transferred in a new 1.5 ml tube and protein concentration was determined using Bradford protein assay. Then 5 µl protein, 5 µl 12% (w/v) SDS and 10 µl DNPH solution for samples and 5 µl protein, 5 µl 12% (w/v) SDS and 10 µl derivatization control solution for controls were mixed and incubated for 15 min at room temperature. Afterwards, 7.5 µl neutralization solution was added to the mixture and the samples were directly run on an SDS-PAGE.

5.5.14 Glutathione fusion assay

To investigate redox-induced protein oligomerization in splenocytes, the glutathione fusion assay was performed. Cell lysates were prepared for the treatment with reduced glutathione (GSH) or oxidized glutathione disulfide (GSSG). For one experiment 2.5 µl 10x ATP/succinate mix (10 mM ATP (K⁺), 50 mM sodium succinate, 0.8 mM adenosine diphosphate (ADP) and 20 mM K₂HPO₄, pH 7.4 with KOH), 1 mM guanosine triphosphate (GTP), 1.25 µl 20x fusion buffer (700 mM sucrose, 0.8 M KCl, 5 mM ethylene glycol-bis(2-aminoethyl ether)-N,N,N',N'-tetraacetic acid (EGTA), 20 mM MgAc₂ and 200 mM HEPES, pH 7.4) and 5 mM GSH or GSSG were mixed and filled up to 12.5 µl with nuclease-free water. 12.5 µl cell lysate was added to the reaction mix and incubated for 1 h at 37°C. To stop the reaction Coomassie Brilliant Blue G-250 or 5x SDS sample loading buffer (50% (v/v) glycerol, 10% (w/v) SDS, 77 mg/ml DTT, 25%

5 METHODS

(v/v) 1 M Tris, pH 6.8 and 2 mg/ml bromphenol blue) with or without DTT was pipetted to the glutathione fusion assay and a Blue Native PAGE or SDS-PAGE was run.

5.5.15 Dual-Glo® Luciferase assay

In the Dual-Glo® Luciferase assay, a luminescent signal from two reporter genes was detected. The activity of the firefly luciferase reporter is linked to a specific stimulus (NFAT translocation and IL-2 promotor induction) and can be normalized to the activity of the co-transfected renilla luciferase control reporter. Therefore 2500 MEF cells were plated in a white 96-well plate. The next day, cells were co-transfected with NFAT firefly luciferase construct under the expression control of the IL-2 promotor and renilla luciferase construct under the control of the CAG promotor. After 48 h, the Dual-Glo® Luciferase assay from Promega was performed according to manufacturer's instructions. In brief, growth medium was changed to one without phenol red and Dual-Glo® Reagent equal to the volume of growth medium (75 µl) was added to each well, mixed and incubated for 20 min at room temperature. The firefly luminescence was detected with the microplate detection system SpectraMax® i3 (Molecular Devices). Next, 75 µl Dual-Glo® Stop & Glo® Reagent was added to each well, mixed and incubated for another 20 min before the renilla luminescence was measured. As a control, a well with untransfected cells was measured as well. Quantification of NFAT activity after 10 µM DMF treatment for 24 h and 1 h was calculated with Microsoft Excel.

5.5.16 Immunocytochemistry

Immunocytochemistry (ICC) was performed to visualize the localization of proteins inside cells. Here it was used to specifically study nuclear translocation of the two transcription factors NFκB and NFATc1. Hence, 1×10^6 splenocytes or 20 000 MEF cells were seeded on coverslips (Ø 12 mm) in 24-well plates. Coverslips were sterilized with 100% ethanol and the ones used for splenocytes were additionally coated with 100 µl 5 mg/ml BSA for 1 h at 37°C and 0.01% poly-L-lysine for 2-24 h at 37°C. Cells were treated with 10 ng TNF-α for 10 min (NFκB samples) or 1 µg/ml Iono/ 5 ng/ml PMA for 4 h (NFATc1 samples). Cells were washed with PBS for 5 min and fixed with 4% (v/v) Roti®-Histofix for 15-20 min. Subsequently, cells were permeabilized with 0.3% (v/v) Triton X-100 in PBS for 10 min or with 100% methanol for 2 min. A 1 h incubation with 1x Roti®-ImmunoBlock in PBS or normal goat serum (NGS) blocking solution

5 METHODS

(1% (w/v) BSA in PBS with 0.3% (v/v) Triton X-100 and 10% (v/v) NGS) followed to block unspecific binding of antibodies. Primary antibodies were added overnight at 4°C. Next, cells were incubated with fluorophore-conjugated secondary antibodies for another hour in the dark, followed by cell nuclei staining with 300 nM DAPI for 5 min. Coverslips were mounted with Dako Fluorescent Mounting Medium onto microscope slides. Between each incubation step, the cells were washed three times with PBS for 5 min. If not indicated differently, all steps were performed on a shaker at room temperature.

Table 25: Antibodies used in ICC

Primary antibodies	Sekundary antibodies
Anti-NFATc1 1:100 and Anti- $\alpha\beta$ -Tubulin 1:1000 in 1x Roti [®] -ImmunoBlock in PBS containing 0.1% (v/v) Triton X-100	Anti-mouse Alexa Fluor [®] 488 1:500 and Anti-rabbit Alexa Fluor [®] 568 1:500 in 1x Roti [®] -ImmunoBlock in PBS containing 0.1% (v/v) Triton X-100
Anti-NF- κ B p65 1:400 and Anti-Actin 1:4000 in 1x Roti [®] -ImmunoBlock in PBS containing 0.1% (v/v) Triton X-100	Anti-rabbit Alexa Fluor [®] 488 1:500 and Anti-mouse Alexa Fluor [®] 568 1:500 in 1x Roti [®] -ImmunoBlock in PBS containing 0.1% (v/v) Triton X-100
Anti-NF- κ B p65 1:400 in 1% (w/v) BSA in PBS containing 0.3% (v/v) Triton X-100 and 10% (v/v) NGS	Anti-rabbit Alexa Fluor [®] 568 1:500 in 1% (w/v) BSA in PBS containing 0.3% (v/v) Triton X-100 and 10% (v/v) NGS

5.5.17 Microsomal preparation

For Microsomal preparation, confluent, SERCA2b WT and C674S PMT2 transfected COS1 cells were harvested in PBS with 5 mM NaEDTA, pH7.5, washed with PBS and kept on ice in 2 ml hypotonic buffer (0.5 mM MgCl₂·6H₂O, 10 mM Tris-HCl, pH 7.5 and protease inhibitors) for 10 min. Cells were homogenized by 40 strokes in a glass Dounce homogenizer, followed by addition of 2 ml of the 1 M solution (0.5 M sucrose, 40 μ M CaCl₂, 0.23 mM PMSF, 1 mM DTT, 10 mM Tris-HCl, pH 7.3 and protease inhibitors) and further 20 strokes. Lysates were centrifuged at 10 414x g for 20 min at 4°C and the resulting supernatant fraction was centrifuged in an Optima XPN90 ultracentrifuge (Beckman Coulter) at 200 000x g for 35 min at 4°C. The resulting microsomal pellet was resuspended in 0.25 M sucrose.

5 METHODS

5.5.18 ATPase activity assay

Microsomal fractions were quantified using the Qubit™ Protein Assay Kit (Thermo Fisher Scientific) and 2.5-10 µg of microsomal proteins supplemented with 4 µM ionophore A23187 were taken for ATPase activity assay. The calcium (Ca²⁺)-dependent ATP hydrolysis activity of SERCA2b was measured by monitoring the release of free inorganic phosphate (Pi) from ATP (Baginski et al., 1967). Pi reacts with ammonium molybdate and the colorimetric reaction into blue can be photometrically measured (Fiske and Subbarow, 1925). ATPase activity measurement was performed in a medium containing 100 mM KCl, 7 mM MgCl₂·6H₂O, 1 mM EGTA, pH 7.0, 50 mM TES/Tris, pH 7.0 and different Ca²⁺ solutions (pCa of 5.25, 5.5, 5.75, 6, 6.25, 6.5, 6.75, 7, 7.25, 7.5 and 8) for 30 min at 37°C. The reaction was initiated by the addition of ATP to a final concentration of 5 mM. The measurement was terminated with a stopping solution (3% (w/v) ascorbic acid in 0.5 N HCl and 0.5% (w/v) ammonium heptamolybdate solution) and samples were put on ice for 5 min. After adding a mixture of 2% (w/v) sodium-(m)- arsenite, 2% (w/v) sodium citrate and 2% (v/v) acetic acid to the plate, an incubation for 5 min at 37°C followed. The absorbance at 850 nm of replicates was measured on a FlexStation 3 Multi-Mode Microplate Reader (Molecular Devices) and analyzed in Origin (OriginLab).

5.6 HIGH-RESOLUTION RESPIROMETRY

5.6.1 Coupling control protocol

The high-resolution respirometer Oxygraph-2k (Oroboros Instruments) was used to measure the mitochondrial oxygen consumption of cells as oxygen flow per million cells (pmol/s*10⁶ cells) in 2 s intervals. The coupling control protocol was followed (Pesta and Gnaiger, 2012). Therefore, 8.1x 10⁶ splenocytes were resuspended in their growth medium and filled in two 2 ml glass chambers, where the oxygen consumption was observed with polarographic oxygen sensors under continuous stirring at 750 rpm and 37°C using DatLab Software 5.1 (Oroboros Instruments). After 10 min, the chambers were closed to measure routine respiration. By adding 2 µg/ml of oligomycin with a Hamilton gastight syringe, the ATP synthase was inhibited and leak respiration determined. To monitor the electron transfer system capacity, carbonyl cyanide 4-(trifluoromethoxy) phenylhydrazone (FCCP) was titrated in 0.5 µM steps until the respiratory chain was uncoupled. After the addition of 0.5 µM rotenone (inhibitor of complex

5 METHODS

l) and 2.5 μM antimycin A (inhibitor of complex III), respiration was completely inhibited and the non-mitochondrial residual oxygen consumption was recorded. All experiments were carried out after daily calibration of the oxygen sensors with splenocytes growth medium.

5.7 ELECTROPHYSIOLOGY

5.7.1 Whole-cell patch clamping

In electrophysiology, patch clamping is a technique to study the transport of currents through single ion channels and was introduced by Neher, Sakmann and colleagues (Hamill et al., 1981). During a patch clamp recording, an electrical circuit is formed between the chlorided silver recording and reference electrode with the cell of interest in between. The reference ground electrode is placed in a bath surrounding the cell. A glass pipette, filled with an electrolyte solution and a recording electrode that is connected to an amplifier, is positioned to the membrane surface of a single cell. After suction is applied, the membrane and the glass pipette form a high resistance "gigaohm ($\text{G}\Omega$) seal". In order to get a whole-cell clamp, more suction is applied to rupture the membrane patch. Then voltage is applied and currents through multiple channels simultaneously over the membrane of an entire cell can be recorded. Current changes within cell membranes can be altered by applying compounds to block or open channels.

1×10^6 splenocytes from 6-12-week old C57BL/6 mice were allowed to attach to coverslips (\emptyset 12 mm, coated with 0.01 % poly-L-lysine for 2-4 h at 37°C) in 24-well plates for at least 1 h, before being whole-cell clamped on an inverted Nikon microscope. The microscope was placed on an air table and surrounded by a Faraday cage. Pipettes were pulled from thick-walled borosilicate glass capillaries with a P-97 Flaming/Brown micropipette puller (Sutter Instrument Company) having a resistance of 3–7 $\text{M}\Omega$. Cells were superfused in a solution containing 124 mM NaCl, 26 mM NaHCO_3 , 1 mM NaH_2PO_4 , 2.5 mM KCl, 10 mM D-glucose, 1 mM MgCl_2 , 2 mM CaCl_2 , bubbled with 95% O_2 and 5% CO_2 , pH 7.3. The intracellular solution contained either 130 mM K-gluconate, 2 mM NaCl, 10 mM HEPES, 10 mM 1,2-bis(2-aminophenoxy) ethane-N,N',N'-tetra-acetic acid (BAPTA), 2 mM Na_2ATP , 0.5 mM Na_2GTP , 0.5 mM CaCl_2 and 2 mM MgCl_2 , pH 7.2 or 140 mM K-gluconate, 10 mM HEPES, 10 mM EGTA, 2 mM Mg^{2+}ATP and 1 mM CaCl_2 , pH 7.2. Splenocytes with an access resistance not higher than 20 $\text{M}\Omega$ were voltage

5 METHODS

clamped at -80 mV and $+36$ mV. To record the voltage-gated currents of splenocytes and the current-voltage (IV) relationship of drug-evoked currents, 20 mV voltage steps of 200 ms duration were applied from a holding potential of -80 mV (voltage range from -140 mV to $+40$ mV). To see the transient reaction, cells were voltage clamped at $+36$ mV. In different experiments the following drugs were applied by adding to the superfusing extracellular solution: 10 μ M DMF, 50 μ M A967079 (A96), 100 μ M HC030031 (HC), 10 μ M ruthenium red (RuRed), 500 μ M flufenamic acid (FFA) and 1 μ M H_2O_2 . A96 and HC are specific transient receptor potential ankyrin 1 (TRPA1) channel blockers (McNamara et al., 2007; Chen et al., 2011), whereas RuRed already blocks a broad spectrum of transient receptor potential (TRP) channels like TRPA1 and TRPV1-6 (Dray et al., 1990; Caterina et al., 1997; Caterina et al., 1999; Strotmann et al., 2000; Hoenderop et al., 2001; Peier et al., 2002; Story et al., 2003). FFA is a TRPA1 agonist (Hu et al., 2010), but inhibits most other TRP channels (Guinamard et al., 2013). H_2O_2 was used to study the reaction of redox-sensitive channels like TRPA1 (Andersson et al., 2008) or TRPM2 (Hara et al., 2002). Responses were recorded using a Digidata 1440A digitizer (Molecular Devices), Axon Instruments' Multiclamp 700B amplifier, Clampex 9 and Axoscope 9 software. Data were analyzed offline using Clampfit 9 (Axon Instruments).

5.8 FLOW CYTOMETRY

Flow cytometry is a method which allows phenotyping of cells by their surface molecules and quantitative determination of extracellular and intracellular proteins, molecules or structures as well as cell vitality. Thus, fluorescence, size, and granularity of individual cells are measured. After target structures are tagged with fluorophore-labeled antibodies, single cells pass through a laser beam at high speed. The laser light stimulates the fluorophores and fluorescence is measured directly along with scattered light. Forward scatter light defines the relative cell size and side scattered light represents the granularity of the cell. In order to subtract autofluorescence or background staining of cells from the true fluorescence signal, an unstained cell control is measured. In the case of multiple stains in one experiment a control for each fluorescent dye is needed to compensate for overlapping emission spectra of fluorescent dyes (Macey, 2007).

5 METHODS

5.8.1 Ca²⁺ and reactive oxygen species

To determine cellular Ca²⁺ levels and reactive oxygen species (ROS), CalciFluor Fluo-8, AM and CellRox™ Orange Reagent were used. For mitochondrial superoxide detection, cells were stained with MitoSox™ Red Mitochondrial Superoxide Indicator Reagent. The acetoxymethyl ester (AM) form of the CalciFluor Fluo-8 dye is cell permeable. Inside the cell esterases cleave the esters, the anionic carboxy group is set free and can bind to Ca²⁺. Due to the stable complex formation of Ca²⁺ and anionic carboxy groups, the fluorescence of the dye is increased more than a hundredfold and can be detected. The CellRox™ Orange Reagent and the MitoSox™ Red Mitochondrial Superoxide Indicator Reagent are cell permeable and non-fluorescent in their reduced state. Oxidation of CellRox™ Orange Reagent by ROS results in orange fluorescence, whereas oxidation of MitoSox™ Red Mitochondrial Superoxide Indicator Reagent only by superoxide in mitochondria results in red fluorescence.

For this experiment 3x 10⁵-1x 10⁶ splenocytes, treated with 10 μM DMF for 1 h or 24 h or splenocytes, isolated from mice treated with 75 mg DMF/kg mouse/day for 17 or 29 days, were used. For another set of experiments 10 μM DMF plus 50 μM A967079 (A96), 100 μM HC030031 (HC), 10 μM ruthenium red (RuRed) or 1 mM lanthanum(III) chloride (LaCl₃) were incubated for 1 h with splenocytes. A96 and HC are specific TRPA1 channel blockers (McNamara et al., 2007; Chen et al., 2011), whereas RuRed and LaCl₃ block a broad spectrum of TRP channels (Dray et al., 1990; Caterina et al., 1997; Caterina et al., 1999; Strotmann et al., 2000; Hoenderop et al., 2001; Peier et al., 2002; Bouron et al., 2015). After incubation, splenocytes were transferred to fluorescence-activated cell sorting (FACS) tubes, washed with PBS and centrifuged. Centrifugation steps were always carried out at 600x g for 5 min at 4°C or at 300x g, 10 min, 4°C. The supernatant was discarded and the cells were stained in 100 μl PBS or PBS with 10 mM EGTA with antibodies against CD3 (1:50) and CD45R/B220 (1:100) to identify T cells and B cells. Splenocytes were additionally loaded with 5 μM CalciFluor Fluo-8, AM and 5 μM CellRox™ Orange Reagent or 5 μM MitoSox™ Red Mitochondrial Superoxide Indicator Reagent. To exclude dead cells, LIVE/DEAD™ Fixable Violet Dead Cell Stain solution (1:1000) was added at last and samples were incubated for 15-30 min in the dark. After another centrifugation step, all samples were measured in 300 μl PBS or PBS with 10 mM EGTA

5 METHODS

on a FACS Canto II (BD Biosciences) and analyzed with FlowJo, LLC (Tree Star, Inc.) and Microsoft Excel.

5.8.2 Ca²⁺ store depletion and SOCE

For kinetic measurements 5×10^6 splenocytes were loaded with 3 μM CalciFluor Fluo-8, AM in cell loading medium (DMEM High Glucose medium supplemented with 10% (v/v) FCS, 20 mM HEPES, 100 U/ml penicillin and 100 $\mu\text{g}/\text{ml}$ streptomycin) for 30 min in the dark. Cells were washed once with 250 μl washing medium (DMEM High Glucose medium without phenol red supplemented with 10% (v/v) FCS, 100 U/ml penicillin and 100 $\mu\text{g}/\text{ml}$ streptomycin) (600x g, 5 min or 300x g, 10 min) and resuspended at 40×10^6 cells per ml in washing medium.

To observe Ca²⁺ store depletion a total of 2×10^6 cells was transferred into 500 μl sterofundin (supplemented with 5 mM HEPES) and baseline Ca²⁺ was recorded for 1 min. 10 mM EGTA was added to the cells to buffer extracellular Ca²⁺ ions and kinetics were measured for 3 min before adding 1 μM of ionomycin to release Ca²⁺ from intracellular stores. The ionophore increases the Ca²⁺ permeability of the membrane (Liu and Hermann, 1978; Beeler et al., 1979) and Ca²⁺ can leak to the cytosol. Since the ER is the biggest Ca²⁺ store, the data recorded for another 5 min represent the depletion of the Ca²⁺ stored in the ER.

For the SOCE experiment a total of 2×10^6 cells was resuspended in 500 μl Hank's Balanced Salt Solution with calcium and magnesium (HBSS +/+). After recording the baseline for 1 min, 2 mM EGTA and 2 μM thapsigargin were added to the cells and measured for 5 min. EGTA binds Ca²⁺ ions in solution and the lactone thapsigargin inhibits the ATP-dependent SERCA pumps (Thastrup et al., 1990). The combination of inhibiting the refill of the cells' Ca²⁺ reservoirs by SERCA inhibition and Ca²⁺ leaking through Ca²⁺ leak channels in the ER, causes SOCE after adding 20 mM of Ca²⁺ (Dutta, 2000). Data were recorded for another 5 min. All samples were measured on a FACSCanto II (BD Biosciences) at low speed and analyzed with FlowJo, LLC (Tree Star, Inc.).

5.8.3 STIM1 expression

STIM1 staining is based on an antigen-antibody reaction. Anti-STIM1 antibody labeling was performed according to manufacturer's instructions with the LYNX Rapid Fluorescein Antibody Conjugation Kit[®] (Biorad). In brief, 20 μl Modifier reagent and 200 μl anti-STIM1 antibody were

5 METHODS

mixed before being pipetted onto the LYNX lyophilized mix. After resuspending, the mixture was incubated overnight at room temperature in the dark before 20 μ l Quencher reagent was added.

For surface staining, 3×10^5 splenocytes were transferred to FACS tubes, centrifuged and washed with PBS. Centrifugation steps were always carried out at 300x g for 10 min at 4°C. Cells were taken up in 100 μ l PBS with 3 μ l (~0.5 μ g) of the labeled anti-STIM1 antibody and incubated for 40 min at 4°C in the dark. The stained cells were centrifuged and washed with PBS before the pellet was resuspended in 200 μ l PBS and measured. For intracellular staining, 3×10^5 cells were transferred to FACS tubes, washed with PBS and centrifuged. Cells were fixed in 500 μ l 4% Roti®-Histofix for 10 min at room temperature. The fixed cells were centrifuged and washed with PBS before a permeabilization step in 1 ml PBS with 0.1% Triton X-100 followed for 30 min at room temperature. After another PBS washing step, cells were stained in the same way as described for surface staining. To determine STIM1 specifically in T and B cells, a T and B cell staining with antibodies against CD3 (1:50) and CD45R/B220 (1:100) was carried out prior to STIM1 staining. All samples were measured on a FACSCanto II (BD Biosciences) and analyzed with FlowJo, LLC (Tree Star, Inc.).

5.8.4 Glucose uptake

To monitor glucose uptake in living cells, the fluorescent glucose analog 2-(N-(7-nitrobenz-2-oxa-1,3-diazol-4-yl)amino)-2-deoxyglucose (2-NBDG) was used. For this experiment, 3×10^5 splenocytes were transferred to FACS tubes, washed with PBS and centrifuged. Centrifugation steps were always carried out at 600x g for 5 min at 4°C. The supernatant was discarded and the cells were stained in 100 μ l PBS with antibodies against CD3 (1:50) and CD45R/B220 (1:100) to identify T cells and B cells. To test cell vitality, LIVE/DEAD™ Fixable Violet Dead Cell Stain solution (1:1000) was added and samples were incubated for 15 min in the dark. After another centrifugation step, the cells were stained with 100 μ M 2-NBDG for 15 min at 37°C. Cells were spun down and all samples were measured in 300 μ l PBS on a FACS Canto II (BD Biosciences) and analyzed with FlowJo, LLC (Tree Star, Inc.) and Microsoft Excel.

5 METHODS

5.8.5 NFAT translocation

NFAT translocation was measured in activated T cells. All centrifugation steps before fixation were performed at 600x g for 5 min at 4°C, whereas cells were centrifuged at 1000x g after fixation. First, 10×10^6 cells were transferred to 1.5 ml tubes, centrifuged and washed with PBS. T cell staining with an antibody against CD3 (1:50) was carried out for 20 min at room temperature in the dark. Stained cells were centrifuged and washed with PBS before the pellet was resuspended in 500 μ l PBS. For fixation 500 μ l 4% Roti[®]-Histofix was added for 20 min at 4°C. Fixed cells were centrifuged and washed with PBS before a permeabilization step in 1 ml PBS with 0.3% Triton X-100 followed for 10 min at room temperature. After washing with PBS, cells were incubated with Alexa Fluor[®]488 anti-NFATc1 (1:100) for 20 min at room temperature in the dark. Cells were washed with PBS and resuspended in 50 μ l FACS buffer (0.5% BSA in PBS). Cell nuclei were stained with 0.25 μ g 7-Aminoactinomycin D (7-AAD) 5 min prior to the measurement with the imaging flow cytometer Amnis ImageStream X mk II (Merck). The device combines the phenotyping capability of flow cytometry with the abilities of microscopy to locate and quantitate signals in cells. Therefore, a picture was taken from every cell that passes the laser beam. A total of 5702 to 11627 activated T cells were analyzed with the Ideas Software (Amnis).

5.9 MICROSCOPY

5.9.1 Confocal laser scanning microscopy

1×10^6 splenocytes were seeded in 8-well glass bottom slides and incubated for 2.5 h. Then cells were loaded with 5 μ g/ml CalciFluor Fluo-8, AM in PBS and incubated for 15 min at 37°C in the dark. The measurement at the TCS SP5 confocal microscope (Leica Microsystems) was performed in PBS. For the first experiment, three consecutive images were taken: baseline, 1 min after 10 μ M DMF was applied and 1 min after adding 2 μ M of thapsigargin as a positive control. For the second measurement, four consecutive images were taken: baseline, 10 seconds after applying 2 mM EGTA, 1 min after 10 μ M DMF treatment and 1 min after 1 μ M ionomycin incubation as a positive control. The analysis was performed with ImageJ (Fiji).

5 METHODS

5.9.2 High content screening microscopy

High content light microscopy was performed with an Opera Phenix™ spinning disc high content screening microscope (Perkin Elmer) containing two 16 bit sCMOS cameras and a 40x, 1.1 NA water immersion objective. Obtained images were processed and analyzed using Columbus 2.8.0 software, that includes the PhenoLOGIC™ machine learning plugin (Perkin Elmer). Some experiments were performed at an ArrayScan® VTI HCS Reader by Thermo Fisher Scientific with a 10x objective. Samples were measured in molecular translocation assay mode with Cellomics® vHCS:View and Cellomics® Scan software (Thermo Fisher Scientific).

5.9.2.1 *Live cell imaging*

For live cell imaging, all five STIM1 MEF cell lines were stained with Hoechst (1:1000) in plain growth medium for 10-15 min at 37°C. After washing with plain growth medium and PBS, growth medium with supplements was applied to the cells again. The Opera Phenix™ spinning disc high content screening microscope (Perkin Elmer) was heated to 37°C and 5% CO₂ was supplied. Laser lines used in this experiment were mcherry (Excitation (Ex) 561/Emission (Em) 599) to see the different STIM1 proteins and DAPI (Ex 405/Em 456) for nuclei stained with Hoechst. All measurements were performed in a black 96-well plate in extracellular buffer (130 mM NaCl, 4.6 mM KCl, 2 mM MgCl₂·6H₂O, 10 mM HEPES/Na, 5 mM D-glucose, pH7.4) with 100 μM EGTA. Cells were treated with 1 μM thapsigargin for 10 min, 100 μM H₂O₂ for 20 min and with 10 μM DMF for 1 h and 24 h before measurement. Images of untreated cells were taken as a control. For analysis, cells were identified by their DAPI stained nuclei. The Columbus software was programmed to distinguish texture properties. Thus, the mcherry signal and the STIM1 protein structure could be divided into punctae, reticular or smooth and cells were classified respectively.

5.9.2.2 *Fixed cell imaging*

MEF cells and splenocytes used for ICC were measured. The laser lines DAPI (Ex 405/Em 456) to identify the cells' nuclei, Alexa 488 (Ex 488/ Em 522) to see NFAT or NF-κB and either mcherry (Ex 561/Em 599) or Alexa 568 (Ex 561/Em 599) to detect the cells' cytoplasm, were used in these experiments. For analysis, cells were identified by their DAPI stained nuclei. Masks surrounding the nuclei and cytoplasm were created and the mean fluorescence

5 METHODS

intensity ratio of nuclear to cytoplasmic NF- κ B or NFAT was determined. A total of 8299 to 75076 MEF cells, 6583 to 10997 splenocytes and 1752 to 25996 activated T cells were analyzed.

5.9.3 Ca²⁺ imaging microscopy

The Ca²⁺ indicator Fura-2 was developed by Grynkiewicz et al. (Grynkiewicz et al., 1985). It can be excited at 340 nm and 380 nm, which allows an accurate determination of the intracellular Ca²⁺ concentration. The ratiometric measurement reduces artificial effects of uneven dye loading and photobleaching because they equally affect both measurements. The fluorescence excitation maximum shifts from 362 nm (Ca²⁺-free Fura-2) to 335 nm when Fura-2 binds Ca²⁺. The maximum fluorescence emission, however, stays stable around 510 nm (Grynkiewicz et al., 1985). Fura-2-AM is an esterified cell-permeant form of the Ca²⁺ indicator Fura-2. Inside the cell, it is cleaved by esterases to Fura-2, which is then able to bind Ca²⁺. Pluronic™ F-127 is a nonionic tenside polyol, often used to help disperse the water-insoluble acetoxymethyl ester in the loading medium.

For Ca²⁺ imaging, the different STIM1 MEF cell lines, as well as primary MEF cells, were used. In general, 20 000-40 000 cells were seeded to the 14 mm glass bottom in the center of a 35 mm fibronectin coated dish (1:40 in PBS for 30 min at 37°C). The following day, the cells' growth medium was replaced by 1 ml plain growth medium and cells were loaded with 5 μ M Fura-2-AM and 0.04% (v/v) Pluronic™ F-127 for 1 h at 37°C in the dark. Cells were washed by incubating them in 1 ml extracellular buffer (130 mM NaCl, 4.6 mM KCl, 2 mM MgCl₂·6H₂O, 10 mM HEPES/Na, 5 mM D-glucose, pH7.4) with 2 mM Ca²⁺ for 30 min. To record cytosolic Ca²⁺, cells were taken up in 1 ml extracellular buffer with 100 μ M EGTA and a picture was taken every 2 sec at 340 nm and 380 nm. For controls at the end of the experiments, a maximum signal was caused by the application of 5 μ M ionomycin and a minimum signal by adding 8 mM manganese(II) chloride, which quenched the Fura-2 signal. A High Speed InCyt Im2™ Dual-Wavelength Fluorescence Imaging System from Intracellular Imaging Inc. with a monochromator from Bentham Instruments and a system with a Nikon Eclipse Ti-E inverted microscope, an Optoscan monochromator (Cairn Research) and an iXon 897 EM-CCD camera (Andor Technology) were applied to study cytosolic Ca²⁺ (using F₃₄₀/F₃₈₀ ratio) of individual cells. Software used to perform and monitor the experiments were InCyt_Im2 (Intracellular

5 METHODS

Imaging Inc.) and Winfluor V3.4.0. Background fluorescence was subtracted from the obtained images and analysis was performed with ImageJ (Fiji) software and Microsoft Excel.

5.9.3.1 *Ca²⁺ store depletion*

For Ca²⁺ store depletion, a baseline signal was measured for 1 min before 1 μM (primary MEF cells) or 100 nM ionomycin (STIM1 -/- + STIM1 WT MEF cells) was added to release Ca²⁺ from intracellular stores. The ionophore increases the Ca²⁺ permeability of the membrane (Liu and Hermann, 1978; Beeler et al., 1979) and Ca²⁺ can leak to the cytosol.

5.9.3.2 *SOCE*

For SOCE, a baseline signal was recorded for 1 min before 5 μM thapsigargin for 5 min (primary MEF cells) or 1 μM thapsigargin for 10 min (STIM1 -/- + STIM1 WT MEF cells) was added. The lactone thapsigargin inhibits the ATP-dependent SERCA pumps (Thastrup et al., 1990). Thus Ca²⁺ leaking through Ca²⁺ leak channels results in Ca²⁺ store depletion, which evokes SOCE in response to the addition of 2 mM Ca²⁺ (Dutta, 2000).

5.9.3.3 *Oxidative stress-induced Ca²⁺ entry through H₂O₂*

To test if Ca²⁺ entry can be induced by oxidative stress produced by H₂O₂, cells were incubated with or without 100 μM H₂O₂ for 20 min before a baseline signal was recorded for 1 min. Then 2 mM Ca²⁺ was added and the reaction of the cells was measured.

5.10 STATISTICAL ANALYSIS

Statistical analysis was performed with GraphPad Prism 6 (GraphPad). Data are displayed as mean ± standard deviation (SD) or Tukey's box and whiskers plot. Statistical significance between results was determined by the parametric two-tailed t-test or the non-parametric Mann-Whitney or Wilcoxon matched-pairs signed rank test. To compare more than two datasets, one-way ANOVA variance test with Tukey's multiple comparison test or Kruskal Wallis or Friedman test with Dunn's multiple comparison test was used. Column significance against zero was determined with the one sample t-test. P-values < 0.05 were considered significant. Normal distribution of data was tested with the D'Agostino and Pearson omnibus normality test. Outliers were removed with the ROUT method.

6 RESULTS

6.1 DMF CAUSES SHORT-TERM OXIDATIVE STRESS AND ACTIVATES THE ANTIOXIDANT RESPONSE LEADING TO INCREASED GLUTATHIONE LEVELS

I performed the following experiments in splenocytes to verify that dimethyl fumarate (DMF) causes oxidative stress and induces the antioxidant response in these cells. Splenocytes were isolated from Swiss Jim Lambert (SJL) mice and treated with 10 μ M DMF, a concentration found to be effective without affecting cell viability (Albrecht et al., 2012), for 1 h or 24 h.

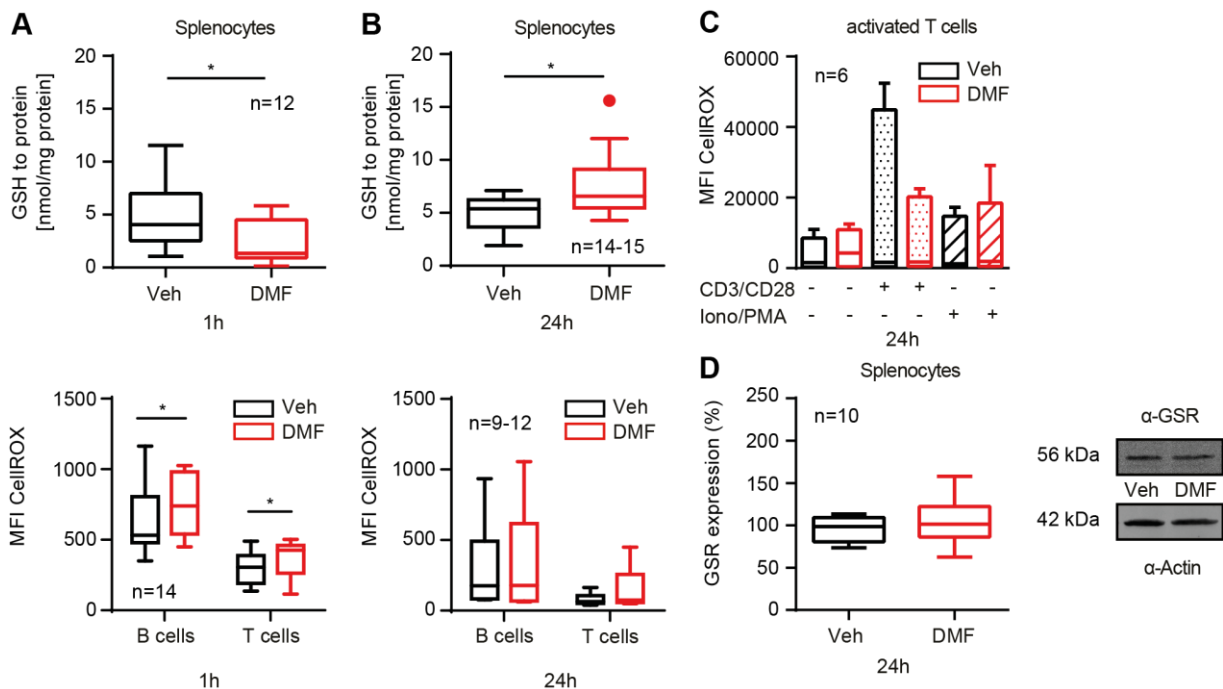


Figure 9: DMF causes short-term oxidative stress and activates the antioxidant response leading to increased glutathione levels.

Splenocytes were isolated from Swiss Jim Lambert (SJL) mice and treated ex vivo with vehicle (Veh) or 10 μ M dimethyl fumarate (DMF) for 1 h or 24 h. A) DMF decreased glutathione (GSH) and increased reactive oxygen species (ROS) levels in B and T cells after 1 h. B) Upon 24 h of DMF treatment, GSH levels were significantly increased and there was no difference in ROS levels anymore. C) ROS levels in activated T cells (not reactivated or reactivated with ionomycin/phorbol 12-myristate 13-acetate (Iono/PMA) or CD3/CD28 were not altered after 24 h treatment with DMF. D) DMF did not significantly change glutathione reductase (GSR) expression after 24 h of DMF treatment. Cytosolic ROS levels were analyzed by flow cytometry using the median fluorescence intensity of the ROS dye CellRox™. T cells were stained with Anti-CD3, B cells with Anti-CD45R/B220. GSH was measured enzymatically and GSR abundance in immunoblots was normalized to actin. One exemplary blot is shown, size is indicated. Data are displayed as Tukey's box and whiskers plots. Statistical significance was calculated using the parametric two-tailed t-test, except for the use of the Wilcoxon matched-pairs signed rank test for 24 h GSH in B), * $p < 0.05$, n=number of mice is indicated

6 RESULTS

As expected, enzymatically measured glutathione (GSH) levels were decreased after 1 h, whereas flow cytometric analysis of the reactive oxygen species (ROS) dye CellRox™ in B and T lymphocytes showed elevated ROS levels (Figure 9A). Upon 24 h of DMF treatment, GSH levels were significantly increased and compared to vehicle (Veh) there was no difference in ROS levels anymore (Figure 9B). The CellRox™ measurement in B and T lymphocytes was performed during my Master's thesis (Herrmann, 2014) and is shown here for illustration purposes only. After 24 h of DMF treatment, there are no signs of oxidative stress anymore in activated T cells, no matter if T cells were not reactivated or reactivated with ionomycin/phorbol 12-myristate 13-acetate (Iono/PMA) or CD3/CD28 (Figure 9C). Next, I examined glutathione reductase (GSR), the enzyme that catalyzes the reduction of GSSG to GSH to study if DMF alters GSH recycling. In splenocytes, DMF treatment did not significantly change GSR expression after 24 h (Figure 9D). Overall, I confirmed the DMF-evoked short-term oxidative stress and the DMF-induced antioxidant answer leading to increased GSH levels but not to elevated GSR expression and GSH recycling. As redox processes can alter intracellular calcium (Ca^{2+}) signaling, I determined cytosolic Ca^{2+} levels in further experiments.

6.2 CYTOSOLIC Ca^{2+} INCREASES AS AN IMMEDIATE RESPONSE TO DMF

I studied the immediate response of cytosolic Ca^{2+} levels to DMF in splenocytes, as ROS and Ca^{2+} signaling pathways are closely intertwined. Splenocytes from SJL micewere incubated with CalciFluor Fluo-8, AM (Fluo-8) and live cell images, taken by confocal microscopy, were analyzed before and after treating the cells with 10 μM DMF for 1 min. Figure 10A reveals a significant immediate increase of cytosolic Ca^{2+} concentration in splenocytes triggered by DMF, which was potentiated by the application of 2 μM thapsigargin (TG). Elevated Ca^{2+} levels in splenocytes treated with 10 μM DMF for 1 min were abolished, when measured in phosphate buffered saline (PBS) with 2 mM of the Ca^{2+} buffer ethylene glycol-bis(2-aminoethyl ether)-N,N,N',N'-tetraacetic acid (EGTA; Figure 10B), hinting to a Ca^{2+} influx from the extracellular space. The positive control, 1 μM ionomycin (Iono), was added to release Ca^{2+} from intracellular stores. The ionophore increases the Ca^{2+} permeability of the membrane (Liu and Hermann, 1978; Beeler et al., 1979) and Ca^{2+} can leak to the cytosol, thus increasing cytosolic Ca^{2+} levels. The significant reaction to DMF in splenocytes led to whole-cell patch clamping experiments to find the reason for the cytosolic Ca^{2+} increase.

6 RESULTS

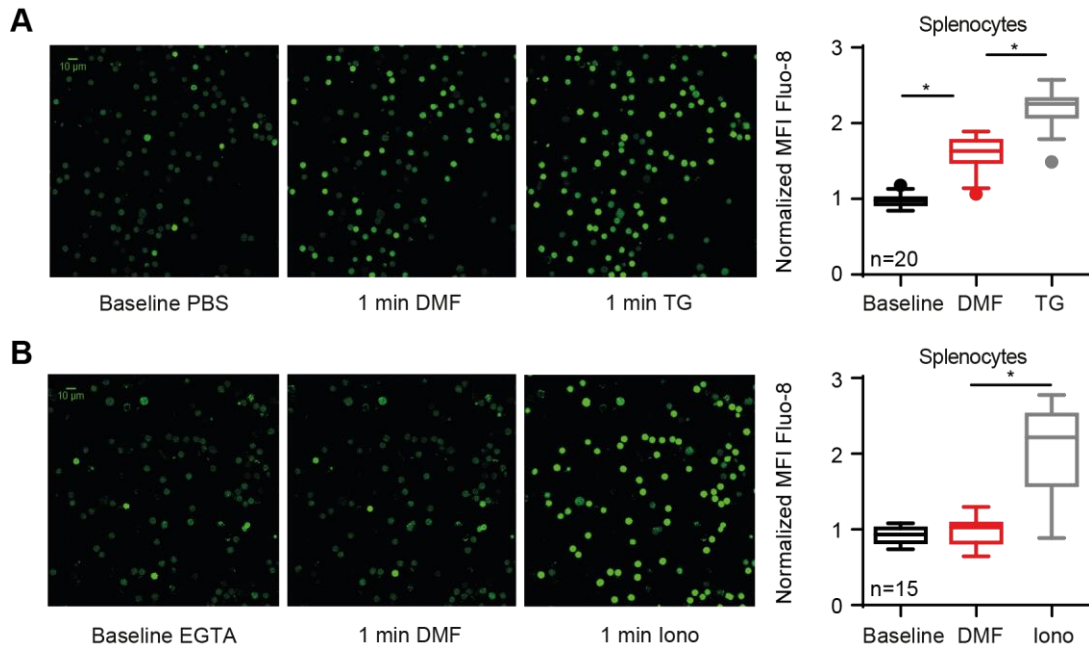


Figure 10: Cytosolic Ca²⁺ increases as an immediate response to DMF.

Splenocytes from SJL mice were incubated with 10 μ M DMF for 1 min. A) DMF increased cytosolic Ca²⁺ levels in splenocytes after 1 min treatment. Adding 2 μ M thapsigargin (TG) for 1 min led to a further increase. B) DMF-elevated cytosolic Ca²⁺ levels were abolished in splenocytes when measured in phosphate buffered saline (PBS) with 2 mM ethylene glycol-bis(2-aminoethyl ether)-N,N,N',N'-tetraacetic acid (EGTA). 1 μ M ionomycin (Iono) increased cytosolic Ca²⁺ levels. Live cell images were taken by confocal microscopy. Cytosolic Ca²⁺ levels were analyzed with ImageJ (Fiji) using the mean fluorescence intensity of the Ca²⁺dye CalciFluo-8, AM (Fluo-8). Data were normalized to baseline. Statistical variation is shown as Tukey's box and whiskers plots and significance was calculated using the Friedman test with Dunn's multiple comparison test (A) and the one-way ANOVA variance test with Tukey's multiple comparison test (B), *p<0.05, n=number of analyzed visual fields is indicated

6.3 DURING PATCH CLAMPING OF SPLENCYTES, DMF CREATES A CURRENT WITH CHARACTERISTICS OF A TRP CHANNEL

The immediate increase in cytosolic Ca²⁺ levels in splenocytes after the addition of 10 μ M DMF revealed that DMF elicits Ca²⁺ influx from the extracellular space. To find the source, I performed whole-cell patch clamping to measure potential DMF-evoked currents. First, I reproduced the DMF-triggered cytosolic Ca²⁺ increase in B and T cells after 1 h incubation in lymphocytes of C57BL/6 mice (Figure 11A) because these mice were used for patch clamping due to legal regulations that restrict the use of SJL mice in the UK, where these experiments were conducted. A voltage step protocol of 10 steps with 20 mV increment from -140 mV to +40 mV showed a depolarized resting IV in splenocytes (Figure 11B). In order to maximize the currents generated by the treatment with 10 μ M DMF for 1-5 min, cells were held at +36mV.

6 RESULTS

An example curve of an outward current caused by DMF is shown in Figure 11C, which recovered to baseline when DMF was washed out. The DMF-evoked IV (Figure 11D) revealed that the current reversed at -15 mV and showed characteristics of a transient receptor potential (TRP) channel with inward rectification at negative voltages, and outward rectification at positive voltages. Figure 11E displays the significant maximum current after 1-5 min of DMF treatment. These results suggested that a TRP channel has a role in DMF-induced immediate Ca^{2+} entry from the extracellular space.

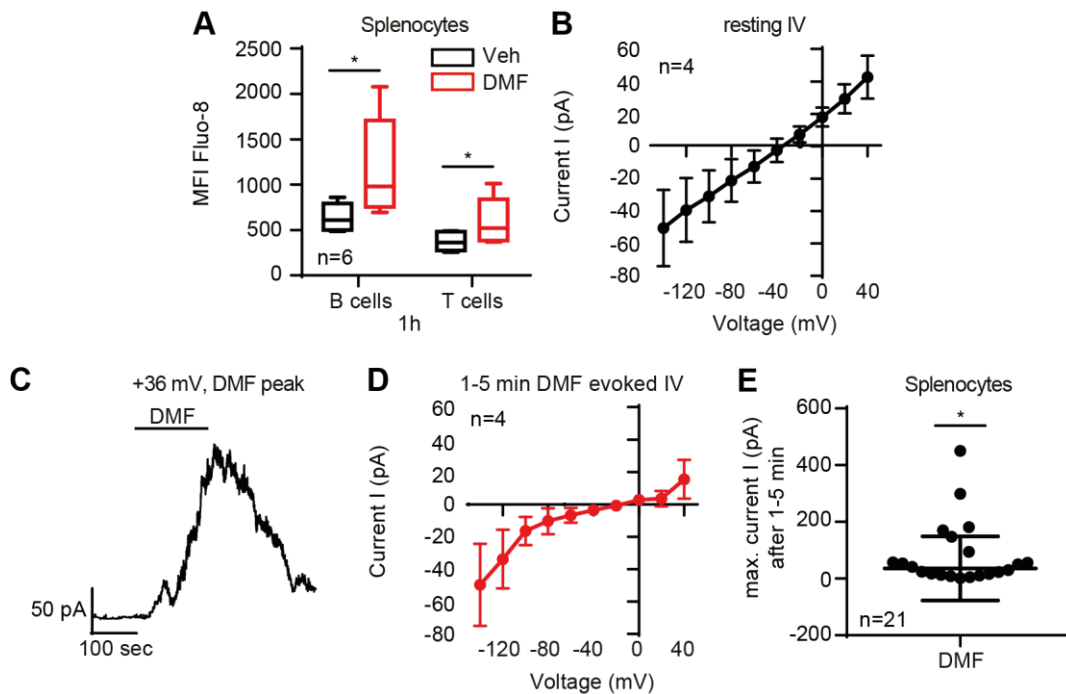


Figure 11: During patch clamping of splenocytes, DMF creates a current with characteristics of a TRP channel.

Splenocytes of C57BL/6 mice were isolated and treated with Veh or 10 μM DMF. A) DMF triggered cytosolic Ca^{2+} increase in B and T cells after 1 h incubation compared to Veh. B) The resting IV of splenocytes was depolarized. C) An example curve of an outward current caused by DMF is shown. Cells were held at +36 mV. D) The DMF-evoked IV revealed that the current reversed at -15 mV, with both inward rectification at negative voltages and outward rectification at positive voltages. E) After 1-5 min treatment with 10 μM DMF the maximum current was significantly changed. Cytosolic Ca^{2+} levels were analyzed by flow cytometry using the median fluorescence intensity of the Ca^{2+} dye Fluo-8. T cells were stained with Anti-CD3, B cells with Anti-CD45R/B220. IV's were generated with a voltage step protocol of 10 steps with 20 mV increment from -140 mV to +40 mV. Cells were held at +36 mV when DMF was applied by adding to the superfusing extracellular solution. Data are displayed as Tukey's box and whiskers plots or as scatter dot plot with SD. Statistical significance was calculated using the parametric two-tailed t-test (A) or the one-sample t-test (E), * $p < 0.05$, n=number of mice (A) or cells (B, D and E) is indicated

6 RESULTS

6.4 TRPA1 INHIBITORS ABOLISH DMF-EVOKED CYTOSOLIC Ca^{2+} INCREASE

After patch clamping results indicated that Ca^{2+} entry through a TRP channel could be the reason for the DMF-evoked increase of cytosolic Ca^{2+} levels in splenocytes, I performed a flow cytometric analysis to examine especially the non-selective ion channel transient receptor potential ankyrin 1 (TRPA1) because of its redox-sensitivity (Andersson et al., 2008). Splenocytes from SJL mice were treated with 10 μ M DMF or Veh for 1 h. Additionally, samples were co-incubated with different TRP channel inhibitors.

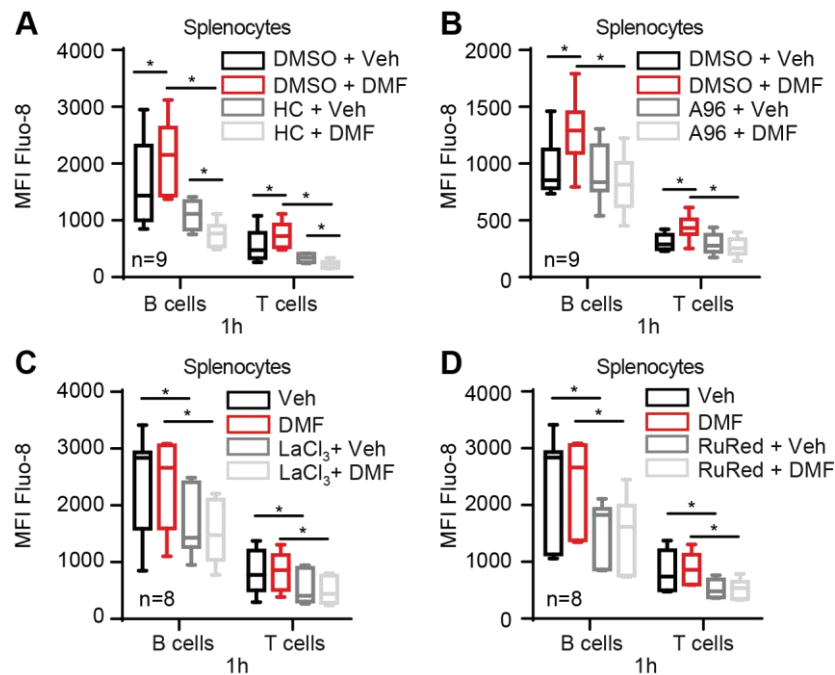


Figure 12: TRPA1 inhibitors abolish DMF-evoked cytosolic Ca^{2+} increase.

Splenocytes from SJL mice were treated with Veh or 10 μ M DMF for 1 h. TRP channel inhibitors were co-incubated. A) and B) The specific transient receptor potential ankyrin 1 (TRPA1) antagonists HC030031 (HC, 100 μ M) in A) and A967079 (A96, 50 μ M) in B) abolished the DMF-evoked cytosolic Ca^{2+} increase. Ca^{2+} levels of lymphocytes co-incubated with DMF and HC (A) were even more reduced compared to the ones in cells co-incubated with Veh and HC. C and D) Incubation of inhibitors that block a broad spectrum of TRP channels, 1 mM lanthanum (III) chloride ($LaCl_3$) in C) and 10 μ M ruthenium red (RuRed) in D), led to a reduction of cytosolic Ca^{2+} concentration in both, Veh- and DMF-treated B and T lymphocytes respectively. Cytosolic Ca^{2+} levels were analyzed by flow cytometry using the median fluorescence intensity of the Ca^{2+} dye Fluo-8. T cells were stained with Anti-CD3, B cells with Anti-CD45R/B220. Data are displayed as Tukey's box and whiskers plots. Statistical significance was calculated using the one-way ANOVA variance test with Tukey's multiple comparison test, * $p < 0.05$, n=number of mice is indicated

The specific TRPA1 antagonists HC030031 (HC) (McNamara et al., 2007) and A967079 (A96) (Chen et al., 2011) abolished the DMF-evoked cytosolic Ca^{2+} increase (Figure 12A and B). Interestingly, Ca^{2+} levels of lymphocytes co-incubated with DMF and 100 μ M HC were even

6 RESULTS

more reduced compared to the ones in cells co-incubated with Veh and HC, indicating an increased DMF-mediated Ca^{2+} efflux either into the extracellular space or into the endoplasmic reticulum (ER). In B and T cells treated with 50 μM A96, I found the same tendency. Lanthanum (III) chloride (LaCl_3) and ruthenium red (RuRed), inhibitors that block a broad spectrum of TRP channels (Dray et al., 1990; Caterina et al., 1997; Caterina et al., 1999; Strotmann et al., 2000; Hoenderop et al., 2001; Peier et al., 2002; Bouron et al., 2015), were used to test if the same effect could be shown (Figure 12C and D). Compared to cells without inhibitor treatment, 1 mM LaCl_3 and 10 μM RuRed incubation led to a reduction of cytosolic Ca^{2+} concentration in both, Veh- and DMF-treated B and T lymphocytes respectively. Thus, this effect seems to be a general one and cannot be traced back to DMF. To further investigate TRPA1, I performed whole-cell patch clamping with TRP inhibitors to verify the data obtained with flow cytometry.

6.5 PATCH CLAMPING OF SPLENOCYTES WITH TRP INHIBITORS IS INCONCLUSIVE

Flow cytometric results point to Ca^{2+} entry through TRPA1 as the reason for the DMF-evoked immediate increase of cytosolic Ca^{2+} levels in splenocytes. I performed whole-cell patch clamping to verify that TRPA1 was mediating the DMF-evoked current. Cells were held at +36mV. Hydrogen peroxide (H_2O_2) is known to activate redox-sensitive TRP channels like TRPA1 (Andersson et al., 2008) or transient receptor potential melastatin (TRPM) 2 (Hara et al., 2002), but 1 μM H_2O_2 had no significant maximum current after being incubated for 1-5 min (Figure 13A). In order to determine if TRPA1 or another TRP channel was mediating the DMF-evoked current, multiple antagonists were applied in the presence of 10 μM DMF. After incubating 10 μM DMF alone, 100 μM HC + 10 μM DMF or 50 μM A96 +10 μM DMF followed as a second application for 1-5 min (Figure 13B). Surprisingly the specific TRPA1 antagonists did not inhibit the current, hinting that TRPA1 is not the reason for the immediate cytosolic Ca^{2+} increase. As a third drug the broad TRP channel inhibitor RuRed (10 μM or 30 μM) was added together with 10 μM DMF for 1-5 min (Figure 13C), but again there was no current inhibition. Last, as the fourth application, 500 μM flufenamic acid (FFA) was applied with 10 μM DMF for 1-5 min to inhibit especially TRPM2 (Hill et al., 2004), but interestingly FFA evoked a current (Figure 13D). In summary, these patch clamping data regarding whether TRPA1 plays a role in DMF-induced Ca^{2+} entry from the extracellular space are inconclusive. To

6 RESULTS

exclude TRPA1 or specify another TRP channel to be responsible for the immediate cytosolic Ca^{2+} increase clearly not enough experiments were done due to the limited time of my stay in the UK, where these experiments were performed.

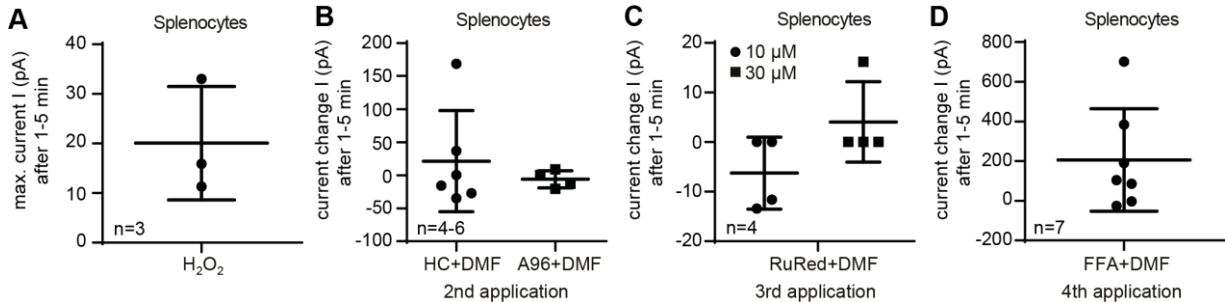


Figure 13: Patch clamping of splenocytes with TRP inhibitors is inconclusive.

Splenocytes of C57BL/6 mice were isolated and whole-cell patch clamped. A) After 1-5 min treatment with 1 μM hydrogen peroxide (H_2O_2), the maximum current was not significantly changed. B-D) Multiple TRP antagonists were applied in the presence of 10 μM DMF after preincubation of 10 μM DMF alone. B) As a second application, the specific TRPA1 inhibitors HC (100 μM) or A96 (50 μM) did not inhibit the current. C) The broad TRP channel inhibitor RuRed (10 μM or 30 μM) did not show any current inhibition, as a third drug applied. D) The fourth application, 500 μM flufenamic acid (FFA), evoked a current. Cells were held at +36 mV when drugs were applied by adding to the superfusing extracellular solution. Data are displayed as scatter dot plots with SD. Statistical significance was calculated using the one-sample t-test, * $p < 0.05$, n=number of cells is indicated

6.6 MRNA EXPRESSION OF TRP CHANNELS IS NOT CHANGED BY DMF

Because patch clamping data could neither verify the involvement of TRPA1 in increasing cytosolic Ca^{2+} levels nor specify another TRP channel to be responsible, I tested mRNA expression levels of several TRP channels after DMF treatment. Splenocytes from SJL micewere treated ex vivo with 10 μM DMF or Veh for 1 h or 24 h, whereas for in vivo experiments 75 mg DMF/kg mouse/day for 17-29 days was used. mRNA from splenocytes was isolated, transcribed into cDNA and quantitative real-time PCR (qPCR) was performed to test TRPA1, TRPM2 and TRPM7 levels. Neither ex vivo DMF-treated cells (Figure 14A), nor cells from in vivo treatment (Figure 14B) showed an altered expression of TRPA1, TRPM2 or TRPM7 compared to Veh-treated cells. Interestingly the expression level of TRPM2, in general, was significantly higher after 24 h in culture, whereas the expression level of TRPA1 was considerably decreased (Figure 14A). Thus, DMF does not alter the amount of TRP channels expressed in splenocytes.

6 RESULTS

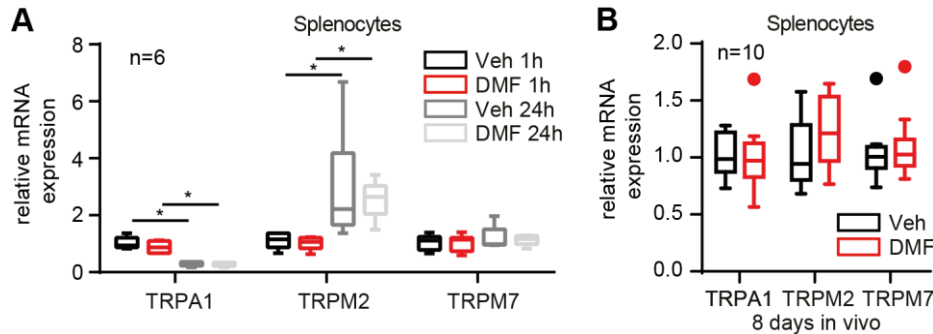


Figure 14: mRNA expression of TRP channels is not changed by DMF.

Splenocytes from SJL mice were treated ex vivo with Veh or 10 μ M DMF for 1 h or 24 h or in vivo with 75 mg DMF/kg mouse/day for 8 days. A) Ex vivo treated cells did not show expression changes in TRPA1, TRPM2 or TRPM7 levels after 1 h or 24 h DMF treatment compared to Veh-treated cells. TRPM2, in general, was significantly higher expressed after 24 h in culture, whereas TRPA1 was considerably decreased. B) In cells from in vivo experiments, no alterations in TRPA1, TRPM2 or TRPM7 expression levels could be detected compared to control mice. mRNA of splenocytes from SJL mice was isolated, transcribed into cDNA and quantitative real-time PCR (qPCR) with the TaqMan method was performed. Data are displayed as Tukey's box and whiskers plots. Statistical significance was calculated using the Friedman test with Dunn's multiple comparison test (A) and the parametric two-tailed t-test (B), * $p < 0.05$, n = number of mice is indicated

6.7 CYTOSOLIC Ca^{2+} INCREASES AS A LONG-TERM EFFECT OF DMF

After I discovered that DMF increases cytosolic Ca^{2+} immediately, I wanted to clarify if there were any long-term effects on Ca^{2+} homeostasis by studying cytosolic Ca^{2+} levels via flow cytometry and Fluo-8. Interestingly the Ca^{2+} concentration in DMF-treated splenocytes of SJL mice was increased throughout all experiments. In contrast to the immediate response to DMF, which was abolished in the presence of EGTA, this did not make a difference for the long-term effect. B and T lymphocytes treated with 10 μ M DMF for 1 h showed a higher cytosolic Ca^{2+} concentration in absence and presence of 10 mM EGTA (Figure 15A). This indicates that either Ca^{2+} is released from intracellular stores, Ca^{2+} uptake into the stores is reduced or Ca^{2+} transport into the extracellular space is attenuated. In splenocytes incubated ex vivo with 10 μ M DMF for 24 h cytosolic Ca^{2+} levels were increased as well (Figure 15B). Only activated T cells reactivated with Iono/PMA showed significantly higher cytosolic Ca^{2+} levels in DMF-treated cells compared to Veh control (Figure 15C). The Ca^{2+} measurement in B and T lymphocytes in PBS after 1 h and 24 h DMF treatment was performed during my Master's thesis (Herrmann, 2014) and is shown here for illustration purposes only. Intrigued by the fact that DMF increases the cytosolic Ca^{2+} concentration not only immediately but also as a long-term effect, I investigated the influence of DMF in mice in vivo.

6 RESULTS

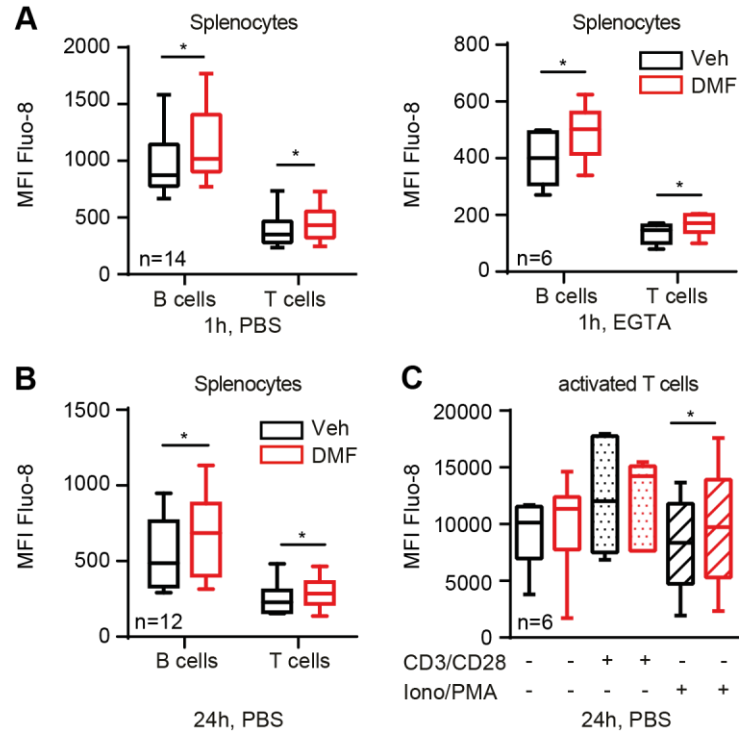


Figure 15: Cytosolic Ca²⁺ increases as a long-term effect of DMF.

Splenocytes were isolated from SJL mice and treated ex vivo with Veh or 10 μ M DMF for 1 h or 24 h. A) DMF increased cytosolic Ca²⁺ levels after 1 h, measured in PBS with or without 10 mM EGTA. B) After 24 h of DMF incubation Ca²⁺ levels were still increased. C) Only T cells reactivated with Iono/PMA showed higher cytosolic Ca²⁺ after 24 h of DMF treatment. Cytosolic Ca²⁺ levels were analyzed by flow cytometry using the median fluorescence intensity of the Ca²⁺ dye Fluo-8. T cells were stained with Anti-CD3, B cells with Anti-CD45R/B220. Data are displayed as Tukey's box and whiskers plots. Statistical significance was calculated using the parametric two-tailed t-test, except for the use of the Wilcoxon matched-pairs signed rank test for 24 h Ca²⁺ in T cells in B), *p<0.05, n=number of mice is indicated

6.8 IN VIVO TREATMENT WITH DMF SHOWS INCREASED CA²⁺ LEVELS, BALANCED GLUTATHIONE LEVELS, BUT STILL INCREASED ROS LEVELS IN B CELLS

So far, I performed ex vivo experiments to study the effect of DMF regarding oxidative stress and Ca²⁺ signaling. Here I examined Ca²⁺, ROS and GSH levels as well as GSR abundance in B and T cells of SJL mice treated in vivo with 75 mg DMF/kg mouse/day for 17-29 days. Cytosolic Ca²⁺ levels were significantly increased in B and T lymphocytes of DMF-treated mice (Figure 16A). I found no significant differences in GSH levels compared to control mice (Figure 16B), but ROS levels in B cells were increased in DMF-treated mice and T cells showed the same tendency (Figure 16C). DMF treatment did not significantly change GSR expression after 17-29

6 RESULTS

days in vivo (Figure 16D). Altogether, the results of the in vivo treatment with DMF were not as conclusive in terms of oxidative stress and DMF-induced antioxidant answer as ex vivo experiments. I assume that the antioxidative system is insufficiently balancing ROS levels here. The fact that cytosolic Ca^{2+} concentration is increased as a long-term effect ex vivo and in vivo led to the investigation of possible mechanisms causing this Ca^{2+} increase.

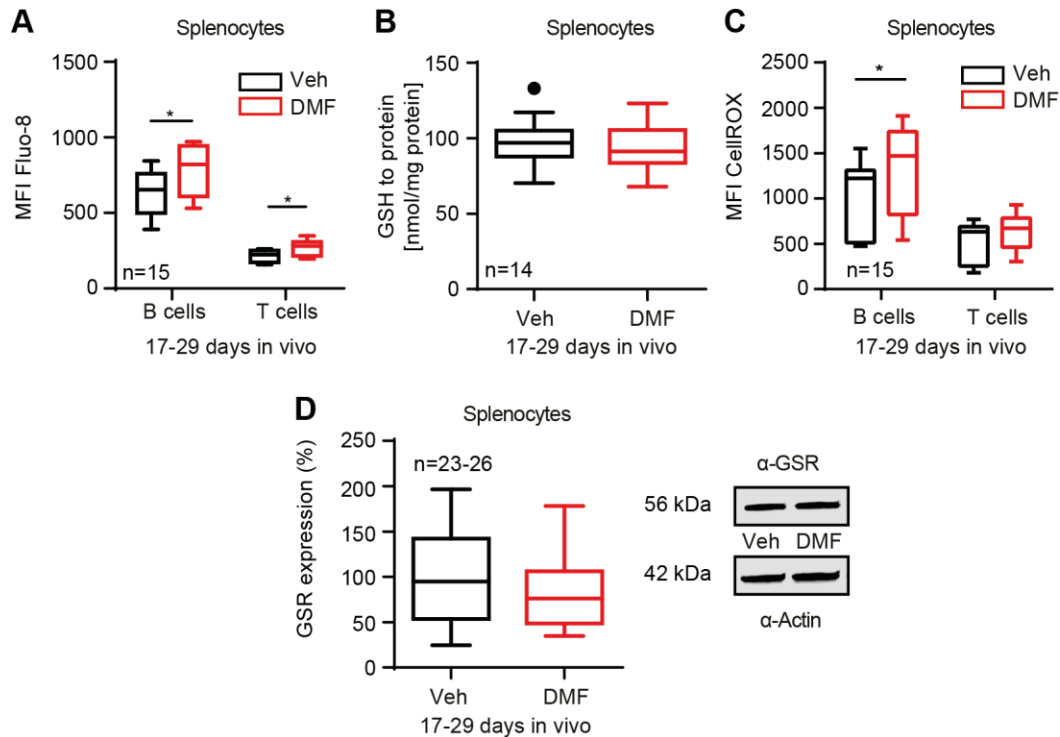


Figure 16: In vivo treatment with DMF shows increased Ca^{2+} levels, balanced glutathione levels, but still increased ROS levels in B cells.

Splenocytes from SJL mice were treated in vivo with 75 mg DMF/kg mouse/day for 17-29 days. A) DMF significantly upregulated intracellular Ca^{2+} concentration after in vivo treatment. B) Splenocytes treated in vivo with DMF showed no alterations in GSH levels compared to control mice. C) ROS levels in B lymphocytes were increased in DMF-treated mice and T cells showed the same tendency. D) DMF did not significantly change GSR expression after 17-29 days in vivo treatment. Cytosolic Ca^{2+} and ROS levels were analyzed by flow cytometry using the median fluorescence intensity of the Ca^{2+} dye Fluo-8 and the ROS dye CellRox™. T cells were stained with Anti-CD3, B cells with Anti-CD45R/B220. GSH was measured enzymatically and GSR abundance in immunoblots was normalized to actin. One exemplary blot is shown, size is indicated. Data are displayed as Tukey's box and whiskers plots. Statistical significance was calculated using the parametric two-tailed t-test, except for the use of the non-parametric Mann-Whitney test in B cells in A) and in C), * $p < 0.05$, n=number of mice is indicated

6.9 DMF REDUCES Ca^{2+} STORE CONTENT IN SPLENOCYTES AFTER 24 H OF INCUBATION

To further clarify how DMF causes increased long-term cytosolic Ca^{2+} levels, I studied if there were any changes in the Ca^{2+} store content. I used Ca^{2+} imaging microscopy with the Ca^{2+} indicator Fura-2-AM to measure Ca^{2+} store content in primary mouse embryonic fibroblast (MEF) cells or the STIM1 $^{-/-}$ + STIM1 WTmcherry MEF cell line after 24 h treatment with 10 μM DMF or Veh. Splenocytes from SJL micewere treated ex vivo with 10 μM DMF or Veh for 1 h or 24 h or in vivo with 75 mg DMF/kg mouse/day for 23 days before Ca^{2+} store content was measured using Fluo-8 and flow cytometry.

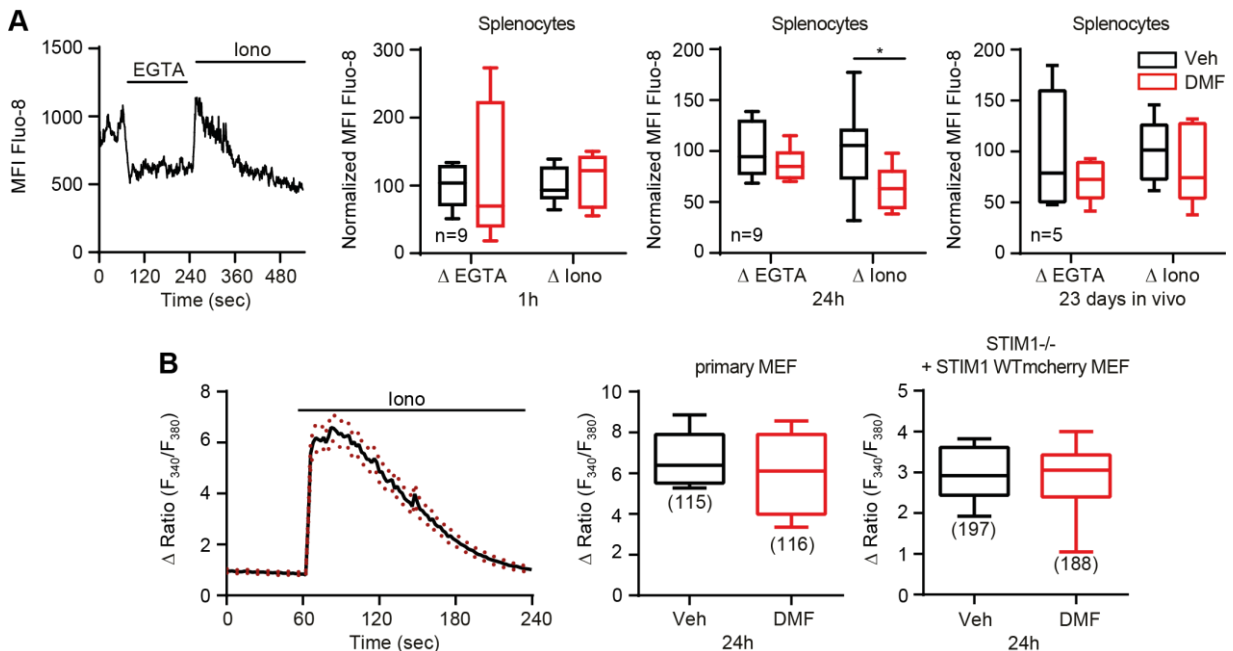


Figure 17: DMF reduces Ca^{2+} store content in splenocytes after 24 h of incubation.

Splenocytes from SJL micewere treated ex vivo with Veh or 10 μM DMF for 1 h or 24 h or in vivo with 75 mg DMF/kg mouse/day for 23 days. Primary mouse embryonic fibroblast (MEF) cells or STIM1 $^{-/-}$ + STIM1 WTmcherry MEF cells were treated with Veh or 10 μM DMF for 24 h. A) An example curve for the kinetic measurement of Ca^{2+} store depletion is shown, where first 10 mM EGTA was added to the cells before 1 μM of Iono was applied. After 1 h, 24 h or 23 days of DMF incubation, there was no difference in Δ EGTA (mean MFI baseline - mean MFI EGTA) compared to Veh, whereas Δ Iono (peak MFI Iono - mean MFI EGTA), on the other hand, was significantly reduced in lymphocytes treated with DMF for 24 h. B) An example curve for the measurement of Ca^{2+} store depletion in primary MEF cells and STIM1 $^{-/-}$ + STIM1 WTmcherry MEF cells is shown. 100 μM EGTA was added before 1 μM (primary MEF cells) or 100 nM (STIM1 $^{-/-}$ + STIM1 WTmcherry MEF cells) Iono was applied. DMF treatment for 24 h did neither change Ca^{2+} store depletion (peak Fura-2-AM ratio Iono - Fura-2-AM ratio before Iono application) in primary MEF cells nor in STIM1 $^{-/-}$ + STIM1 WTmcherry MEF cells compared to Veh. Ca^{2+} store content in splenocytes was measured via flow cytometry using the mean fluorescence intensity of the Ca^{2+} dye Fluo-8, whereas in MEF cells Ca^{2+} store content was studied via Ca^{2+} imaging microscopy

6 RESULTS

using the fluorescence ratio (F_{340}/F_{380}) of the Ca^{2+} indicator Fura-2-AM. Data are displayed as Tukey's box and whiskers plots. Statistical significance was calculated using the parametric two-tailed t-test, except for the use of the non-parametric Mann-Whitney test in in vivo experiments in A), * $p < 0.05$, n=number of mice (A) or cells (B) is indicated

Figure 17A shows an example curve for the kinetic measurement of Ca^{2+} store depletion via flow cytometry. First, 10 mM EGTA was added to the cells to buffer extracellular Ca^{2+} ions before 1 μ M of Iono was applied, resulting in a Ca^{2+} leak to the cytosol. After 1 h, 24 h or 23 days of DMF incubation, I observed no difference in Δ EGTA (mean MFI baseline - mean MFI EGTA) compared to Veh, whereas Δ Iono (peak MFI Iono - mean MFI EGTA), on the other hand, was significantly reduced in lymphocytes treated with DMF for 24 h (Figure 17A). Figure 17B shows an example curve for the measurement of Ca^{2+} store depletion in primary MEF cells and STIM1 -/- + STIM1 WT mcherry MEF cells, in which first 100 μ M EGTA was added to the cells before 1 μ M (primary MEF cells) or 100 nM (STIM1 -/- + STIM1 WTmcherry MEF cells) Iono was applied. In contrast to the flow cytometric analysis in splenocytes, I did not observe a difference in Ca^{2+} store content (peak Fura-2-AM ratio Iono - Fura-2-AM ratio before Iono application) in primary MEF cells nor in STIM1 -/- + STIM1 WTmcherry MEF cells after 24 h of DMF incubation compared to Veh (Figure 17B). The flow cytometric measurement of Ca^{2+} store content after 1 h and 24 h DMF treatment was performed during my Master's thesis (Herrmann, 2014) and is shown here for illustration purposes only. Taken together, less Ca^{2+} stored in the ER in splenocytes explains the higher Ca^{2+} levels in the cytosol. Thus, suggesting either a higher leakage of Ca^{2+} from the ER into the cytosol or the inhibition of the ATPase-mediated Ca^{2+} transport into the ER after 24 h of DMF treatment.

6.10 SERCA2B EXPRESSION IS REDUCED WHILE ITS ACTIVITY IS INCREASED BECAUSE OF S-GLUTATHIONYLATION OF ITS C674

I investigated sarco/endoplasmic reticulum Ca^{2+} -ATPase (SERCA) 2b, the ATPase isoform which is expressed in various tissues (Wu et al., 1995), to figure out if the protein is involved in causing increased cytosolic Ca^{2+} levels and empty ER stores. CV-1 in Origin Simian-1 (COS1) cells and Chinese hamster ovary (CHO) cells were transfected with SERCA2b WT or C674S, the SERCA2b mutant in which the cysteine 674 is mutated into a serine. Transfected COS1 and CHO cells were incubated with 10 μ M DMF or Veh for 24 h, as well as splenocytes.

6 RESULTS

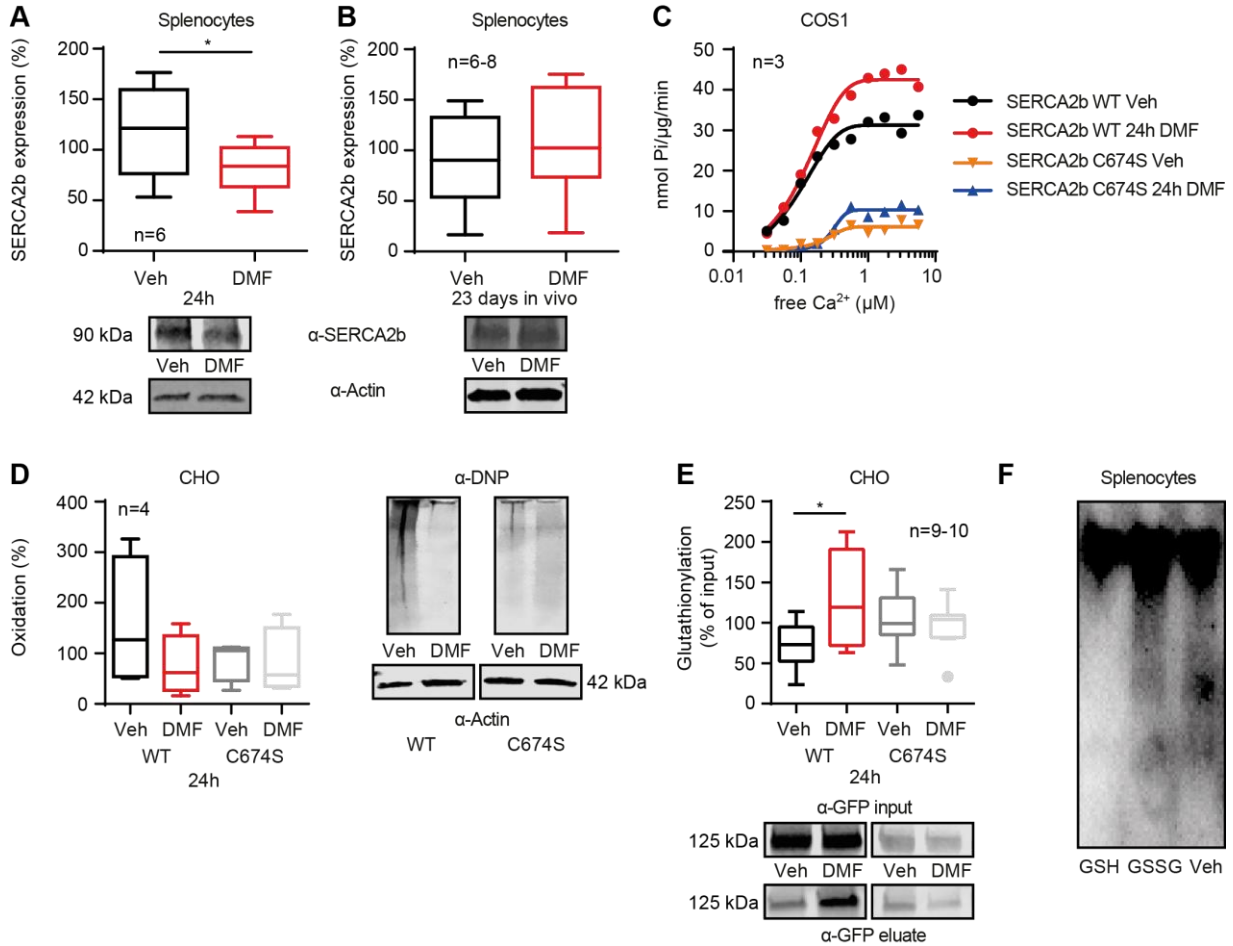


Figure 18: SERCA2b expression is reduced while its activity is increased because of S-glutathionylation of its C674.

CV-1 in Origin Simian-1 (COS1) cells and Chinese hamster ovary (CHO) cells were transfected with sarco/endoplasmic reticulum Ca²⁺-ATPase (SERCA) 2b WT or C674S and incubated with 10 µM DMF or Veh for 24 h. Splenocytes from SJL micewere treated ex vivo with 10 µM DMF or Veh for 24 h or in vivo with 75 mg DMF/kg mouse/day for 23 days. A) DMF significantly reduced SERCA2b expression in splenocytes after 24 h. B) No alterations in SERCA2b abundance were detected upon 23 days of DMF treatment. C) SERCA2b WT activity was increased in DMF-treated cells compared to Veh. SERCA2b C674 mutant activity was barely detectable. D) Oxidation at C674 was not significantly altered in SERCA2b WT or C674S mutant after incubation with DMF. E) DMF significantly increased S-glutathionylation of C674 in SERCA2b WT compared to Veh, whereas the SERCA2b C674S mutant was not affected at all. F) GSH-treated splenocytes showed a different pattern in redox-induced protein oligomerization in Blue Native PAGE compared to GSSG treatment or Veh. SERCA2b activity was determined with the ATPase activity assay. SERCA2b expression or oxidation in immunoblots was normalized to actin. Oxidation of C674 was determined after the GFP-Trap assay was accomplished. S-glutathionylation of C674 was studied with the BIOGEE assay. One exemplary blot for each experiment is shown, size is indicated. Data are displayed as an XY line plot or Tukey's box and whiskers plots. Statistical significance was calculated using the parametric two-tailed t-test (A and B) or the one-way ANOVA variance test with Tukey's multiple comparison test (C, D and E), *p<0.05, n= number of mice (A and B) or experiments (C, D and E) is indicated

6 RESULTS

DMF significantly reduced SERCA2b expression in splenocytes after 24 h of treatment with 10 μ M DMF (Figure 18A), whereas 23 days of treatment with 75 mg DMF/kg mouse/day did not affect SERCA2b abundance (Figure 18B). Lower abundance in DMF-treated cells was compensated by increased SERCA2b WT activity (Figure 18C). As SERCA activity is prone to stimulatory and inhibitory oxidative posttranslational modifications, especially at cysteine 674 (C674) (Grover et al., 2003; Adachi et al., 2004), I determined the oxidative status as well as S-glutathionylation of SERCA2b WT and the mutant C674S. Figure 18C shows clearly, by abolishing C674 in the mutant, its activity was marginal. As expected by a higher SERCA2b WT activity, oxidation at C674 was not significantly altered in SERCA2b WT after DMF treatment nor in the C674S mutant (Figure 18D). For the BIOGEE assay, CHO cells, transfected with SERCA2b-GFP fusion proteins, were treated with 250 μ M biotinylated glutathione ethyl ester (BIOGEE) for 1 h. The strong affinity of streptavidin to biotin was used to isolate glutathionylated proteins. For analysis, the percentage of isolated S-glutathionylated SERCA2b protein was calculated from total SERCA2b protein input. The BIOGEE assay showed that DMF significantly increased S-glutathionylation of SERCA2b WT compared to Veh (Figure 18E), whereas the SERCA2b C674S mutant was not affected at all, suggesting that glutathionylation occurs at C674. Besides, GSH-treated splenocytes showed a different pattern in redox-induced protein oligomerization in Blue Native PAGE compared to GSSG treatment or Veh (Figure 18F). Summarized, DMF has two different ways of affecting SERCA2b. First, it reduces the expression after 24 h treatment and second, it increases the S-glutathionylation of C674 and therefore increases Ca^{2+} -ATPase activity. Thus, less SERCA2b abundance can only be a partial reason for DMF-mediated alterations in Ca^{2+} homeostasis.

6.11 DMF DECREASES SOCE IN MEF CELLS AFTER 24 H OF INCUBATION

My observations of an increase in cytosolic Ca^{2+} levels and a reduced Ca^{2+} store content are similar to the phenotype of a constitutively active STIM1 EF-hand mutant, that activates Ca^{2+} entry independently from ER Ca^{2+} stores (Henke et al., 2012). As STIM1 is the main regulator of store-operated Ca^{2+} entry (SOCE) (Liou et al., 2005; Roos et al., 2005) and can be altered by oxidative posttranslational modifications (Hawkins et al., 2010), I analyzed if there were any DMF-mediated changes regarding SOCE.

6 RESULTS

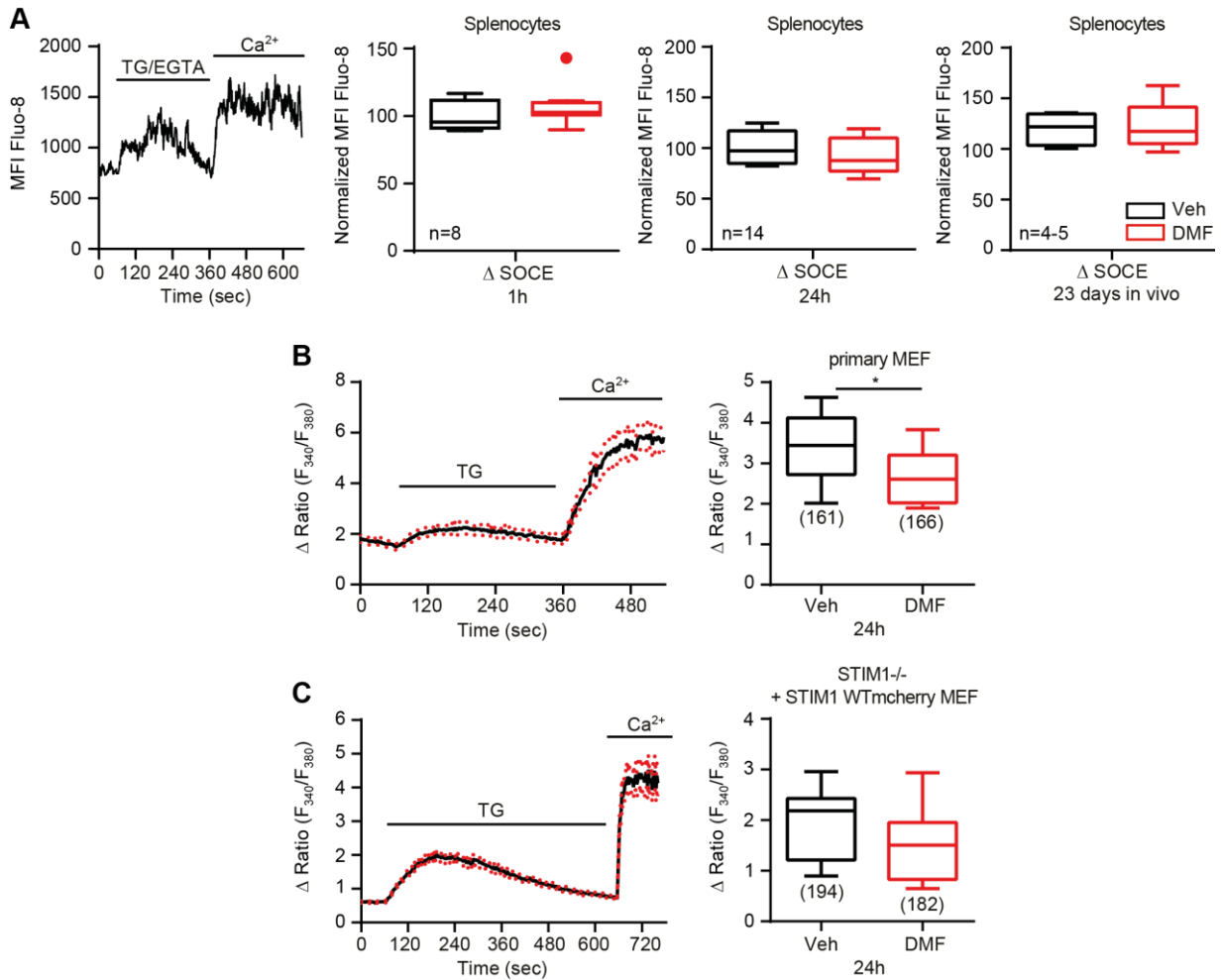


Figure 19: DMF decreases SOCE in MEF cells after 24 h of incubation.

Splenocytes from SJL micewere treated ex vivo with Veh or 10 μ M DMF for 1 h or 24 h or in vivo with 75 mg DMF/kg mouse/day for 23 days. Primary MEF cells or STIM1 ^{-/-} + STIM1 WTMcherry MEF cells were treated with Veh or 10 μ M DMF for 24 h. A) An example curve for the kinetic measurement of SOCE in splenocytes is shown. 2 mM EGTA was added together with 2 μ M TG before SOCE was induced by applying 20 mM of Ca²⁺. DMF treatment for 1 h, 24 h or 23 days did not significantly change Δ SOCE (peak MFI after Ca²⁺ application) compared to Veh. B and C) An example curve for the SOCE measurement in MEF cells is shown. First, 100 μ M EGTA was added, then 5 μ M TG was incubated for 5 min (B) or 1 μ M TG for 10 min (C) before SOCE was induced by applying 2 mM of Ca²⁺. DMF significantly decreased SOCE (peak Fura-2-AM ratio Ca²⁺ – Fura-2-AM ratio before Ca²⁺ application) in primary MEF cells (B), but not in STIM1 ^{-/-} + STIM1 WTMcherry MEF cells (C). SOCE in splenocytes was measured via flow cytometry using the mean fluorescence intensity of the Ca²⁺ dye Fluo-8, whereas in MEF cells SOCE was studied via Ca²⁺ imaging microscopy using the fluorescence ratio (F₃₄₀/F₃₈₀) of the Ca²⁺ indicator Fura-2-AM. Data are displayed as Tukey's box and whiskers plots. Statistical significance was calculated using the parametric two-tailed t-test. The non-parametric Mann-Whitney test was used for in vivo experiments, *p<0.05, n=number of mice (A) or cells (B and C) is indicated

I applied a well-established Ca²⁺ imaging microscopy protocol using the ratiometric Ca²⁺ indicator Fura-2-AM to measure SOCE in primary MEF cells or STIM1 ^{-/-} + STIM1 WTMcherry MEF cells after 24 h treatment with 10 μ M DMF or Veh. Splenocytes from SJL micewere treated

6 RESULTS

ex vivo with 10 μM DMF or Veh for 1 h or 24 h or in vivo with 75 mg DMF/kg mouse/day for 23 days before SOCE was measured using Fluo-8 and flow cytometry. Figure 19A shows an example curve for the kinetic measurement of SOCE in splenocytes via flow cytometry. First, 2 mM EGTA was added together with 2 μM TG, to bind Ca^{2+} ions in solution and inhibit the Ca^{2+} reuptake to the ER through the ATP-dependent SERCA. SOCE was induced by applying 20 mM of Ca^{2+} . DMF treatment for 1 h, 24 h or 23 days did not significantly change Δ SOCE (peak MFI after Ca^{2+} application) in splenocytes compared to Veh (Figure 19A). Although there is a tendency for a reduction in Δ SOCE after 24 h DMF treatment. Figure 19B shows an example curve for the measurement of SOCE in primary MEF cells, whereas Figure 19C shows the one for STIM1 $-/-$ + STIM1 WTmcherry MEF cells. Both differ in the duration and amount of TG treatment, which was optimized for the respective cells. In general, 100 μM EGTA was added before 5 μM TG for 5 min (primary MEF cells) or 1 μM TG for 10 min (STIM1 $-/-$ + STIM1 WT mcherry MEF cells) and 2 mM of Ca^{2+} were applied. DMF significantly decreased SOCE (peak Fura-2-AM ratio Ca^{2+} – Fura-2-AM ratio before Ca^{2+} application) in primary MEF cells (Figure 19B). SOCE was not significantly altered in STIM1 $-/-$ + STIM1 WTmcherry MEF cells (Figure 19C), but showed the same tendency. This deviant SOCE behavior in MEF cells led to further research of proteins involved in SOCE regulation as a potential DMF target.

6.12 DMF REDUCES STIM1 EXPRESSION IN MEF CELLS AND SPLENOCYTES

I investigated STIM1 abundance in STIM1 WT MEF cells and splenocytes next, because STIM1 is the main regulator of SOCE (Liou et al., 2005; Roos et al., 2005) and can be altered by oxidative posttranslational modifications (Hawkins et al., 2010). STIM1 WT MEF cells were incubated with 2, 4, 6, 8 and 10 μM DMF for 24 h to test STIM1 expression in a dose-dependent manner. I determined STIM1 expression in splenocytes from SJL mice, treated ex vivo with 10 μM DMF or Veh for 1 h or 24 h or in vivo with 75 mg DMF/kg mouse/day for 17-29 days, by using flow cytometric detection of a fluorescence STIM1 antibody and via immunoblotting. DMF significantly decreased STIM1 abundance dose-dependently (Figure 20A), with 8 μM and 10 μM DMF being the most effective concentrations. Not after 1 h but after 24 h incubation with 10 μM DMF, I detected a significant STIM1 reduction in splenocytes (Figure 20B). In vivo DMF treatment showed no difference in STIM1 levels compared to control mice (Figure 20C). Flow cytometric analysis revealed that DMF neither changed STIM1 expression at the cell

6 RESULTS

surface (Figure 20D) nor intracellular (Figure 20E) upon 1 h or 24 h incubation. Dose-dependent STIM1 expression in STIM1 WT MEF cells and flow cytometric STIM1 analysis in B and T lymphocytes after 1 h and 24 h DMF treatment was performed during my Master's thesis (Herrmann, 2014) and is newly analyzed shown here for illustration purposes only. Altogether, less STIM1 protein would be an explanation for the reduced SOCE response seen in DMF-treated cells.

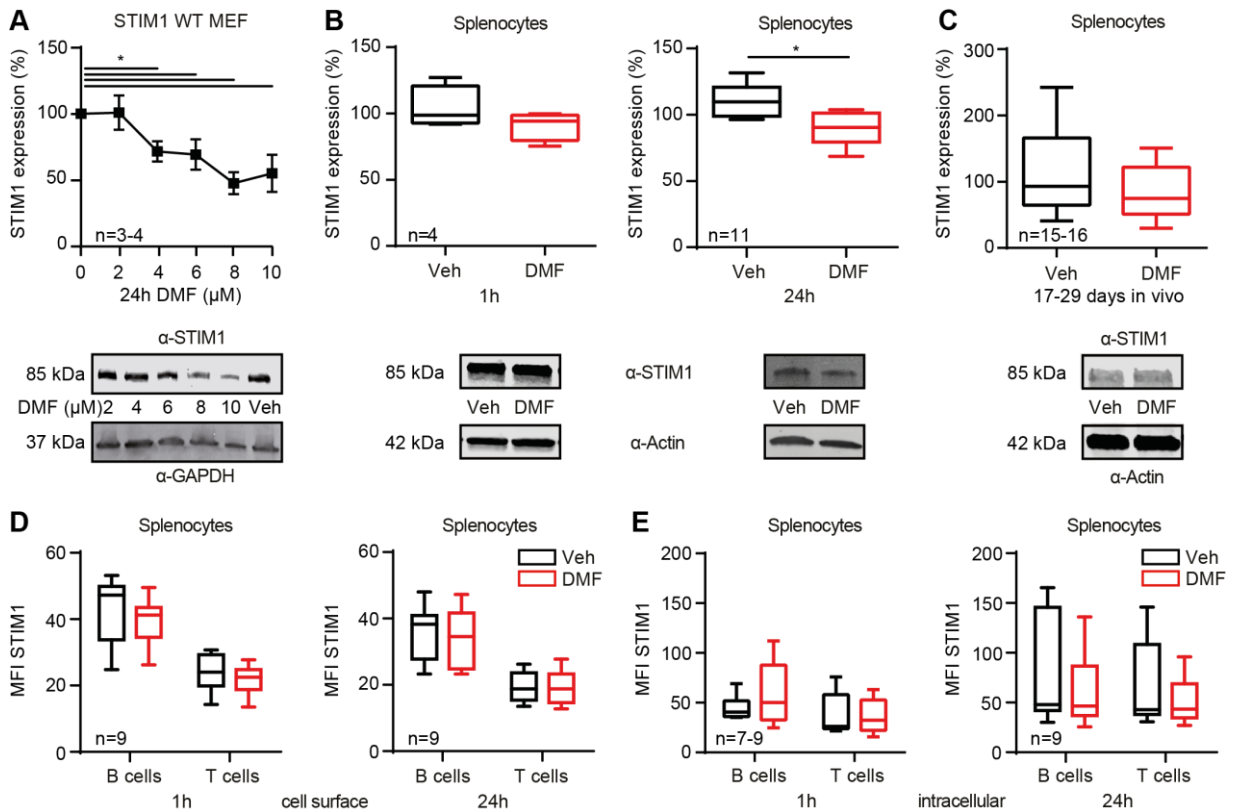


Figure 20: DMF reduces STIM1 expression in MEF cells and splenocytes.

STIM1 WT MEF cells were incubated with 2, 4, 6, 8 and 10 μM DMF for 24 h. Splenocytes from SJL mice were treated ex vivo with Veh or 10 μM DMF for 1 h or 24 h or in vivo with 75 mg DMF/kg mouse/day for 17-29 days. A) DMF significantly decreased STIM1 abundance dose-dependently after 24 h. B) Not after 1 h, but after 24 h of DMF incubation, STIM1 expression was significantly decreased in splenocytes. C) Splenocytes treated in vivo with DMF showed no difference in STIM1 levels compared to control mice. D and E) STIM1 expression was neither changed at the cell surface (D) nor intracellular (E) after 1 h and 24 h DMF treatment. Cell surface and intracellular STIM1 abundance were analyzed by flow cytometry using the median fluorescence intensity of a fluorescence-labeled STIM1 antibody. T cells were stained with Anti-CD3, B cells with Anti-CD45R/B220. STIM1 expression in immunoblots was normalized to GAPDH or actin. One exemplary blot for each experiment is shown, size is indicated. Data are displayed as an XY line plot or as Tukey's box and whiskers plots. Statistical significance was calculated using the parametric two-tailed t-test (B, C, D and E), except for the use of the one-way ANOVA variance test with Tukey's multiple comparison test for A, * $p < 0.05$, n=number of blots (A) or mice (B, C, D and E) is indicated

6 RESULTS

6.13 GSH DECREASES STIM1 OLIGOMERIZATION

S-glutathionylation of STIM1 at cysteine 56 (C56) is an oxidative posttranslational modification which activates STIM1 (Hawkins et al., 2010). Upon activation, STIM1 oligomerizes and forms punctae to initiate SOCE (Luik et al., 2008). To investigate redox-induced protein oligomerization in splenocytes, I performed a glutathione fusion assay. Cell lysates from freshly isolated splenocytes were treated with reduced glutathione (GSH) or oxidized glutathione disulfide (GSSG) for 1 h. For analysis, the bands of the oligomeric STIM1 (shifted) were compared to the monomeric STIM1 bands (non-shifted).

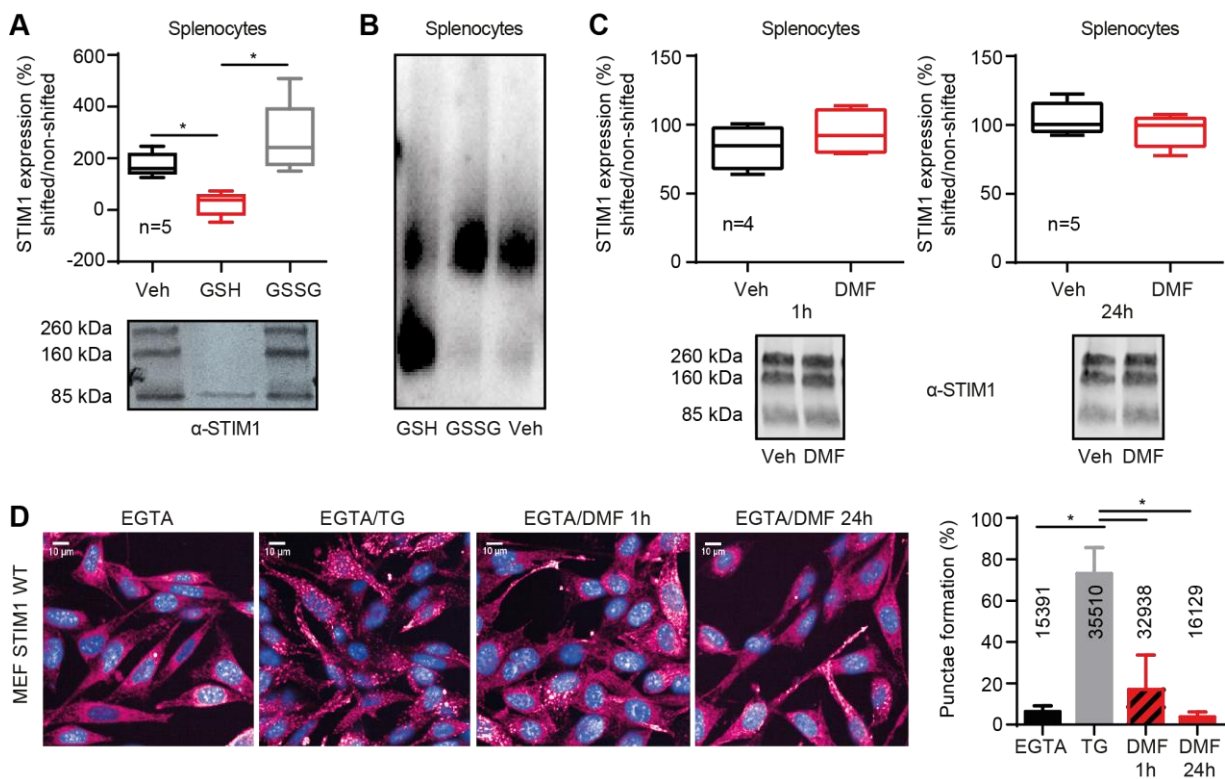


Figure 21: GSH decreases STIM1 oligomerization.

Splenocytes from SJL mice and STIM1 $-/-$ + STIM1 WTmcherry MEF cells were treated with 10 μ M DMF or Veh for 1 h or 24 h. Cell lysates from freshly isolated splenocytes were treated with reduced glutathione (GSH) or oxidized glutathione disulfide (GSSG) for 1 h. A and B) GSH-treated samples showed significant less oligomerization (A) and a different pattern in Blue Native PAGE (B) compared to GSSG treatment or Veh. C and D) There were neither significant differences in STIM1 oligomerization in Veh- or DMF-treated splenocytes (C) nor in punctae formation in STIM1 $-/-$ + STIM1 WTmcherry MEF cells (D), incubated with DMF for 1 h and 24 h, when compared to the negative control (100 μ M EGTA). The glutathione fusion assay and DMF treatment were performed before STIM1 oligomerization was analyzed by comparing the bands of the oligomeric STIM1 (shifted) to the monomeric STIM1 bands (non-shifted) on non-reducing immunoblots or a Blue Native PAGE. One exemplary blot for each experiment is shown, size is indicated. Punctae formation was measured in living cells via a high content screening microscope. For analysis, cells were identified by their DAPI stained nuclei and the software

6 RESULTS

distinguished texture properties. The STIM1 mcherry signal and protein structure was divided into punctae, reticular or smooth and cells were classified respectively. Data are displayed as Tukey's box and whiskers plots or column bar graphs with SD. Statistical significance was calculated using the one-way ANOVA variance test with Tukey's multiple comparison test (A and D) or the parametric two-tailed t-test (C), * $p < 0.05$, n =number of mice (A and C) or cells (D) is indicated

GSH-treated samples showed significant less oligomerization compared to Veh- or GSSG-treated samples (Figure 21A). Complex detection by Blue Native PAGE showed a different redox-induced protein oligomerization pattern in GSH-treated splenocytes compared to GSSG treatment or Veh (Figure 21B) that confirmed the findings displayed in Figure 21A. To investigate if DMF affects STIM1 oligomerization, I incubated splenocytes with 10 μ M DMF for 1 h or 24 h before analyzing the complexes on a non-reducing gel. I did not find any significant differences in STIM1 oligomerization in Veh- or DMF-treated cells (Figure 21C). Punctae formation was also measured in living STIM1 $-/-$ + STIM1 WTmcherry MEF cells via a high content screening microscope. For analysis, cells were identified by their DAPI stained nuclei and the Columbus software (Perkin Elmer) was programmed to distinguish texture properties. The STIM1 mcherry signal and protein structure was classified as punctae, reticular or smooth. Adding 100 μ M EGTA as negative control did not show any STIM1 oligomerization in the different cell lines. I found no differences in punctae formation in cells treated with 10 μ M DMF for 1 h and 24 h compared to the negative control, either (Figure 21D). Thus, GSH but not DMF influences STIM1 oligomerization. If highly conserved cysteines in STIM1 are important for its oligomerization, was determined next.

6.14 PUNCTAE FORMATION IS REDUCED IN STIM1 MUTANTS

STIM1 has two highly conserved cysteines in its luminal part, C49 and C56, which are susceptible to oxidative posttranslational modifications. In our laboratory, different MEF cell lines were generated from STIM1 $-/-$ cells in order to investigate their differences in functionality: STIM1 $-/-$ with STIM1 WT or the mutants STIM1 C49M, STIM1 C56M and the double mutant STIM1 C49M/C56M (DM). All cell lines express a STIM1-mcherry fusion protein. Figure 22A shows that STIM1 was expressed in all MEF cell lines, except for the STIM1 $-/-$ + empty vector (EV) mcherry one, which served as a negative control. Punctae formation was measured in living cells using a high content screening microscope. For analysis, cells were identified by their DAPI stained nuclei and the Columbus software (Perkin Elmer) was

6 RESULTS

programmed to distinguish texture properties. The STIM1 mcherry signal and protein structure was classified as punctae, reticular or smooth. Adding 100 μ M EGTA as a negative control did not show any STIM1 oligomerization in the different cell lines (Figure 22A). Punctae formation was significantly reduced in all mutants compared to STIM1 WT cells after triggering Ca^{2+} store depletion by adding 1 μ M TG for 10 min (Figure 22B). STIM1 oligomerization in the DM was even more decreased than in the C56M mutant. Figure 22C shows that punctae formation in STIM1 WT cells was triggered by 20 min treatment with 100 μ M H_2O_2 , but not in the mutants. These results led to further research in STIM1 mutants regarding their behavior in Ca^{2+} store depletion and SOCE.

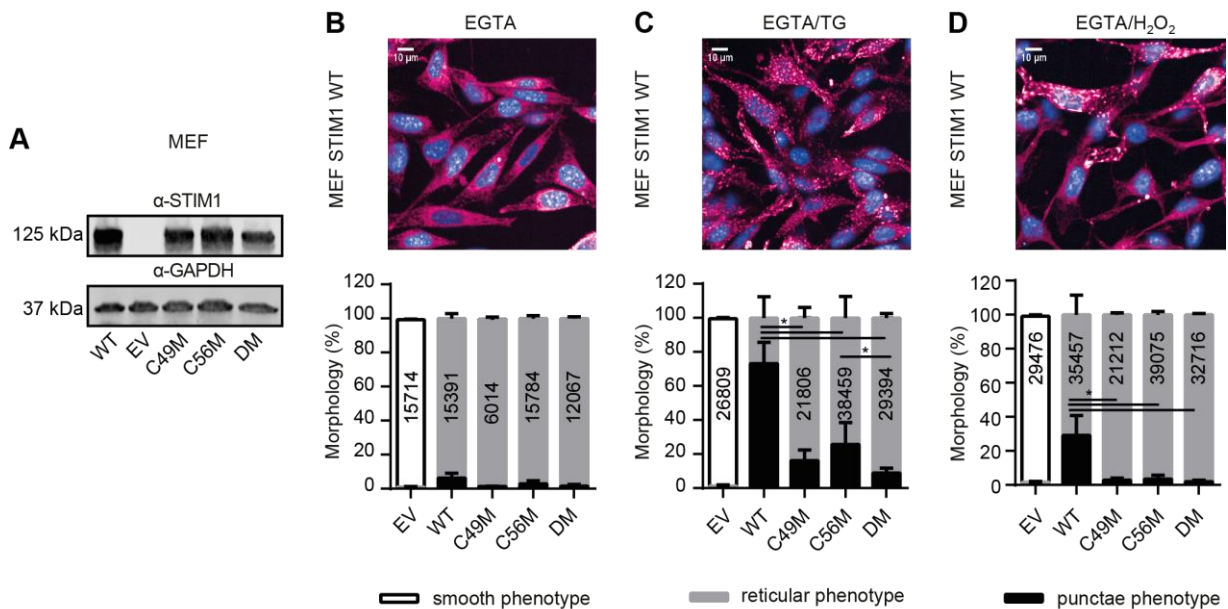


Figure 22: Punctae formation is reduced in STIM1 mutants.

The MEF cell lines STIM1 $^{-/-}$ + empty vector (EV) mcherry, STIM1 $^{-/-}$ + STIM1 WTmcherry, STIM1 $^{-/-}$ + STIM1 C49Mmcherry, STIM1 $^{-/-}$ + STIM1 C56Mmcherry and STIM1 $^{-/-}$ + STIM1 C49M/C56Mmcherry (DM) were used for these experiments. A) STIM1 is expressed in all MEF cell lines, except for the STIM1 $^{-/-}$ + EVmcherry one, which served as a negative control. B) Adding 100 μ M EGTA as a negative control showed no STIM1 oligomerization. C) Punctae formation was significantly reduced in all mutants compared to STIM1 WT after adding 1 μ M TG for 10 min and triggering Ca^{2+} store depletion. STIM1 oligomerization in the DM was even more decreased than in the C56M mutant. D) 20 min treatment with 100 μ M H_2O_2 triggered punctae formation in STIM1 WT cells, but not in the mutants. STIM1 expression was verified via immunoblotting. One exemplary blot is shown, size is indicated. Punctae formation was measured in living cells via a high content screening microscope. For analysis, cells were identified by their DAPI stained nuclei and the software distinguished texture properties. The STIM1 mcherry signal and protein structure was divided into punctae, reticular or smooth and cells were classified respectively. Data are displayed as stacked bar graphs with SD. Statistical significance was calculated using the Kruskal Wallis test with Dunn's multiple comparison test (B and D) or the one-way ANOVA variance test with Tukey's multiple comparison test (C), * $p < 0.05$, n=number of cells is indicated

6 RESULTS

6.15 SOCE IS INCREASED IN STIM1 MUTANTS

Hawkins et al. showed that oxidative stress enhanced Ca^{2+} influx into the cells and mutation of STIM1 C56 or STIM1 C49 and C56 leads to constitutive Ca^{2+} entry independent of intracellular stores (Hawkins et al., 2010), whereas Prins et al. reported SOCE is inhibited in the STIM1 C49A/C56A double mutant (Prins et al., 2011). These contradictory results led to the performance of the next experiments to test the STIM1 mutants created in our laboratory.

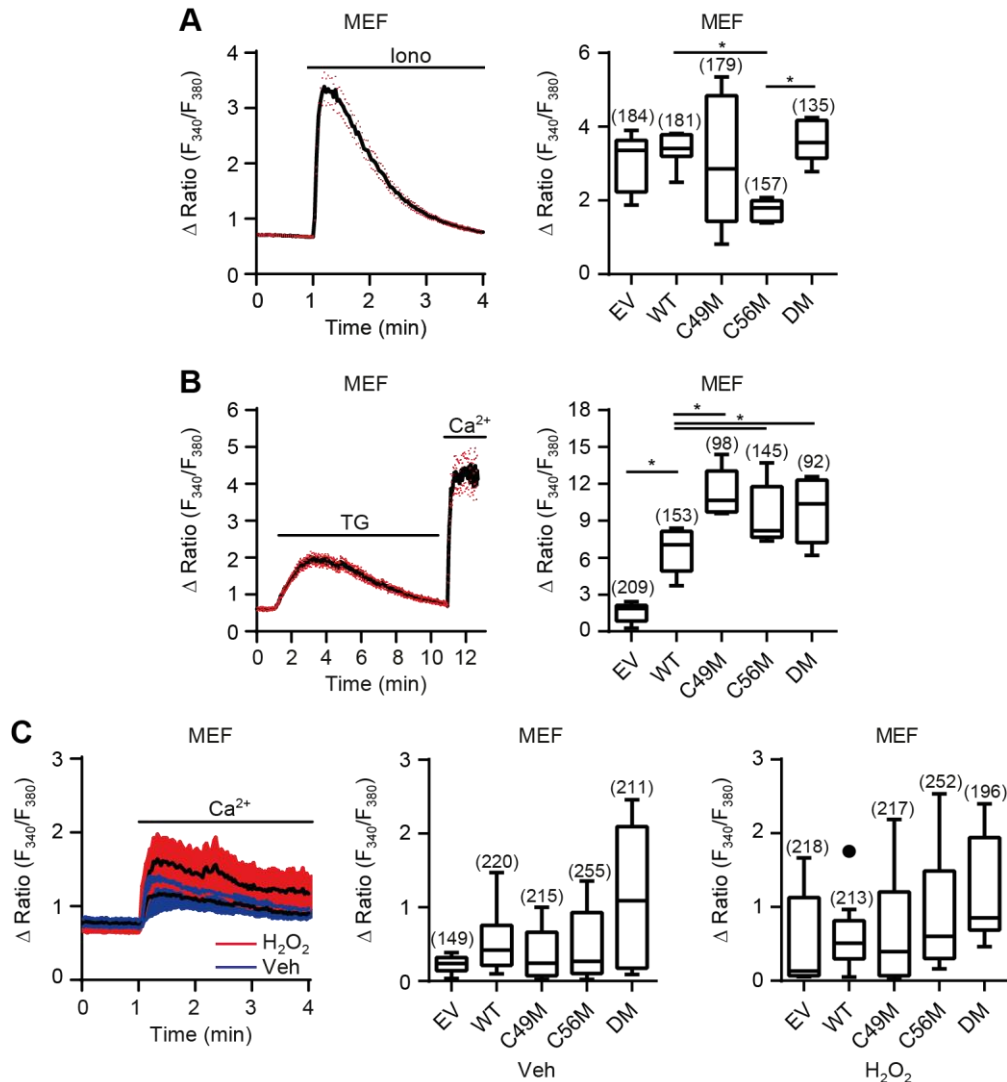


Figure 23: SOCE is increased in STIM1 mutants.

The MEF cell lines STIM1 ^{-/-} + empty vector (EV) mcherry, STIM1 ^{-/-} + STIM1 WTmcherry, STIM1 ^{-/-} + STIM1 C49Mmcherry, STIM1 ^{-/-} + STIM1 C56Mmcherry and STIM1 ^{-/-} + STIM1 C49M/C56Mmcherry (DM) were used for these experiments. A) An example curve for the measurement of Ca^{2+} store depletion in MEF cells is displayed, in which first 100 μM EGTA was added to the cells before or 100 nM lono was applied. The C56M mutant had a significantly decreased Ca^{2+} store depletion (peak Fura-2-AM ratio lono – Fura-2-AM ratio before lono application) compared to STIM1 WT or DM. B) An example curve for the measurement of SOCE is shown, where 100 μM EGTA was added before 1 μM TG and

6 RESULTS

finally 2 mM of Ca^{2+} were applied. All mutants had a significantly increased SOCE (peak Fura-2-AM ratio Ca^{2+} – Fura-2-AM ratio before Ca^{2+} application) compared to STIM1 WT, whereas the negative control, STIM1 $-/-$ + Evmcherry, did not show any SOCE activity after Ca^{2+} was added. C) An example curve of oxidative-stress induced Ca^{2+} entry is shown. 100 μM EGTA was added before cells were incubated with or without 100 μM H_2O_2 for 20 min and 2 mM Ca^{2+} was applied. There was no increase in Ca^{2+} entry after applying Ca^{2+} in cells incubated with or without H_2O_2 (peak Fura-2-AM ratio Ca^{2+} – Fura-2-AM ratio before Ca^{2+} application). Ca^{2+} levels were measured via fluorescence ratio (F_{340}/F_{380}) of the Ca^{2+} indicator Fura-2-AM. Data are displayed as Tukey's box and whiskers plots. Statistical significance was calculated using the one-way ANOVA variance test with Tukey's multiple comparison test (A and B) or the Kruskal Wallis test with Dunn's multiple comparison test (C), * $p < 0.05$, $n =$ number of cells is indicated

An example curve for the measurement of Ca^{2+} store depletion in MEF cells is displayed in Figure 23A, in which first 100 μM EGTA was added to the cells before 100 nM Iono was applied. Ca^{2+} levels were measured via fluorescence ratio (F_{340}/F_{380}) of the Ca^{2+} indicator Fura-2-AM and revealed decreased Ca^{2+} store depletion (peak Fura-2-AM ratio Iono – Fura-2-AM ratio before Iono application) in the C56M mutant compared to STIM1 WT or DM (Figure 23A). Figure 23B shows an example curve for the measurement of SOCE, where 100 μM EGTA was added before 1 μM TG and finally 2 mM of Ca^{2+} were applied. All mutants had a significantly increased SOCE (peak Fura-2-AM ratio Ca^{2+} – Fura-2-AM ratio before Ca^{2+} application) compared to STIM1 WT, whereas the negative control, STIM1 $-/-$ + EV mcherry, did not show any SOCE activity after Ca^{2+} was added (Figure 23B). An example curve of oxidative-stress induced Ca^{2+} entry is shown in Figure 23C. Here 100 μM EGTA was added before cells were incubated with or without 100 μM H_2O_2 for 20 min and 2 mM Ca^{2+} was applied. I did not find any increase in Ca^{2+} entry after applying Ca^{2+} in cells incubated with or without H_2O_2 (peak Fura-2-AM ratio Ca^{2+} – Fura-2-AM ratio before Ca^{2+} application). These results suggest that negative regulation of SOCE might not function in STIM1 mutants and although H_2O_2 causes punctae formation in STIM1 WT cells, it is not enough to cause oxidative stress-induced Ca^{2+} entry.

6.16 DMF DOES NOT ALTER GLUCOSE-UPTAKE, BUT MITOCHONDRIAL RESPIRATION AND SUPEROXIDE LEVELS

Due to the hypothesis that SERCA C674 is oxidized by high glucose (Tong et al., 2008) and the resulting inactivation could be responsible for the diminished Ca^{2+} content in the ER, I studied if there were any alterations in glucose-uptake in DMF-treated cells. Therefore, I performed a flow cytometric measurement of splenocytes incubated with 2-(N-(7-nitrobenz-2-oxa-1,3-

6 RESULTS

diazol-4-yl)amino)-2-deoxyglucose (2-NBDG), a fluorescent glucose analog. SJL mice treated in vivo with 75 mg DMF/kg mouse/day for 23 days showed no difference in glucose-uptake compared to control mice (Figure 24A). In addition to the glucose-uptake, mitochondrial respiration plays an important role in the energy balance of the cell and can be affected by oxidative stress (Kowaltowski and Vercesi, 1999). DMF is reported to inactivate glyceraldehyde 3-phosphate dehydrogenase (GAPDH) by succination of its catalytic cysteine and thereby downregulating aerobic glycolysis in mitochondria (Kornberg et al., 2018). Thus, I investigated mitochondrial oxygen consumption via high-resolution respirometry and the existence of superoxide in mitochondria via flow cytometric analysis of MitoSox™. Splenocytes were isolated from SJL mice and treated with 10 μ M DMF or Veh for 24 h. Similar to the results in 6.1, Figure 24B reveals that there was significantly less mitochondrial superoxide in T cells incubated with DMF for 24 h, whereas there was no effect in B cells. In this case, superoxide dismutase could be upregulated to protect from DMF-induced oxidative stress. In Figure 24C an example picture of a high-resolution respirometric experiment following the coupling control protocol is displayed with the different treatments and resulting respiration measured. First, the routine respiration (routine, R) was recorded, before 2 μ g/ml of oligomycin (Omy) inhibited the ATP synthase and leak respiration (leak, L) was determined. Then, FCCP (F) was titrated in 0.5 μ M steps until the respiratory chain was uncoupled. The electron transfer system (ETS, E) capacity was measured at the maximum oxygen flux with optimum FCCP concentration. This is a state of experimentally induced maximum non-coupled respiration (Pesta and Gnaiger, 2012) and shows the value of oxygen consumption that would occur if all enzymes functioned at maximum activity. After the addition of 0.5 μ M rotenone (Rot; inhibitor of complex I) and 2.5 μ M antimycin A (Ama; inhibitor of complex III), respiration was completely inhibited and the non-mitochondrial residual oxygen consumption (ROX) was recorded. ROX was used to correct routine, leak and ETS, which allows comparison of mitochondrial oxygen consumption between cells and experiments. Figure 24D shows that splenocytes, treated with 10 μ M DMF for 24 h, consumed similar oxygen levels at routine and leak respiration as Veh-treated cells. DMF significantly reduced ETS but interestingly, also increased ROX in lymphocytes (Figure 24D). Reduced ETS levels in DMF-treated cells indicate DMF-induced alterations at the four enzyme complexes.

6 RESULTS

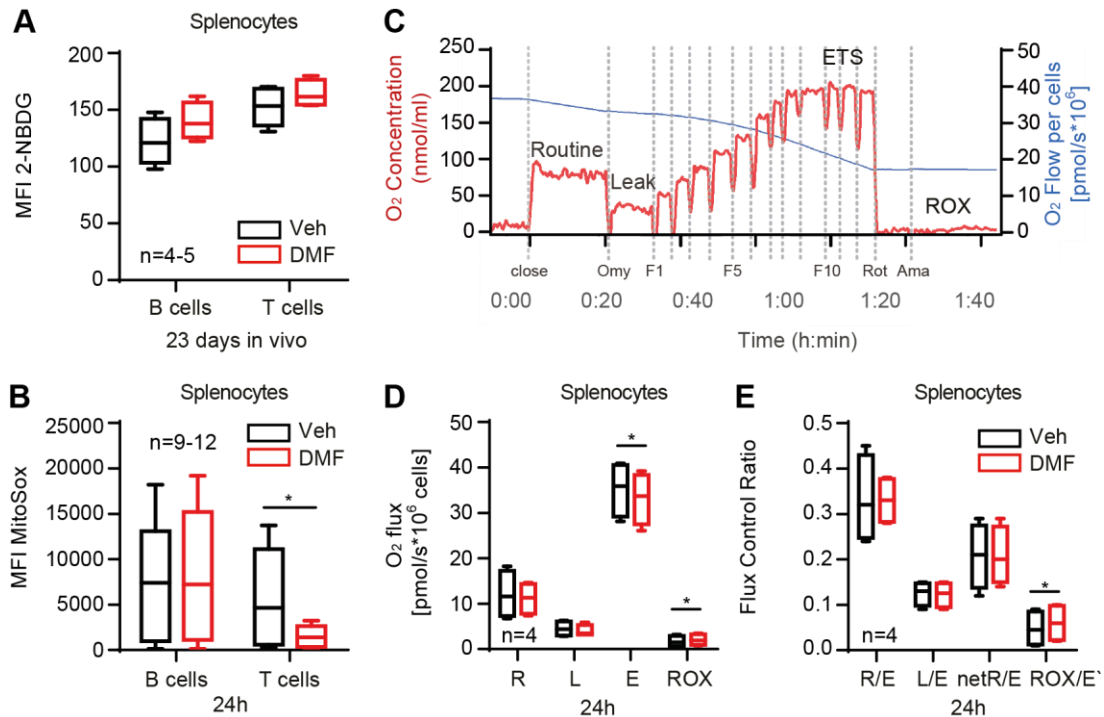


Figure 24: DMF does not alter glucose-uptake, but mitochondrial respiration and superoxide levels. Splenocytes from SJL mice were treated in vivo with 75 mg DMF/kg mouse/day for 23 days and ex vivo with 10 μ M DMF or Veh for 24 h. A) SJL mice treated in vivo with DMF showed no difference in glucose-uptake compared to control mice. B) Significantly less mitochondrial superoxide was measured in T cells incubated with DMF for 24 h, whereas there was no effect in B cells. C) An example picture of a high-resolution respirometric experiment following the coupling control protocol is displayed. Oxygen concentration (nmol/ml) and the rate of respiration, defined as oxygen flow ($\text{pmol/s} \cdot 10^6$ cells) are indicated as blue and red traces, respectively. First, the routine respiration (R) was recorded, before 2 μ g/ml of oligomycin (Omy) inhibited the ATP synthase and leak respiration (L) was determined. Then, FCCP (F) was titrated in 0.5 μ M steps to measure the electron transfer system (ETS, E) capacity. After the addition of 0.5 μ M rotenone (Rot; inhibitor of complex I) and 2.5 μ M antimycin A (Ama; inhibitor of complex III), the non-mitochondrial residual oxygen consumption (ROX) was recorded. D) DMF-treated splenocytes consumed similar amounts of oxygen in ROX-corrected routine and leak respiration as Veh-treated cells, but DMF significantly reduced ROX-corrected ETS and increased ROX in lymphocytes. E) A difference between Veh- or DMF-treated cells was not discovered in the corrected respiratory states R/E, L/E or netR/E (netR=R-L). DMF significantly increased ROX, normalized to the uncorrected ETS state E'. Glucose-uptake and mitochondrial superoxide levels were analyzed by flow cytometry using the median fluorescence intensity of the fluorescent glucose analog 2-(N-(7-nitrobenz-2-oxa-1,3-diazol-4-yl)amino)-2-deoxyglucose (2-NBDG) or the mitochondrial superoxide dye MitoSoxTM. T cells were stained with Anti-CD3, B cells with Anti-CD45R/B220. Mitochondrial respiration was determined via high-resolution respirometry. Statistical variation is shown as Tukey's box and whiskers plots and significance was calculated using the parametric two-tailed t-test, * $p < 0.05$, n=number of mice (A and B) or experiments (D and E) is indicated

In order to compare the fractions of the ETS capacity used for routine, leak or netR (netR=routine-leak; the fraction used for ATP production) in the cells irrespective of mitochondrial content and cell size, the respiratory states were expressed as flux control ratios

6 RESULTS

in relation to the maximum ETS capacity (states R/E, L/E or net R/E). I did not detect a difference between Veh- or DMF-treated cells in any of the corrected respiratory states shown in Figure 24E. Apart from that, DMF significantly increased ROX, normalized to the uncorrected ETS state E' (ROX/ E'). The non-mitochondrial oxygen consumption ROX can be explained by autooxidation reactions and the activity of oxygen-consuming enzymes, including oxidases (Pesta and Gnaiger, 2012), which are most probably upregulated in order to reduce the DMF-induced oxidative stress. To conclude, glucose-uptake is not altered by DMF, but mitochondrial respiration and mitochondrial superoxide levels are.

6.17 DMF DOES NOT CAUSE ER STRESS

Disturbances in cellular redox-maintenance or Ca^{2+} levels, can affect ER functioning and trigger a cellular stress reaction, the unfolded protein response (UPR), to compensate for damage (Boyce and Yuan, 2006). As DMF causes short-term oxidative stress, increases intracellular Ca^{2+} levels and decreases Ca^{2+} store content in splenocytes, SERCA2b inhibition by oxidation of C674 was hypothesized. ER stress mechanisms were subject of my further research to test if DMF-evoked SERCA2b inhibition is a trigger for ER stress. Upon UPR activation different stress sensors are stimulated. Activating transcription factor 6 (ATF6) induces the mRNA of X box-binding protein 1 (XBP1) and inositol-requiring enzyme 1 α (IRE1 α) splices the XBP1 mRNA to produce an active transcription factor (Yoshida et al., 2001). To analyze XBP1 mRNA expression levels of the unspliced and spliced forms, I isolated mRNA from STIM1 WT MEF cells and splenocytes and performed qPCR with the TaqMan method. This method is based on TaqMan probes that are complementary to the target sequence and anneal during qPCR. They consist of a fluorophore, covalently attached to its 5'-end, and a quencher at its 3'-end. The quencher molecule quenches fluorescence emitted by the fluorophore when excited, as long as both are in proximity. 5' to 3' exonuclease activity of the Taq polymerase degrades the probe during extension. This degradation releases the fluorophore from the quencher. Hence, fluorescence intensity detected in the qPCR is directly proportional to the fluorophore released and the amount of cDNA template present. Figure 25 A shows no alterations in the spliced and unspliced form of XBP1 mRNA expressed in STIM1 WT MEF cells after 1 h or 24 h incubation with 10 μM DMF compared to Veh. DMF did not significantly increase the relative mRNA expression of spliced XBP1 in splenocytes treated ex vivo with 10 μM DMF for 24 h nor in vivo

6 RESULTS

with 75 mg DMF/kg mouse/day for 23 days (Figure 25B). I could not detect expression changes in calnexin after 23 days of in vivo incubation of DMF (Figure 25C) nor was binding immunoglobulin protein (BiP) abundance altered upon 17-29 days of DMF treatment (Figure 25D). Taken all together, these results suggest that DMF does not cause ER stress, which is in line with my finding that SERCA2b is not inhibited but rather activated by DMF.

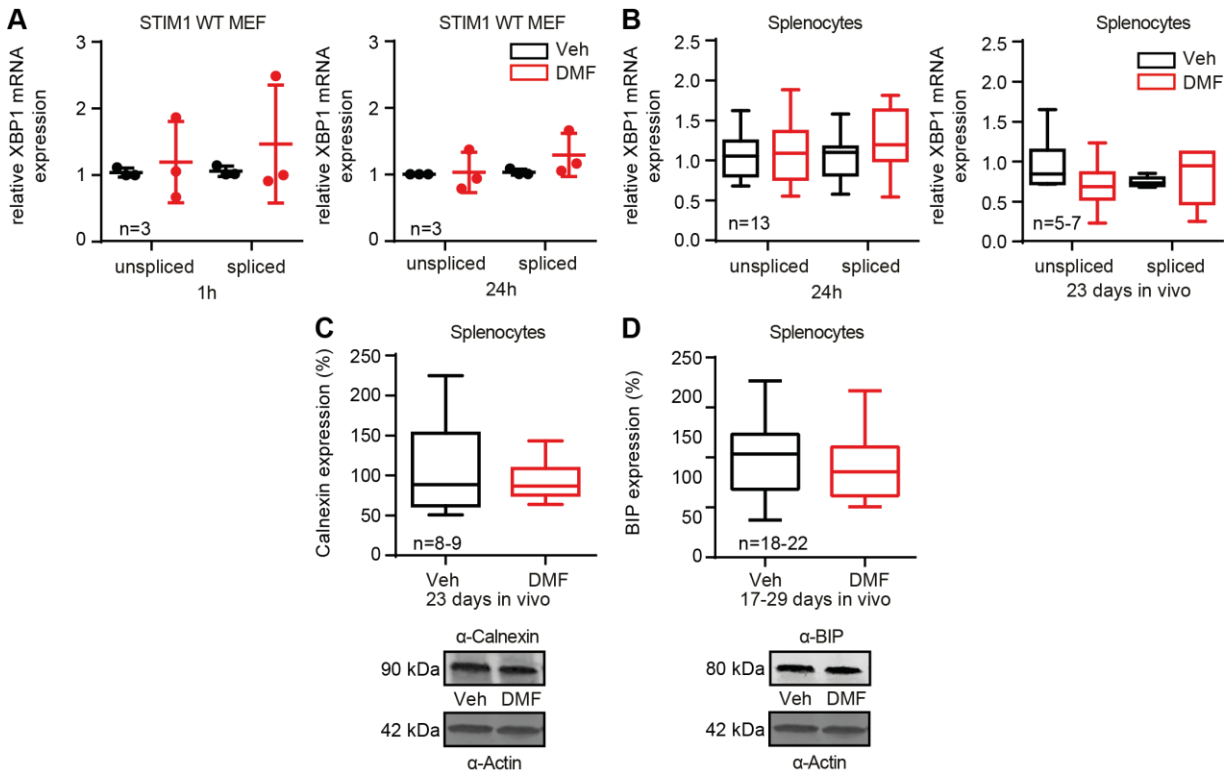


Figure 25: DMF does not cause ER stress.

STIM1 WT MEF cells were incubated with 10 μ M DMF or Veh for 1 h or 24 h. Splenocytes from SJL mice were treated ex vivo with 10 μ M DMF or Veh for 24 h or in vivo with 75 mg DMF/kg mouse/day for 17-29 or 23 days. A) mRNA expression of the spliced and unspliced form of relative X box-binding protein 1 (XBP1) was not altered in STIM1 WT MEF cells after 1 h or 24 h of DMF incubation. B) Ex vivo or in vivo treatment of DMF did not change relative XBP1 mRNA expression in splenocytes. C) DMF did not cause expression changes in calnexin after 23 days of incubation. D) Binding immunoglobulin protein (BiP) abundance was not altered after 17-29 days of DMF treatment. mRNA from STIM1 WT MEF cells and splenocytes was isolated and qPCR with the TaqMan method was performed to test XBP1 mRNA expression levels. Calnexin and BiP abundance in immunoblots was normalized to actin. One exemplary blot for each experiment is shown, size is indicated. Data are displayed as Tukey's box and whiskers plots or scatter dot plots with SD. Statistical significance was calculated using the one-way ANOVA variance test with Tukey's multiple comparison test (A and B) or the parametric two-tailed t-test (C and D), n=number of experiments (A) or mice (B, C and D) is indicated

6.18 NFAT EXPRESSION IS NOT ALTERED BY DMF, BUT ITS TRANSLOCATION INTO THE NUCLEUS IS INCREASED

Disturbances in Ca^{2+} homeostasis can affect intracellular signaling of transcription factors. As DMF increases cytosolic Ca^{2+} levels but decreases SOCE and reduces Ca^{2+} in intracellular stores, nuclear factor of activated T cells (NFAT) was the focus of research in the next experiments. In order to examine NFAT abundance, SJL mice were treated ex vivo with 10 μM DMF or Veh for 24 h or in vivo with 75 mg DMF/kg mouse/day for 8 days.

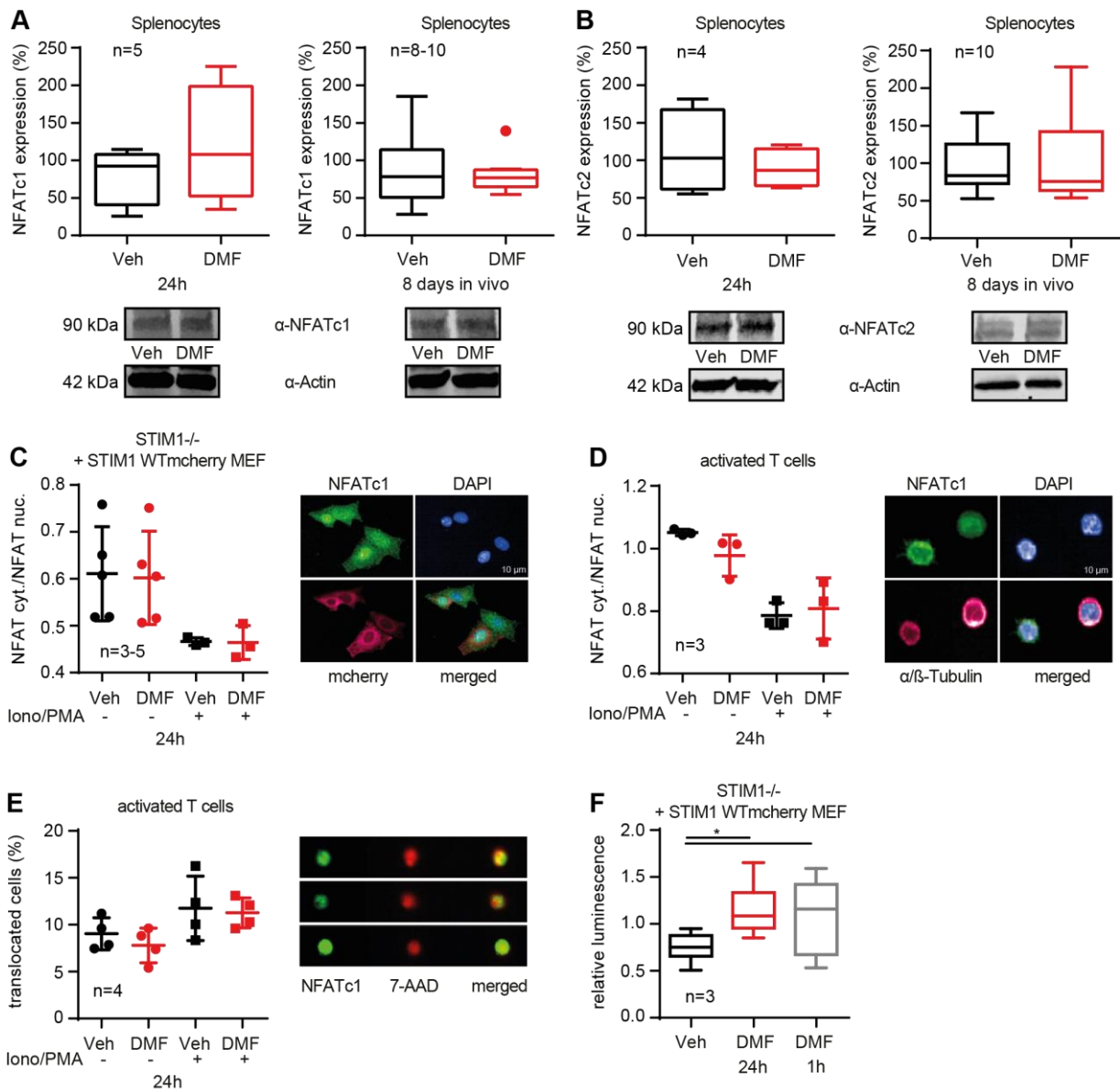


Figure 26: NFAT expression is not altered by DMF, but its translocation into the nucleus is increased. Splenocytes and activated T cells from SJL mice were treated ex vivo with 10 μM DMF or Veh for 24 h or in vivo with 75 mg DMF/kg mouse/day for 8 days. STIM1^{-/-} + STIM1 WTmcherry MEF cells were treated with 10 μM DMF or Veh for 1 h or 24 h. A and B) There were neither alterations in expression

6 RESULTS

levels of nuclear factor of activated T cells c1 (NFATc1) (A) nor of NFATc2 (B) in splenocytes treated ex vivo or in vivo with DMF. C and D) DMF did not alter the ratio of NFATc1 in cytoplasm (cyt.) to NFATc1 in nucleus (nuc.) in ICC samples of STIM1 $-/-$ + STIM1 Wtmcherry MEF cells, treated with or without Iono/PMA (C) or activated T cells, not reactivated or reactivated with Iono/PMA (D). E) In DMF-treated samples of activated T cells (not reactivated or reactivated with Iono/PMA) the number of cells in which NFAT translocated to the nucleus did not differ from that in Veh when counted by imaging flow cytometry. F) The relative luciferase luminescence and therefore NFAT promotor activity was significantly increased after 1 h and 24 h of DMF treatment. NFATc1 and NFATc2 abundance in immunoblots was normalized to actin. One exemplary blot for each experiment is shown, size is indicated. NFAT translocation was analyzed using high content screening microscopy, imaging flow cytometry or the Dual-Glo[®] Luciferase assay. For ICC the DNA dye DAPI and antibodies against NFATc1 and α/β -tubulin were used. Imaging flow cytometry was performed using an NFATc1 antibody and the DNA dye 7-AAD. T cells were stained with Anti-CD3. For the Dual-Glo[®] Luciferase assay, NFAT firefly luciferase was co-transfected with the control, renilla luciferase, and normalized to it. Data are displayed as Tukey's box and whiskers plots or scatter dot plots with SD. Statistical significance was calculated using the parametric two-tailed t-test (A and B) or the one-way ANOVA variance test with Tukey's multiple comparison test (C, D, E and F). The non-parametric Mann-Whitney test was used for in vivo experiments in A) and B), * $p < 0.05$, n=number of mice (A and B) or experiments (C, D, E and F) is indicated

I found neither alterations in expression levels of NFATc1 (Figure 26A) nor of NFATc2 (Figure 26B) in splenocytes treated ex vivo or in vivo with DMF compared to controls. The activation and thus translocation of NFAT into the nucleus was examined next. STIM1 $-/-$ + STIM1 Wtmcherry MEF cells, treated with or without Iono/PMA or activated T cells, not reactivated or reactivated with Iono/PMA, were incubated with 10 μ M DMF or Veh for 24 h and translocation of NFATc1 was examined via immunocytochemistry (ICC) or imaging flow cytometry. I analyzed the ratio of NFATc1 in the cytoplasm (cyt.) to NFATc1 in the nucleus (nuc.) in ICC samples, but neither in STIM1 $-/-$ + STIM1 Wtmcherry MEF cells (Figure 26C), nor in activated T cells (Figure 26D) I saw changes in NFATc1 translocation. In DMF-treated samples of activated T cells, the number of cells in which NFAT translocated to the nucleus did not differ from that in Veh when counted by imaging flow cytometry (Figure 26E). Figure 26F shows the result of the Dual-Glo[®] Luciferase assay. STIM1 $-/-$ + STIM1 Wtmcherry MEF cells were transfected with an NFAT firefly luciferase construct under the expression control of the interleukin-2 (IL-2) promotor and a renilla luciferase construct under the control of the CAG promotor. The firefly luciferase reporter is linked to a specific stimulus (NFAT translocation and IL-2 promotor induction) and can be normalized to the activity of the co-transfected renilla luciferase control reporter. After 1 h and 24 h treatment with 10 μ M DMF the relative

6 RESULTS

luciferase luminescence and therefore NFAT promoter activity was significantly increased. Next, I investigated another transcription factor known to be affected by Ca^{2+} signaling.

6.19 DMF DOES NOT CHANGE NF-KB EXPRESSION AND TRANSLOCATION

A second transcription factor that could be affected by disturbed Ca^{2+} homeostasis is the nuclear factor kappa-light-chain-enhancer of activated B cells (NF- κ B).

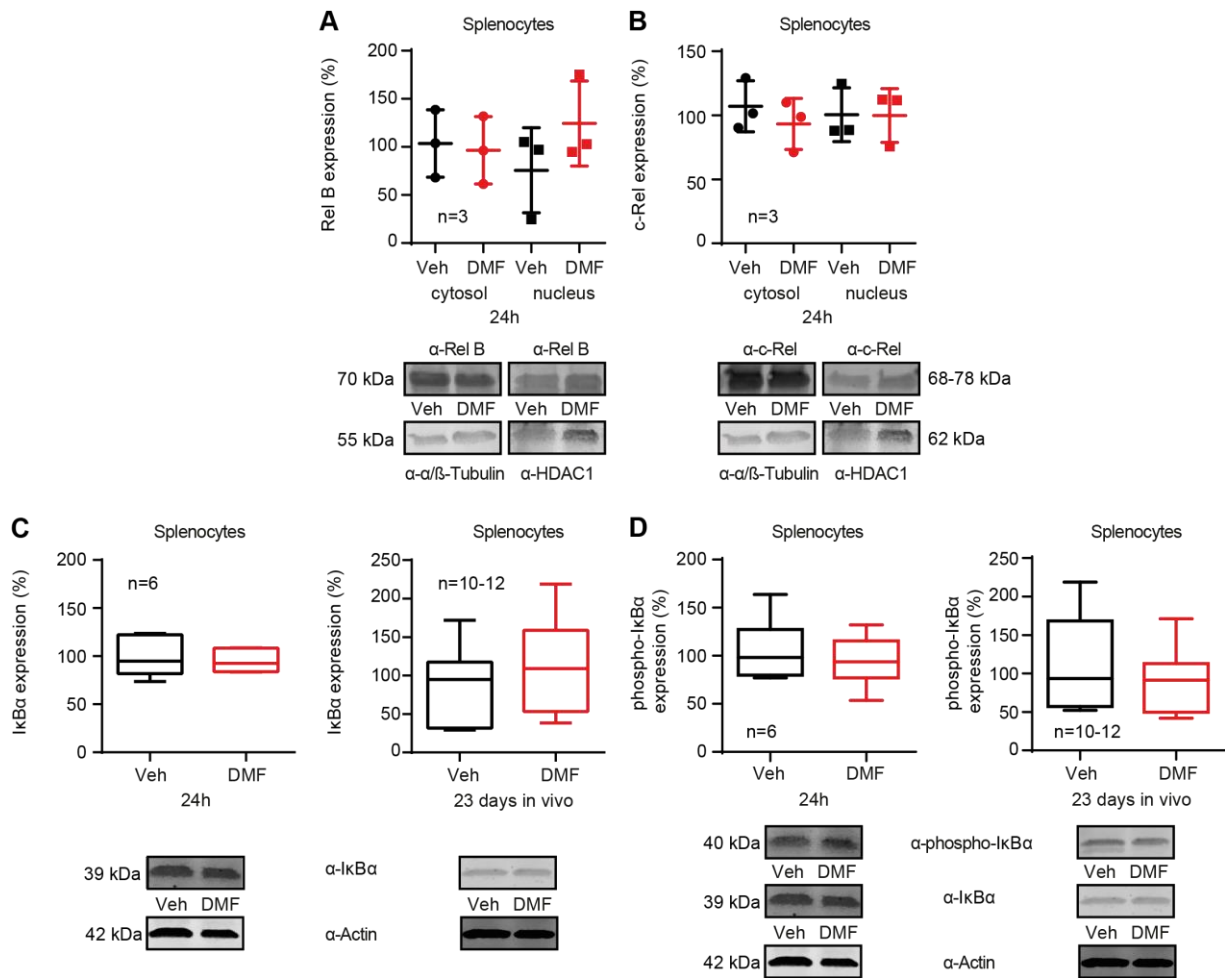


Figure 27: DMF does not change NF- κ B expression.

Splenocytes from SJL mice were treated ex vivo with 10 μM DMF or Veh for 24 h or in vivo with 75 mg DMF/kg mouse/day for 23 days. A and B) There were no DMF-evoked alterations in expression levels of RelB (A) or c-Rel (B) in the cytosolic or in the nuclear fraction. C and D) Neither total I κ B α (C) nor phospho-I κ B α (D) abundance was changed in splenocytes treated ex vivo or in vivo with DMF compared to controls. RelB and c-Rel expression were normalized to α/β -tubulin (cytosolic fraction) or HDAC1 (nuclear fraction). Total I κ B α abundance was normalized to actin and phospho-I κ B α expression to the already normalized total I κ B α . One exemplary blot for each experiment is shown, size is indicated. Data are displayed as Tukey's box and whiskers plots or scatter dot plots with SD. Statistical significance was calculated using the one-way ANOVA variance test with Tukey's multiple comparison test (A and B) or the parametric two-tailed t-test (C and D), n=number of mice is indicated

6 RESULTS

In order to test NF- κ B abundance, SJL mice were treated ex vivo with 10 μ M DMF or Veh for 24 h or in vivo with 75 mg DMF/kg mouse/day for 23 days. NF- κ B proteins of the canonical and non-canonical pathway were tested. I found no DMF-provoked alterations in expression levels of RelB (Figure 27A) or c-Rel (Figure 27B) in the cytosolic or in the nuclear fraction. Neither total I κ B α (Figure 27C) nor phospho-I κ B α (Figure 27D) abundance was changed in splenocytes treated ex vivo or in vivo with DMF compared to controls.

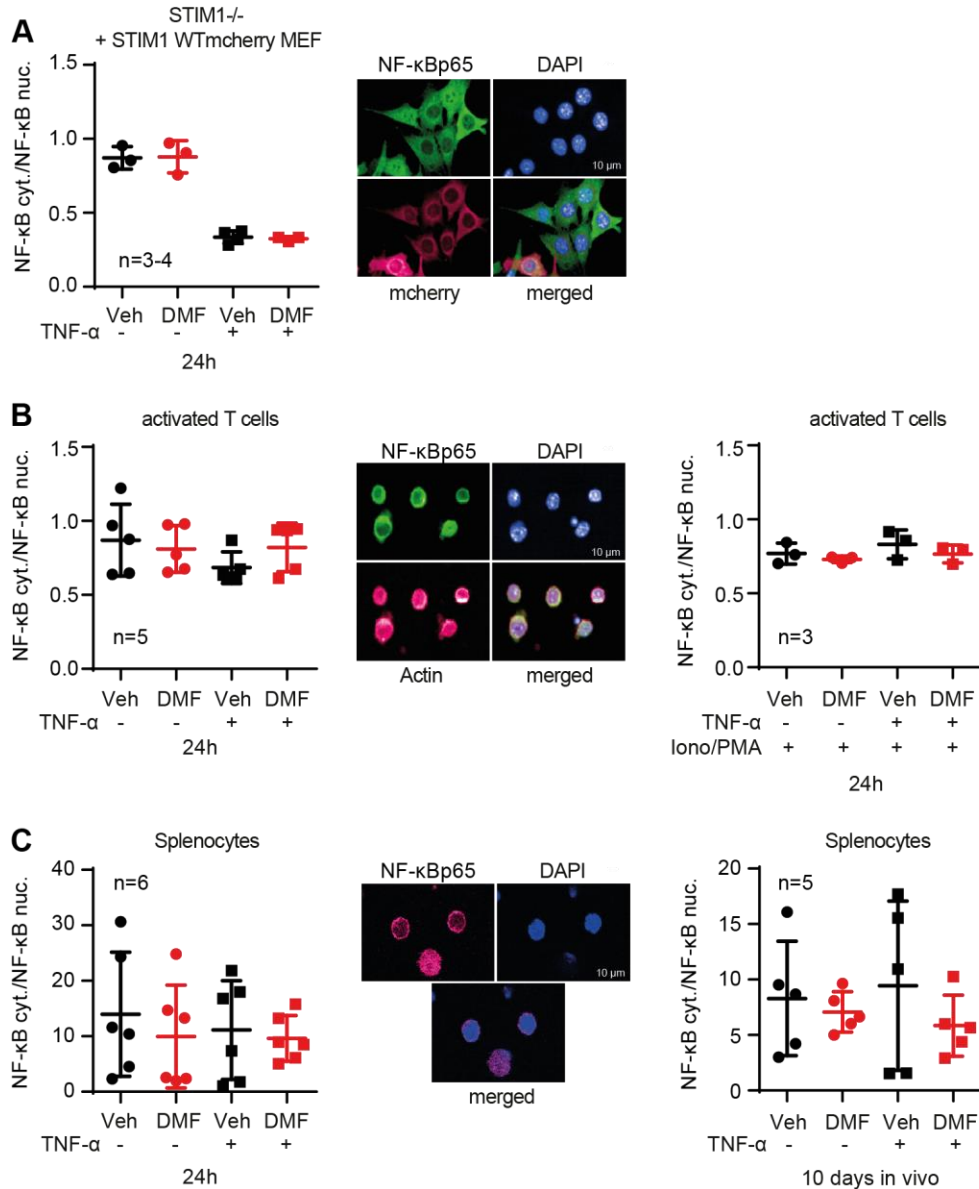


Figure 28: DMF does not change NF- κ B translocation.

Splenocytes were isolated from SJL mice and treated ex vivo with Veh or 10 μ M DMF for 24 h or in vivo with 75 mg DMF/kg mouse/day for 10 days. STIM1^{-/-} + STIM1 WTmcherry MEF cells and activated T cells were treated with 10 μ M DMF or Veh for 1 h or 24 h. A, B and C) There were no DMF-evoked alterations in nuclear factor kappa-light-chain-enhancer of activated B cells (NF- κ B) translocation in

6 RESULTS

STIM1 $-/-$ + STIM1 Wtmcherry MEF cells (A), activated T cells, not reactivated or reactivated with Iono/PMA (B) or in splenocytes treated ex vivo or in vivo with DMF (C), irrespective of the absence or presence of TNF- α . NF- κ B translocation was analyzed using high content screening microscopy. The DNA dye DAPI and antibodies against NF- κ B p65 and actin were used for ICC. Data are displayed as scatter dot plots with SD. Statistical significance was calculated using the one-way ANOVA variance test with Tukey's multiple comparison test, n=number of experiments is indicated

The activation and thus translocation of NF- κ B into the nucleus was examined next. STIM1 $-/-$ + STIM1 Wtmcherry MEF cells, splenocytes and activated T cells, not reactivated or reactivated with Iono/PMA, were incubated with 10 μ M DMF or Veh for 24 h and translocation of NF- κ B was examined after the incubation with 10 ng TNF- α for 10 min. I analyzed the ratio of NF- κ B in the cytoplasm (cyt.) to NF- κ B in the nucleus (nuc.) in ICC samples, but neither in STIM1 $-/-$ + STIM1 Wtmcherry MEF cells (Figure 28A), nor in activated T cells (Figure 28B) I saw DMF-evoked changes in NF- κ B translocation. Splenocytes treated in vivo with 75 mg DMF/kg mouse/day for 10 days or splenocytes treated ex vivo with DMF did not show any translocation alterations compared to controls, either (Figure 28C). Altogether, I could not find any modifications in the NF- κ B pathway in contrast to, for example, a publication of Loewe et al., in which DMF was reported to inhibit translocation of Rel A (p65) in human endothelial cells (Loewe et al., 2002).

7 DISCUSSION

Dimethyl fumarate (DMF) is a treatment option for the autoimmune diseases multiple sclerosis and psoriasis. Its immunosuppressive effect, however, is poorly understood. As calcium (Ca^{2+}) signaling plays a very important role in the correct functioning of the immune system, this work focused on the understanding how DMF influences the calcium homeostasis in immune cells and if the DMF-induced changes in cellular redox state are responsible for its immunomodulatory effects. My observations present profound but rather pleiotropic effects of DMF on various key players in Ca^{2+} signaling. These changes are most probably caused by thiol modifications induced by DMF-mediated changes in redox homeostasis.

In detail, DMF first caused oxidative stress after 1 h treatment by depleting glutathione (GSH), before it induced the antioxidant defense system, thus increasing GSH levels and decreasing reactive oxygen species (ROS) levels again after 24 h. These results confirm the data recently obtained in neuronal cells (Albrecht et al., 2012), in which the DMF-evoked short-lived oxidative stress activated cellular antioxidant response via the transcription factor nuclear factor erythroid 2-related factor 2 (Nrf2). Held et al. already found in 1988 that DMF depletes intracellular glutathione (Held et al., 1988). Further studies of Schmidt et al. revealed a spontaneous reaction of DMF with GSH due to its α,β -unsaturated electrophilic nature (Schmidt et al., 2007) and showed that glutathione is rapidly deprived by DMF in cultured primary astrocytes (Schmidt and Dringen, 2010). Activation of the Nrf2 pathway prevents oxidative stress-induced neuronal cell death (Li et al., 2005; Satoh et al., 2006). Several studies showed that DMF induces the Nrf2 pathway, hence, having neuroprotective effects (Lin et al., 2011; Linker et al., 2011; Albrecht et al., 2012).

Additionally, activated T cells did not show any signs of oxidative stress anymore after 24 h incubation with DMF and in samples of DMF long-term in vivo treatment, GSH levels and ROS levels in T cells were not altered compared to the control, indicating a restored balance in the redox state here as well. Contrary to the results of Hoffmann et al. in a hippocampal mouse cell line (Hoffmann et al., 2017), DMF treatment did not significantly increase glutathione reductase (GSR) expression and thus GSH recycling in splenocytes, possibly due to differences in the model systems used. My results suggest that GSR does not play a major role in splenocytes in terms of oxidative response.

7 DISCUSSION

DMF and monomethyl fumarate (MMF) are reported to induce an intracellular Ca^{2+} increase in granulocytes (Nibbering et al., 1993) and keratinocytes (Thio et al., 1994). My experiments in splenocytes revealed that DMF affected direct Ca^{2+} influx from the extracellular space. Mouse embryonic fibroblast (MEF) cells showed the same tendency. Patch clamping data point to a transient receptor potential (TRP) channel because DMF induced a significant current and the DMF-evoked IV showed characteristics of a TRP channel. Flow cytometric results suggested the involvement of transient receptor potential ankyrin 1 (TRPA1) because the specific TRPA1 antagonists HC030031 (McNamara et al., 2007) and A967079 (Chen et al., 2011) abolished the DMF-evoked cytosolic Ca^{2+} increase, whereas lanthanum (III) chloride and ruthenium red, which block a broad spectrum of TRP channels (Dray et al., 1990; Caterina et al., 1997; Caterina et al., 1999; Strotmann et al., 2000; Hoenderop et al., 2001; Peier et al., 2002; Bouron et al., 2015), decreased intracellular Ca^{2+} concentration in Veh control and DMF-treated cells. Additionally, TRPA1 was previously shown to be activated by thiol-reactive molecules (Andersson et al., 2008) and the cysteines necessary for channel activation to be modified by cysteine-reactive inflammatory mediators (Takahashi et al., 2008). Incubation of four TRP channel antagonists in a row during whole-cell patch clamping, on the other hand, could neither verify TRPA1 as the source of DMF-mediated direct Ca^{2+} influx into the cell nor specify another TRP channel. TRPA1 antagonists HC030031 (McNamara et al., 2007) and A967079 (Chen et al., 2011) had no effect here, suggesting TRPA1 was not directly involved. Nevertheless, I cannot entirely rule out that Ca^{2+} influx through another Ca^{2+} channel triggers the activation and thus Ca^{2+} entry through TRPA1, as TRPA1 contains a Ca^{2+} binding domain (Hinman et al., 2006) and can be induced by increased intracellular Ca^{2+} levels (Doerner et al., 2007). Ruthenium red application during whole-cell patch clamping did not inhibit the DMF-evoked current either, which excluded the transient receptor potential vanilloid (TRPV) family to be responsible for the increase in Ca^{2+} levels, because RuRed blocks TRPV1-6 (Dray et al., 1990; Caterina et al., 1997; Caterina et al., 1999; Strotmann et al., 2000; Hoenderop et al., 2001; Peier et al., 2002). However, flufenamic acid (FFA) that blocks the transient receptor potential canonical (TRPC) and transient receptor potential melastatin (TRPM) family (Guinamard et al., 2013), especially TRPM2 (Hill et al., 2004), unexpectedly evoked a larger current. This could be because it activated TRPA1 (Hu et al., 2010). To come to a conclusion

7 DISCUSSION

about the involvement of TRPA1 in the immediate Ca^{2+} entry and because of the fact that the splenocytes I used, were a mixture of T and B cells as well as maybe activated and not activated ones, more cells have to be patched in the presence of the different antagonists. mRNA expression of TRPA1, TRPM2, and TRPM7 was not changed after DMF treatment but TRPM2 mRNA, in general, was increased after 24 h incubation. At the same time, TRPA1 expression was decreased. A possible reason for increased TRPM2 levels is cytokine production by activated cells in the splenocytes culture because tumor necrosis factor-alpha (TNF- α) is known to upregulate TRPM2 expression (Wehrhahn et al., 2010). On the other hand, TNF- α production is also reported to increase TRPA1 expression (Hatano et al., 2012).

My experiments also revealed cytosolic Ca^{2+} increase as a long-term effect of DMF treatment in vitro and in vivo, this time indicating a Ca^{2+} release from intracellular stores. Indeed, Ca^{2+} store depletion was significantly reduced in splenocytes after 24 h of DMF treatment. These results suggest either a higher leakage of Ca^{2+} from the endoplasmic reticulum (ER) into the cytosol or the inhibition of the Ca^{2+} transport into the ER after 24 h of DMF treatment. To resolve this, I first clarified whether DMF treatment affects the amount and activity of sarco/endoplasmic reticulum Ca^{2+} -ATPase (SERCA) 2b, the SERCA variant, which is expressed ubiquitously (Wu et al., 1995). I found a significantly reduced SERCA2b expression but surprisingly also a higher activity rate, which probably compensates for the reduced expression or a possibly increased ER Ca^{2+} leak. SERCA activity is reported to be prone to stimulatory and inhibitory oxidative posttranslational modifications, especially at the highly conserved cysteine 674 (C674) (Grover et al., 2003; Adachi et al., 2004). Due to reduced Ca^{2+} store depletion I expected DMF to oxidize C674 and thus inhibit SERCA activity as shown by atherosclerosis or high glucose conditions (Adachi et al., 2004; Tong et al., 2008), but instead I found an increase in C674 S-glutathionylation and an increase in Ca^{2+} -ATPase activity, which is in line with the results reported by Adachi et al. (Adachi et al., 2004). As expected, the SERCA2b C674S mutant had a lower activity compared to the wildtype variant. Additionally, DMF had no effect on SERCA2b C674S activity, thus supporting the finding that DMF alters SERCA activity by changing the redox state of this cysteine residue.

I further investigated if there were any changes regarding store-operated Ca^{2+} entry (SOCE), as a decrease in ER Ca^{2+} concentration initiates SOCE through the ER Ca^{2+} sensor stromal

7 DISCUSSION

interaction molecule 1 (STIM1) (Liou et al., 2005; Roos et al., 2005). Indeed, I found a significant reduced SOCE in DMF-treated primary MEF cells after 24 h of DMF treatment. In the STIM1 $-/-$ + STIM1 WTmcherry MEF cell line and in splenocytes the tendency was the same. DMF induced a significant reduction in STIM1 expression in STIM1 WT MEF cells and splenocytes after 24 h, although flow cytometric results could not confirm the reduced STIM1 expression in splenocytes. S-glutathionylation at cysteine 56 is an oxidative posttranslational modification found in STIM1 (Hawkins et al., 2010). The observation that SERCA2b abundance was reduced as well as STIM1 expression suggests a glutathionylation-induced protein degradation as shown in mitochondrial thymidine kinase 2 (Sun et al., 2012) or destabilization and thus degradation of the proteins by the initially DMF-induced oxidative stress. Marinelli et al. calculated the predicted stability for virtually mutated proteins within an extensive database of non-homologous protein structures containing cysteine residues (Martelli et al., 2002) and revealed a clearly destabilizing effect when cysteines were mutated, which mimics their oxidation (Marinelli et al., 2018). That the loss of STIM1 can affect SOCE was shown in a study from Soboloff et al., which pointed out that the correct stoichiometry of STIM1 and the Ca^{2+} release-activated Ca^{2+} (CRAC) channel Orai1 is required for a functional SOCE (Soboloff et al., 2006). Additionally, another group found that eight STIM1 molecules are necessary for the maximal opening of one CRAC channel (Li et al., 2011). Another reason for a reduced SOCE would be the prevention of STIM1 and Orai1 coupling through a low pH caused by DMF-induced oxidative stress. STIM1-Orai1 uncoupling was recently shown in an hypoxia-stimulated acidic environment (Mancarella et al., 2011). DMF-induced increase in cytosolic Ca^{2+} levels, reduced ER Ca^{2+} content and a reduced SOCE appear to be similar to the phenotype of a constitutively active STIM1 EF-hand mutant, that activates Ca^{2+} entry independently from ER Ca^{2+} stores (Henke et al., 2012), too.

Upon activation, STIM1 oligomerizes and forms punctae, both necessary steps to initiate SOCE (Luik et al., 2008). Punctae formation was significantly reduced in MEF STIM1 mutant cells after thapsigargin or hydrogen oxygen (H_2O_2) treatment, indicating the importance of the highly conserved cysteines 49 and 56 in this process. Prins et al. lately found that mutations of these cysteines inhibit STIM1 punctae formation (Prins et al., 2011). Contrary to the results from Hawkins et al. (Hawkins et al., 2010), GSH treatment and thus probable S-glutathionylation of

7 DISCUSSION

STIM1 cysteines showed less oligomerization of STIM1. Nevertheless, S-nitrosylation, another posttranslational modification, was recently shown to stabilize the N-terminal part of STIM1 in a C49 and C56-dependent manner, thus preventing STIM1 oligomerization (Zhu et al., 2018). I propose a similar reaction in S-glutathionylated STIM1. In contrast to Prins et al. (Prins et al., 2011), SOCE was increased in all MEF STIM1 mutants compared to MEF STIM1 WT, suggesting less interaction with the ER oxidoreductase Erp57 followed by less inhibition of SOCE. Together with the finding of less punctae formation, on the other hand, an accelerated SOCE rather points to a non-STIM1-mediated SOCE in the mutants through, for example, TRP channels. TRPC3 and TRPC6 channels, for instance, are known to be activated by diacylglycerol (DAG) (Hofmann et al., 1999), which is produced by phospholipase C (PLC) during phosphatidylinositol-4,5-bisphosphate (PIP2) cleavage. PLC itself can be activated by Ca^{2+} (Kadamur and Ross, 2013), which is intracellularly increased after ER store depletion. Another possible explanation for a higher SOCE in the MEF STIM1 mutant cells could be a compensatory higher expression or activity of STIM2. To prove this hypothesis, these SOCE experiments have to be repeated in STIM2 $-/-$ cells. Contradictory to the results from Hawkins et al. (Hawkins et al., 2010), I did not find a constitutive Ca^{2+} entry independent from intracellular Ca^{2+} stores in MEF STIM1 mutants or an increased oxidative-stress induced Ca^{2+} entry in MEF STIM1 WT. Differences in the Ca^{2+} dye and the cells used could be responsible for the different results. Contrary to the chicken B cell line DT40 for STIM1 mutants and the MEF STIM1 WT cells in the study of Hawkins et al. (Hawkins et al., 2010), I used STIM1 WTmcherry and mutant MEF cells that were created from STIM1 $-/-$ cells. Whereas Hawkins et al. worked with Fluo-4 (Hawkins et al., 2010), I used the ratiometric dye Fura-2, which allows a more accurate determination of the intracellular Ca^{2+} concentration because the artificial effects of uneven dye loading and photobleaching are reduced within this method.

Although DMF alters the cellular redox state and increases intracellular Ca^{2+} levels, no signs of ER stress could be detected, suggesting that these DMF-induced changes are not stressful enough to trigger ER stress response by activating early and late unfolded protein response (UPR). The abundance of the chaperones binding immunoglobulin protein (BiP) and calnexin was not altered nor was the splicing of the X box-binding protein 1 (XBP1) mRNA, which is downstream of inositol-requiring enzyme 1 α (IRE1 α) (Yoshida et al., 2001). Especially

7 DISCUSSION

lymphocytes should be resistant to oxidative stress and increased Ca^{2+} levels because not only Ca^{2+} signaling but also ROS production is necessary after T and B cell activation (Devadas et al., 2002; Wheeler and Defranco, 2012; Yarosz and Chang, 2018).

Essential for the energy balance of the cell is glucose. I analyzed the glucose-uptake in cells due to the hypothesis that SERCA C674 is oxidized by high glucose (Tong et al., 2008) and the resulting inactivation could be responsible for the diminished Ca^{2+} storage in the ER. Congruent with my findings, that SERCA C674 is not oxidized, I did not find any alterations in glucose-uptake in DMF-treated cells.

DMF is reported to inactivate glyceraldehyde 3-phosphate dehydrogenase (GAPDH) by succination of its catalytic cysteine and thereby downregulating aerobic glycolysis in mitochondria (Kornberg et al., 2018). Mitochondrial respiration plays an important role in the energy balance of the cell and can be affected by oxidative stress (Kowaltowski and Vercesi, 1999). I tested if DMF alters mitochondrial respiration because it induces short-term oxidative stress. Mitochondrial superoxide levels in T cells incubated with DMF for 24 h were reduced similarly to ROS in the cytosol, indicating induction of the antioxidant response by DMF after 24 h of treatment. High-resolution respirometry measurements revealed an increased non-mitochondrial oxygen consumption (ROX), which can be explained by upregulated antioxidant defense enzymes like manganese superoxide-dismutase or heme oxygenase-1 (Lin et al., 2011; Campolo et al., 2017). Contrary to the finding of an increased oxygen consumption rate in fibroblasts by Hayashi et al. (Hayashi et al., 2017) DMF significantly reduced the electron transfer system (ETS) capacity in splenocytes. A decrease in the production of the protein complexes involved in oxidative phosphorylation (OXPHOS) because of the oxidative stress-induced mitochondrial DNA damage may be the explanation (Guo et al., 2013).

To further determine alterations of downstream elements of the Ca^{2+} signaling cascade, I tested the expression and nuclear translocation of the transcription factor nuclear factor of activated T cells (NFAT). In DMF-treated splenocytes or activated T cells, neither NFAT expression was changed compared to vehicle controls nor was NFAT translocation. Gerdes et al. did also report that DMF did not inhibit nuclear binding of NFAT in activated human T cells (Gerdes et al., 2007). In contrast to the results in activated T cells, the luminescence reporter assay showed an increase in NFAT translocation due to DMF treatment in STIM1 -

7 DISCUSSION

/- + STIM1 WTmcherry MEF cells. Contrary to a recently reported downregulation of proinflammatory cytokines, including interleukin-2 (IL-2) and TNF- α , in DMF-treated splenocytes (Albrecht et al., 2012), a higher NFAT translocation rate would come with increased production of IL-2 and TNF- α (Shaw et al., 1988; McCaffrey et al., 1994; Chow et al., 1999). Increased TNF- α levels would activate nuclear factor kappa light chain enhancers of activated B cells (NF- κ B) and lead to its translocation in the nucleus to further regulate cytokine expression. Indeed, the NF- κ B signaling pathway was shown previously to be affected by DMF in an Nrf2-dependent (Campolo et al., 2017) and independent manner (Gillard et al., 2015). DMF was reported to inhibit translocation of Rel A (p65) in human endothelial cells (Loewe et al., 2002), or NF- κ B1 (p50) in human dermal fibroblast cells (Vandermeeren et al., 2001). Others showed DMF inhibits the NF- κ B pathway by covalent modification of p65 in breast cancer cells (Kastrati et al., 2016). However, in contrast to these publications, I did not find any modifications in the NF- κ B pathway. As I worked with splenocytes, I have to consider that the mixture of different cells could be the reason. To counteract the heterogeneity of cells in isolated splenocytes, a presorting of B or T cells may improve or at least specify the responses to DMF for one cell type.

The mechanism of action of DMF definitely involves alterations of redox-sensitive thiols in proteins. Blewett et al. tested >2400 cysteine residues in human T cells with the help of a site-specific chemical proteomic approach to find DMF sensitive proteins. They identified proteins important for the immune response as DMF targets (Blewett et al., 2016). Thus, the effects of DMF I showed on various key players in Ca²⁺ signaling could probably be extended. Further research on thiol modifications altered by DMF has to be accomplished in order to find a better approach to protein thiols as targets for future drugs.

8 LITERATURE

Adachi, T., Weisbrod, R.M., Pimentel, D.R., Ying, J., Sharov, V.S., Schöneich, C., and Cohen, R.A. (2004). S-Glutathiolation by peroxynitrite activates SERCA during arterial relaxation by nitric oxide. *Nature medicine* *10*, 1200-1207.

Albrecht, P., Bouchachia, I., Goebels, N., Henke, N., Hofstetter, H.H., Issberner, A., Kovacs, Z., Lewerenz, J., Lisak, D., and Maher, P., et al. (2012). Effects of dimethyl fumarate on neuroprotection and immunomodulation. *Journal of neuroinflammation* *9*, 163.

Al-Jaderi, Z., and Maghazachi, A.A. (2015). Vitamin D₃ and monomethyl fumarate enhance natural killer cell lysis of dendritic cells and ameliorate the clinical score in mice suffering from experimental autoimmune encephalomyelitis. *Toxins* *7*, 4730-4744.

Anderson, D.M., Makarewich, C.A., Anderson, K.M., Shelton, J.M., Bezprozvannaya, S., Bassel-Duby, R., and Olson, E.N. (2016). Widespread control of calcium signaling by a family of SERCA-inhibiting micropeptides. *Science signaling* *9*, ra119.

Andersson, D.A., Gentry, C., Moss, S., and Bevan, S. (2008). Transient receptor potential A1 is a sensory receptor for multiple products of oxidative stress. *The Journal of neuroscience : the official journal of the Society for Neuroscience* *28*, 2485-2494.

Anzai, K., Ogawa, K., Kuniyasu, A., Ozawa, T., Yamamoto, H., and Nakayama, H. (1998). Effects of hydroxyl radical and sulfhydryl reagents on the open probability of the purified cardiac ryanodine receptor channel incorporated into planar lipid bilayers. *Biochemical and biophysical research communications* *249*, 938-942.

Atoyan, R., Shander, D., and Botchkareva, N.V. (2009). Non-neuronal expression of transient receptor potential type A1 (TRPA1) in human skin. *The Journal of investigative dermatology* *129*, 2312-2315.

Baeuerle, P.A., and Baltimore, D. (1988). I kappa B: a specific inhibitor of the NF-kappa B transcription factor. *Science (New York, N.Y.)* *242*, 540-546.

Baginski, E.S., Foà, P.P., and Zak, B. (1967). Microdetermination of inorganic phosphate, phospholipids, and total phosphate in biologic materials. *Clinical chemistry* *13*, 326-332.

Bautista, D.M., Jordt, S.-E., Nikai, T., Tsuruda, P.R., Read, A.J., Poblete, J., Yamoah, E.N., Basbaum, A.I., and Julius, D. (2006). TRPA1 mediates the inflammatory actions of environmental irritants and proalgesic agents. *Cell* *124*, 1269-1282.

Bautista, D.M., Pellegrino, M., and Tsunozaki, M. (2013). TRPA1: A gatekeeper for inflammation. *Annual review of physiology* *75*, 181-200.

8 LITERATURE

Bayle, D., Weeks, D., and Sachs, G. (1995). The membrane topology of the rat sarcoplasmic and endoplasmic reticulum calcium ATPases by in vitro translation scanning. *The Journal of biological chemistry* *270*, 25678-25684.

Beeler, T.J., Jona, I., and Martonosi, A. (1979). The effect of ionomycin on calcium fluxes in sarcoplasmic reticulum vesicles and liposomes. *The Journal of biological chemistry* *254*, 6229-6231.

Belbasis, L., Bellou, V., Evangelou, E., Ioannidis, J.P.A., and Tzoulaki, I. (2015). Environmental risk factors and multiple sclerosis: an umbrella review of systematic reviews and meta-analyses. *The Lancet Neurology* *14*, 263-273.

Berridge, M.J., Bootman, M.D., and Roderick, H.L. (2003). Calcium signalling: dynamics, homeostasis and remodelling. *Nature reviews. Molecular cell biology* *4*, 517-529.

Blank, V., Kourilsky, P., and Israël, A. (1991). Cytoplasmic retention, DNA binding and processing of the NF-kappa B p50 precursor are controlled by a small region in its C-terminus. *The EMBO journal* *10*, 4159-4167.

Blewett, M.M., Xie, J., Zaro, B.W., Backus, K.M., Altman, A., Teijaro, J.R., and Cravatt, B.F. (2016). Chemical proteomic map of dimethyl fumarate-sensitive cysteines in primary human T cells. *Science signaling* *9*, rs10.

Blond-Elguindi, S., Cwirla, S.E., Dower, W.J., Lipshutz, R.J., Sprang, S.R., Sambrook, J.F., and Gething, M.J. (1993). Affinity panning of a library of peptides displayed on bacteriophages reveals the binding specificity of BiP. *Cell* *75*, 717-728.

Bogeski, I., Kummerow, C., Al-Ansary, D., Schwarz, E.C., Koehler, R., Kozai, D., Takahashi, N., Peinelt, C., Griesemer, D., and Bozem, M., et al. (2010). Differential redox regulation of ORAI ion channels: a mechanism to tune cellular calcium signaling. *Science signaling* *3*, ra24.

Bouron, A., Kiselyov, K., and Oberwinkler, J. (2015). Permeation, regulation and control of expression of TRP channels by trace metal ions. *Pflugers Archiv : European journal of physiology* *467*, 1143-1164.

Boyce, M., and Yuan, J. (2006). Cellular response to endoplasmic reticulum stress: a matter of life or death. *Cell death and differentiation* *13*, 363-373.

Boyer, P.D. (1997). The ATP synthase--a splendid molecular machine. *Annual review of biochemistry* *66*, 717-749.

Braakman, I., and Bulleid, N.J. (2011). Protein folding and modification in the mammalian endoplasmic reticulum. *Annual review of biochemistry* *80*, 71-99.

8 LITERATURE

Bradford, M.M. (1976). A rapid and sensitive method for the quantitation of microgram quantities of protein utilizing the principle of protein-dye binding. *Analytical biochemistry* 72, 248-254.

Brand, M.D., Affourtit, C., Esteves, T.C., Green, K., Lambert, A.J., Miwa, S., Pakay, J.L., and Parker, N. (2004). Mitochondrial superoxide: production, biological effects, and activation of uncoupling proteins. *Free radical biology & medicine* 37, 755-767.

Brandes, N., Schmitt, S., and Jakob, U. (2009). Thiol-based redox switches in eukaryotic proteins. *Antioxidants & redox signaling* 11, 997-1014.

Campolo, M., Casili, G., Biundo, F., Crupi, R., Cordaro, M., Cuzzocrea, S., and Esposito, E. (2017). The Neuroprotective Effect of Dimethyl Fumarate in an MPTP-Mouse Model of Parkinson's Disease: Involvement of Reactive Oxygen Species/Nuclear Factor- κ B/Nuclear Transcription Factor Related to NF-E2. *Antioxidants & redox signaling* 27, 453-471.

Caterina, M.J., Rosen, T.A., Tominaga, M., Brake, A.J., and Julius, D. (1999). A capsaicin-receptor homologue with a high threshold for noxious heat. *Nature* 398, 436-441.

Caterina, M.J., Schumacher, M.A., Tominaga, M., Rosen, T.A., Levine, J.D., and Julius, D. (1997). The capsaicin receptor: a heat-activated ion channel in the pain pathway. *Nature* 389, 816-824.

Chen, J., and Hackos, D.H. (2015). TRPA1 as a drug target--promise and challenges. *Naunyn-Schmiedeberg's archives of pharmacology* 388, 451-463.

Chen, J., Joshi, S.K., DiDomenico, S., Perner, R.J., Mikusa, J.P., Gauvin, D.M., Segreti, J.A., Han, P., Zhang, X.-F., and Niforatos, W., et al. (2011). Selective blockade of TRPA1 channel attenuates pathological pain without altering noxious cold sensation or body temperature regulation. *Pain* 152, 1165-1172.

Chow, C.W., Rincón, M., and Davis, R.J. (1999). Requirement for transcription factor NFAT in interleukin-2 expression. *Molecular and cellular biology* 19, 2300-2307.

Cohen, S.N., Chang, A.C., and Hsu, L. (1972). Nonchromosomal antibiotic resistance in bacteria: genetic transformation of *Escherichia coli* by R-factor DNA. *Proceedings of the National Academy of Sciences of the United States of America* 69, 2110-2114.

Compston, A., and Coles, A. (2008). Multiple sclerosis. *The Lancet* 372, 1502-1517.

Confavreux, C., Aimard, G., and Devic, M. (1980). Course and prognosis of multiple sclerosis assessed by the computerized data processing of 349 patients. *Brain : a journal of neurology* 103, 281-300.

8 LITERATURE

- Coope, H.J., Atkinson, P.G.P., Huhse, B., Belich, M., Janzen, J., Holman, M.J., Klaus, G.G.B., Johnston, L.H., and Ley, S.C. (2002). CD40 regulates the processing of NF-kappaB2 p100 to p52. *The EMBO journal* *21*, 5375-5385.
- Cooper, A.A., Gitler, A.D., Cashikar, A., Haynes, C.M., Hill, K.J., Bhullar, B., Liu, K., Xu, K., Strathearn, K.E., and Liu, F., et al. (2006). Alpha-synuclein blocks ER-Golgi traffic and Rab1 rescues neuron loss in Parkinson's models. *Science (New York, N.Y.)* *313*, 324-328.
- Covington, E.D., Wu, M.M., and Lewis, R.S. (2010). Essential role for the CRAC activation domain in store-dependent oligomerization of STIM1. *Molecular biology of the cell* *21*, 1897-1907.
- Croxford, A.L., Kurschus, F.C., and Waisman, A. (2011). Mouse models for multiple sclerosis: historical facts and future implications. *Biochimica et biophysica acta* *1812*, 177-183.
- Decrock, E., Bock, M. de, Wang, N., Gadicherla, A.K., Bol, M., Delvaeye, T., Vandenabeele, P., Vinken, M., Bultynck, G., and Krysko, D.V., et al. (2013). IP3, a small molecule with a powerful message. *Biochimica et biophysica acta* *1833*, 1772-1786.
- Dendrou, C.A., Fugger, L., and Friese, M.A. (2015). Immunopathology of multiple sclerosis. *Nature reviews. Immunology* *15*, 545-558.
- Devadas, S., Zaritskaya, L., Rhee, S.G., Oberley, L., and Williams, M.S. (2002). Discrete generation of superoxide and hydrogen peroxide by T cell receptor stimulation: selective regulation of mitogen-activated protein kinase activation and fas ligand expression. *The Journal of Experimental Medicine* *195*, 59-70.
- Diezel, W., Kopperschläger, G., and Hofmann, E. (1972). An improved procedure for protein staining in polyacrylamide gels with a new type of Coomassie Brilliant Blue. *Analytical biochemistry* *48*, 617-620.
- Dode, L., Andersen, J.P., Leslie, N., Dhitavat, J., Vilsen, B., and Hovnanian, A. (2003). Dissection of the functional differences between sarco(endo)plasmic reticulum Ca²⁺-ATPase (SERCA) 1 and 2 isoforms and characterization of Darier disease (SERCA2) mutants by steady-state and transient kinetic analyses. *The Journal of biological chemistry* *278*, 47877-47889.
- Doerner, J.F., Gisselmann, G., Hatt, H., and Wetzel, C.H. (2007). Transient receptor potential channel A1 is directly gated by calcium ions. *The Journal of biological chemistry* *282*, 13180-13189.
- Dolmetsch, R.E., Lewis, R.S., Goodnow, C.C., and Healy, J.I. (1997). Differential activation of transcription factors induced by Ca²⁺ response amplitude and duration. *Nature* *386*, 855-858.

8 LITERATURE

- Dong, Z., Shanmughapriya, S., Tomar, D., Siddiqui, N., Lynch, S., Nemani, N., Breves, S.L., Zhang, X., Tripathi, A., and Palaniappan, P., et al. (2017). Mitochondrial Ca²⁺ Uniporter Is a Mitochondrial Luminal Redox Sensor that Augments MCU Channel Activity. *Molecular cell* *65*, 1014-1028.e7.
- Dray, A., Forbes, C.A., and Burgess, G.M. (1990). Ruthenium red blocks the capsaicin-induced increase in intracellular calcium and activation of membrane currents in sensory neurones as well as the activation of peripheral nociceptors in vitro. *Neuroscience letters* *110*, 52-59.
- Dutta, D. (2000). Mechanism of store-operated calcium entry. *Journal of biosciences* *25*, 397-404.
- Duve, C. de, and Baudhuin, P. (1966). Peroxisomes (microbodies and related particles). *Physiological reviews* *46*, 323-357.
- Fagone, P., and Jackowski, S. (2009). Membrane phospholipid synthesis and endoplasmic reticulum function. *Journal of lipid research* *50 Suppl*, S311-6.
- Felgner, P.L., Gadek, T.R., Holm, M., Roman, R., Chan, H.W., Wenz, M., Northrop, J.P., Ringold, G.M., and Danielsen, M. (1987). Lipofection: a highly efficient, lipid-mediated DNA-transfection procedure. *Proceedings of the National Academy of Sciences of the United States of America* *84*, 7413-7417.
- Feske, S. (2007). Calcium signalling in lymphocyte activation and disease. *Nature reviews. Immunology* *7*, 690-702.
- Fiske, C.H., and Subbarow, Y. (1925). The colorimetric determination of phosphorus. *Journal of Biological Chemistry*, 375-400.
- Förster, A., Preussner, L.M., Seeger, J.M., Rabenhorst, A., Kashkar, H., Mrowietz, U., and Hartmann, K. (2013). Dimethylfumarate induces apoptosis in human mast cells. *Experimental dermatology* *22*, 719-724.
- Frantz, B., Nordby, E.C., Bren, G., Steffan, N., Paya, C.V., Kincaid, R.L., Tocci, M.J., O'Keefe, S.J., and O'Neill, E.A. (1994). Calcineurin acts in synergy with PMA to inactivate I kappa B/MAD3, an inhibitor of NF-kappa B. *The EMBO journal* *13*, 861-870.
- Ganchi, P.A., Sun, S.C., Greene, W.C., and Ballard, D.W. (1992). I kappa B/MAD-3 masks the nuclear localization signal of NF-kappa B p65 and requires the transactivation domain to inhibit NF-kappa B p65 DNA binding. *Molecular biology of the cell* *3*, 1339-1352.

8 LITERATURE

- Gerdes, S., Shaker, K., and Mrowietz, U. (2007). Dimethylfumarate inhibits nuclear binding of nuclear factor kappaB but not of nuclear factor of activated T cells and CCAAT/enhancer binding protein beta in activated human T cells. *The British journal of dermatology* *156*, 838-842.
- Gesser, B., Johansen, C., Rasmussen, M.K., Funding, A.T., Otkjaer, K., Kjellerup, R.B., Kragballe, K., and Iversen, L. (2007). Dimethylfumarate specifically inhibits the mitogen and stress-activated kinases 1 and 2 (MSK1/2): possible role for its anti-psoriatic effect. *The Journal of investigative dermatology* *127*, 2129-2137.
- Ghosh, S., May, M.J., and Kopp, E.B. (1998). NF-kappa B and Rel proteins: evolutionarily conserved mediators of immune responses. *Annual review of immunology* *16*, 225-260.
- Gillard, G.O., Collette, B., Anderson, J., Chao, J., Scannevin, R.H., Huss, D.J., and Fontenot, J.D. (2015). DMF, but not other fumarates, inhibits NF- κ B activity in vitro in an Nrf2-independent manner. *Journal of neuroimmunology* *283*, 74-85.
- Gilmore, T.D. (1990). NF-kappa B, KBF1, dorsal, and related matters. *Cell* *62*, 841-843.
- Gluzman, Y. (1981). SV40-transformed simian cells support the replication of early SV40 mutants. *Cell* *23*, 175-182.
- Gordon, G.B., Prochaska, H.J., and Yang, L.Y. (1991). Induction of NAD(P)H:quinone reductase in human peripheral blood lymphocytes. *Carcinogenesis* *12*, 2393-2396.
- Gross, E., Sevier, C.S., Heldman, N., Vitu, E., Bentzur, M., Kaiser, C.A., Thorpe, C., and Fass, D. (2006). Generating disulfides enzymatically: reaction products and electron acceptors of the endoplasmic reticulum thiol oxidase Ero1p. *Proceedings of the National Academy of Sciences of the United States of America* *103*, 299-304.
- Grover, A.K., Kwan, C.-Y., and Samson, S.E. (2003). Effects of peroxynitrite on sarco/endoplasmic reticulum Ca²⁺ pump isoforms SERCA2b and SERCA3a. *American journal of physiology. Cell physiology* *285*, C1537-43.
- Grupe, M., Myers, G., Penner, R., and Fleig, A. (2010). Activation of store-operated I(CRAC) by hydrogen peroxide. *Cell calcium* *48*, 1-9.
- Grynkiewicz, G., Poenie, M., and Tsien, R.Y. (1985). A new generation of Ca²⁺ indicators with greatly improved fluorescence properties. *The Journal of biological chemistry* *260*, 3440-3450.
- Guinamard, R., Simard, C., and Negro, C.D. (2013). Flufenamic acid as an ion channel modulator. *Pharmacology & therapeutics* *138*, 272-284.

8 LITERATURE

Gunteski-Hamblin, A.M., Greeb, J., and Shull, G.E. (1988). A novel Ca²⁺ pump expressed in brain, kidney, and stomach is encoded by an alternative transcript of the slow-twitch muscle sarcoplasmic reticulum Ca-ATPase gene. Identification of cDNAs encoding Ca²⁺ and other cation-transporting ATPases using an oligonucleotide probe derived from the ATP-binding site. *The Journal of biological chemistry* 263, 15032-15040.

Guo, C., Sun, L., Chen, X., and Zhang, D. (2013). Oxidative stress, mitochondrial damage and neurodegenerative diseases. *Neural regeneration research* 8, 2003-2014.

Halestrap, A.P. (2009). What is the mitochondrial permeability transition pore? *Journal of molecular and cellular cardiology* 46, 821-831.

Hamill, O.P., Marty, A., Neher, E., Sakmann, B., and Sigworth, F.J. (1981). Improved patch-clamp techniques for high-resolution current recording from cells and cell-free membrane patches. *Pflugers Archiv : European journal of physiology* 391, 85-100.

Han, B., and Logsdon, C.D. (2000). CCK stimulates mob-1 expression and NF-kappaB activation via protein kinase C and intracellular Ca(2+). *American journal of physiology. Cell physiology* 278, C344-51.

Hara, Y., Wakamori, M., Ishii, M., Maeno, E., Nishida, M., Yoshida, T., Yamada, H., Shimizu, S., Mori, E., and Kudoh, J., et al. (2002). LTRPC2 Ca²⁺-permeable channel activated by changes in redox status confers susceptibility to cell death. *Molecular cell* 9, 163-173.

Hatano, N., Itoh, Y., Suzuki, H., Muraki, Y., Hayashi, H., Onozaki, K., Wood, I.C., Beech, D.J., and Muraki, K. (2012). Hypoxia-inducible factor-1 α (HIF1 α) switches on transient receptor potential ankyrin repeat 1 (TRPA1) gene expression via a hypoxia response element-like motif to modulate cytokine release. *The Journal of biological chemistry* 287, 31962-31972.

Hawkins, B.J., Irrinki, K.M., Mallilankaraman, K., Lien, Y.-C., Wang, Y., Bhanumathy, C.D., Subbiah, R., Ritchie, M.F., Soboloff, J., and Baba, Y., et al. (2010). S-glutathionylation activates STIM1 and alters mitochondrial homeostasis. *The Journal of cell biology* 190, 391-405.

Hayashi, G., Jasoliya, M., Sahdeo, S., Saccà, F., Pane, C., Filla, A., Marsili, A., Puorro, G., Lanzillo, R., and Brescia Morra, V., et al. (2017). Dimethyl fumarate mediates Nrf2-dependent mitochondrial biogenesis in mice and humans. *Human molecular genetics* 26, 2864-2873.

Held, K.D., Epp, E.R., Clark, E.P., and Biaglow, J.E. (1988). Effect of dimethyl fumarate on the radiation sensitivity of mammalian cells in vitro. *Radiation research* 115, 495-502.

Helenius, A., and Aebi, M. (2004). Roles of N-linked glycans in the endoplasmic reticulum. *Annual review of biochemistry* 73, 1019-1049.

8 LITERATURE

- Henke, N., Albrecht, P., Pfeiffer, A., Toutzaris, D., Zanger, K., and Methner, A. (2012). Stromal interaction molecule 1 (STIM1) is involved in the regulation of mitochondrial shape and bioenergetics and plays a role in oxidative stress. *The Journal of biological chemistry* 287, 42042-42052.
- Henkel, T., Zabel, U., van Zee, K., Müller, J.M., Fanning, E., and Baeuerle, P.A. (1992). Intramolecular masking of the nuclear location signal and dimerization domain in the precursor for the p50 NF- κ B subunit. *Cell* 68, 1121-1133.
- Herrmann, A.-K. (2014). Die Rolle von oxidativem Stress in der Regulation von SOCE (Store-operated Ca²⁺ entry). Master`s thesis.
- Hetz, C. (2012). The unfolded protein response: controlling cell fate decisions under ER stress and beyond. *Nature reviews. Molecular cell biology* 13, 89-102.
- Hill, K., Benham, C.D., McNulty, S., and Randall, A.D. (2004). Flufenamic acid is a pH-dependent antagonist of TRPM2 channels. *Neuropharmacology* 47, 450-460.
- Hinman, A., Chuang, H.-H., Bautista, D.M., and Julius, D. (2006). TRP channel activation by reversible covalent modification. *Proceedings of the National Academy of Sciences of the United States of America* 103, 19564-19568.
- Hoenderop, J.G.J., Vennekens, R., Müller, D., Prenen, J., Droogmans, G., Bindels, R.J.M., and Nilius, B. (2001). Function and expression of the epithelial Ca²⁺ channel family: comparison of mammalian ECaC1 and 2. *The Journal of Physiology* 537, 747-761.
- Hoffmann, C., Dietrich, M., Herrmann, A.-K., Schacht, T., Albrecht, P., and Methner, A. (2017). Dimethyl Fumarate Induces Glutathione Recycling by Upregulation of Glutathione Reductase. *Oxidative medicine and cellular longevity* 2017, 6093903.
- Hofmann, T., Obukhov, A.G., Schaefer, M., Harteneck, C., Gudermann, T., and Schultz, G. (1999). Direct activation of human TRPC6 and TRPC3 channels by diacylglycerol. *Nature* 397, 259-263.
- Horsley, V., and Pavlath, G.K. (2002). NFAT: ubiquitous regulator of cell differentiation and adaptation. *The Journal of cell biology* 156, 771-774.
- Hu, H., Tian, J., Zhu, Y., Wang, C., Xiao, R., Herz, J.M., Wood, J.D., and Zhu, M.X. (2010). Activation of TRPA1 channels by fenamate nonsteroidal anti-inflammatory drugs. *Pflugers Archiv : European journal of physiology* 459, 579-592.
- Inesi, G., Kurzmack, M., Coan, C., and Lewis, D.E. (1980). Cooperative calcium binding and ATPase activation in sarcoplasmic reticulum vesicles. *The Journal of biological chemistry* 255, 3025-3031.

8 LITERATURE

Itoh, K., Chiba, T., Takahashi, S., Ishii, T., Igarashi, K., Katoh, Y., Oyake, T., Hayashi, N., Satoh, K., and Hatayama, I., et al. (1997). An Nrf2/small Maf heterodimer mediates the induction of phase II detoxifying enzyme genes through antioxidant response elements. *Biochemical and biophysical research communications* 236, 313-322.

Itoh, K., Wakabayashi, N., Katoh, Y., Ishii, T., Igarashi, K., Engel, J.D., and Yamamoto, M. (1999). Keap1 represses nuclear activation of antioxidant responsive elements by Nrf2 through binding to the amino-terminal Neh2 domain. *Genes & development* 13, 76-86.

Jaquemar, D., Schenker, T., and Trueb, B. (1999). An ankyrin-like protein with transmembrane domains is specifically lost after oncogenic transformation of human fibroblasts. *The Journal of biological chemistry* 274, 7325-7333.

Jong, R. de, Bezemer, A.C., Zomerdijk, T.P., van de Pouw-Kraan, T., Ottenhoff, T.H., and Nibbering, P.H. (1996). Selective stimulation of T helper 2 cytokine responses by the anti-psoriasis agent monomethylfumarate. *European journal of immunology* 26, 2067-2074.

Kadamur, G., and Ross, E.M. (2013). Mammalian phospholipase C. *Annual review of physiology* 75, 127-154.

Kappos, L., Gold, R., Miller, D.H., Macmanus, D.G., Havrdova, E., Limmroth, V., Polman, C.H., Schmierer, K., Yousry, T.A., and Yang, M., et al. (2008). Efficacy and safety of oral fumarate in patients with relapsing-remitting multiple sclerosis: a multicentre, randomised, double-blind, placebo-controlled phase IIb study. *Lancet (London, England)* 372, 1463-1472.

Kastrati, I., Siklos, M.I., Calderon-Gierszal, E.L., El-Shennawy, L., Georgieva, G., Thayer, E.N., Thatcher, G.R.J., and Frasor, J. (2016). Dimethyl Fumarate Inhibits the Nuclear Factor κ B Pathway in Breast Cancer Cells by Covalent Modification of p65 Protein. *The Journal of biological chemistry* 291, 3639-3647.

Kayagaki, N., Yan, M., Seshasayee, D., Wang, H., Lee, W., French, D.M., Grewal, I.S., Cochran, A.G., Gordon, N.C., and Yin, J., et al. (2002). BAFF/BLyS receptor 3 binds the B cell survival factor BAFF ligand through a discrete surface loop and promotes processing of NF-kappaB2. *Immunity* 17, 515-524.

Kiani, A., García-Cózar, F.J., Habermann, I., Laforsch, S., Aebischer, T., Ehninger, G., and Rao, A. (2001). Regulation of interferon-gamma gene expression by nuclear factor of activated T cells. *Blood* 98, 1480-1488.

Kobayashi, A., Kang, M.-I., Okawa, H., Ohtsuji, M., Zenke, Y., Chiba, T., Igarashi, K., and Yamamoto, M. (2004). Oxidative stress sensor Keap1 functions as an adaptor for Cul3-based E3 ligase to regulate proteasomal degradation of Nrf2. *Molecular and cellular biology* 24, 7130-7139.

8 LITERATURE

- Kornberg, M.D., Bhargava, P., Kim, P.M., Putluri, V., Snowman, A.M., Putluri, N., Calabresi, P.A., and Snyder, S.H. (2018). Dimethyl fumarate targets GAPDH and aerobic glycolysis to modulate immunity. *Science (New York, N.Y.)* 360, 449-453.
- Kowaltowski, A.J., and Vercesi, A.E. (1999). Mitochondrial damage induced by conditions of oxidative stress. *Free radical biology & medicine* 26, 463-471.
- Kozovska, M.E., Hong, J., Zang, Y.C., Li, S., Rivera, V.M., Killian, J.M., and Zhang, J.Z. (1999). Interferon beta induces T-helper 2 immune deviation in MS. *Neurology* 53, 1692-1697.
- Kozutsumi, Y., Segal, M., Normington, K., Gething, M.J., and Sambrook, J. (1988). The presence of malformed proteins in the endoplasmic reticulum signals the induction of glucose-regulated proteins. *Nature* 332, 462-464.
- Kuster, G.M., Lancel, S., Zhang, J., Communal, C., Trucillo, M.P., Lim, C.C., Pfister, O., Weinberg, E.O., Cohen, R.A., and Liao, R., et al. (2010). Redox-mediated reciprocal regulation of SERCA and Na⁺-Ca²⁺ exchanger contributes to sarcoplasmic reticulum Ca²⁺ depletion in cardiac myocytes. *Free radical biology & medicine* 48, 1182-1187.
- Laemmli, U.K. (1970). Cleavage of structural proteins during the assembly of the head of bacteriophage T4. *Nature* 227, 680-685.
- Lam, A.K.M., and Galione, A. (2013). The endoplasmic reticulum and junctional membrane communication during calcium signaling. *Biochimica et biophysica acta* 1833, 2542-2559.
- Li, J., Johnson, D., Calkins, M., Wright, L., Svendsen, C., and Johnson, J. (2005). Stabilization of Nrf2 by tBHQ confers protection against oxidative stress-induced cell death in human neural stem cells. *Toxicological sciences : an official journal of the Society of Toxicology* 83, 313-328.
- Li, R., Rezk, A., Ghadiri, M., Luessi, F., Zipp, F., Li, H., Giacomini, P.S., Antel, J., and Bar-Or, A. (2017). Dimethyl Fumarate Treatment Mediates an Anti-Inflammatory Shift in B Cell Subsets of Patients with Multiple Sclerosis. *The Journal of Immunology* 198, 691-698.
- Li, Z., Liu, L., Deng, Y., Ji, W., Du, W., Xu, P., Chen, L., and Xu, T. (2011). Graded activation of CRAC channel by binding of different numbers of STIM1 to Orai1 subunits. *Cell research* 21, 305-315.
- Lin, S.X., Lisi, L., Dello Russo, C., Polak, P.E., Sharp, A., Weinberg, G., Kalinin, S., and Feinstein, D.L. (2011). The anti-inflammatory effects of dimethyl fumarate in astrocytes involve glutathione and haem oxygenase-1. *ASN neuro* 3.

8 LITERATURE

Linker, R.A., Lee, D.-H., Ryan, S., van Dam, A.M., Conrad, R., Bista, P., Zeng, W., Hronowsky, X., Buko, A., and Chollate, S., et al. (2011). Fumaric acid esters exert neuroprotective effects in neuroinflammation via activation of the Nrf2 antioxidant pathway. *Brain : a journal of neurology* *134*, 678-692.

Liou, H.C., Nolan, G.P., Ghosh, S., Fujita, T., and Baltimore, D. (1992). The NF-kappa B p50 precursor, p105, contains an internal I kappa B-like inhibitor that preferentially inhibits p50. *The EMBO journal* *11*, 3003-3009.

Liou, J., Kim, M.L., Heo, W.D., Jones, J.T., Myers, J.W., Ferrell, J.E., and Meyer, T. (2005). STIM is a Ca²⁺ sensor essential for Ca²⁺-store-depletion-triggered Ca²⁺ influx. *Current biology : CB* *15*, 1235-1241.

Litjens, N.H.R., Burggraaf, J., van Strijen, E., van Gulpen, C., Mattie, H., Schoemaker, R.C., van Dissel, J.T., Thio, H.B., and Nibbering, P.H. (2004). Pharmacokinetics of oral fumarates in healthy subjects. *British journal of clinical pharmacology* *58*, 429-432.

Litjens, N.H.R., Nibbering, P.H., Barrois, A.J., Zomerdijk, T.P.L., van den Oudenrijn, A.C., Noz, K.C., Rademaker, M., van de Meide, P.H., van Dissel, J.T., and Thio, B. (2003). Beneficial effects of fumarate therapy in psoriasis vulgaris patients coincide with downregulation of type 1 cytokines. *The British journal of dermatology* *148*, 444-451.

Liu, C., and Hermann, T.E. (1978). Characterization of ionomycin as a calcium ionophore. *The Journal of biological chemistry* *253*, 5892-5894.

Loewe, R., Holnthoner, W., Groger, M., Pillinger, M., Gruber, F., Mechtcheriakova, D., Hofer, E., Wolff, K., and Petzelbauer, P. (2002). Dimethylfumarate Inhibits TNF-Induced Nuclear Entry of NF- B/p65 in Human Endothelial Cells. *The Journal of Immunology* *168*, 4781-4787.

Lublin, F.D., and Reingold, S.C. (1996). Defining the clinical course of multiple sclerosis: Results of an international survey. *Neurology* *46*, 907-911.

Luik, R.M., Wang, B., Prakriya, M., Wu, M.M., and Lewis, R.S. (2008). Oligomerization of STIM1 couples ER calcium depletion to CRAC channel activation. *Nature* *454*, 538-542.

Lyakh, L., Ghosh, P., and Rice, N.R. (1997). Expression of NFAT-family proteins in normal human T cells. *Molecular and cellular biology* *17*, 2475-2484.

Macey, M.G. (2007). *Flow Cytometry. Principles and Applications* (Totowa, NJ: Humana Press Inc).

Macpherson, L.J., Dubin, A.E., Evans, M.J., Marr, F., Schultz, P.G., Cravatt, B.F., and Patapoutian, A. (2007). Noxious compounds activate TRPA1 ion channels through covalent modification of cysteines. *Nature* *445*, 541-545.

8 LITERATURE

Macpherson, L.J., Geierstanger, B.H., Viswanath, V., Bandell, M., Eid, S.R., Hwang, S., and Patapoutian, A. (2005). The pungency of garlic: activation of TRPA1 and TRPV1 in response to allicin. *Current biology* : CB *15*, 929-934.

Madesh, M., Hawkins, B.J., Milovanova, T., Bhanumathy, C.D., Joseph, S.K., Ramachandrarao, S.P., Sharma, K., Kurosaki, T., and Fisher, A.B. (2005). Selective role for superoxide in InsP3 receptor-mediated mitochondrial dysfunction and endothelial apoptosis. *The Journal of cell biology* *170*, 1079-1090.

Maher, P. (2005). The effects of stress and aging on glutathione metabolism. *Ageing research reviews* *4*, 288-314.

Mancarella, S., Wang, Y., Deng, X., Landesberg, G., Scalia, R., Panettieri, R.A., Mallilankaraman, K., Tang, X.D., Madesh, M., and Gill, D.L. (2011). Hypoxia-induced acidosis uncouples the STIM-Orai calcium signaling complex. *The Journal of biological chemistry* *286*, 44788-44798.

Mandel, M., and Higa, A. (1970). Calcium-dependent bacteriophage DNA infection. *Journal of molecular biology* *53*, 159-162.

Marinelli, P., Navarro, S., Graña-Montes, R., Bañó-Polo, M., Fernández, M.R., Papaleo, E., and Ventura, S. (2018). A single cysteine post-translational oxidation suffices to compromise globular proteins kinetic stability and promote amyloid formation. *Redox biology* *14*, 566-575.

Martelli, P.L., Fariselli, P., Malaguti, L., and Casadio, R. (2002). Prediction of the disulfide bonding state of cysteines in proteins with hidden neural networks. *Protein Engineering, Design and Selection* *15*, 951-953.

McCaffrey, P.G., Goldfeld, A.E., and Rao, A. (1994). The role of NFATp in cyclosporin A-sensitive tumor necrosis factor- α gene transcription. *The Journal of biological chemistry* *269*, 30445-30450.

McNamara, C.R., Mandel-Brehm, J., Bautista, D.M., Siemens, J., Deranian, K.L., Zhao, M., Hayward, N.J., Chong, J.A., Julius, D., and Moran, M.M., et al. (2007). TRPA1 mediates formalin-induced pain. *Proceedings of the National Academy of Sciences of the United States of America* *104*, 13525-13530.

McRae, B.L., Kennedy, M.K., Tan, L.J., Dal Canto, M.C., Picha, K.S., and Miller, S.D. (1992). Induction of active and adoptive relapsing experimental autoimmune encephalomyelitis (EAE) using an encephalitogenic epitope of proteolipid protein. *Journal of neuroimmunology* *38*, 229-240.

8 LITERATURE

Means, A.R., and Dedman, J.R. (1980). Calmodulin—an intracellular calcium receptor. *Nature* 285, 73-77.

Meili-Butz, S., Niermann, T., Fasler-Kan, E., Barbosa, V., Butz, N., John, D., Brink, M., Buser, P.T., and Zaugg, C.E. (2008). Dimethyl fumarate, a small molecule drug for psoriasis, inhibits Nuclear Factor-kappaB and reduces myocardial infarct size in rats. *European journal of pharmacology* 586, 251-258.

Meissner, G. (1994). Ryanodine receptor/Ca²⁺ release channels and their regulation by endogenous effectors. *Annual review of physiology* 56, 485-508.

Meseguer, V., Alpizar, Y.A., Luis, E., Tajada, S., Denlinger, B., Fajardo, O., Manenschijn, J.-A., Fernández-Peña, C., Talavera, A., and Kichko, T., et al. (2014). TRPA1 channels mediate acute neurogenic inflammation and pain produced by bacterial endotoxins. *Nature communications* 5, 3125.

Miller, A., Shapiro, S., Gershtein, R., Kinarty, A., Rawashdeh, H., Honigman, S., and Lahat, N. (1998). Treatment of multiple sclerosis with copolymer-1 (Copaxone): implicating mechanisms of Th1 to Th2/Th3 immune-deviation. *Journal of neuroimmunology* 92, 113-121.

Moutsianas, L., Jostins, L., Beecham, A.H., Dilthey, A.T., Xifara, D.K., Ban, M., Shah, T.S., Patsopoulos, N.A., Alfredsson, L., and Anderson, C.A., et al. (2015). Class II HLA interactions modulate genetic risk for multiple sclerosis. *Nature genetics* 47, 1107-1113.

Müller, M.R., and Rao, A. (2010). NFAT, immunity and cancer: a transcription factor comes of age. *Nature reviews. Immunology* 10, 645-656.

Müller, S., Behnen, M., Bieber, K., Möller, S., Hellberg, L., Witte, M., Hänsel, M., Zillikens, D., Solbach, W., and Laskay, T., et al. (2016). Dimethylfumarate Impairs Neutrophil Functions. *Journal of Investigative Dermatology* 136, 117-126.

Mullis, K., Faloona, F., Scharf, S., Saiki, R., Horn, G., and Erlich, H. (1986). Specific enzymatic amplification of DNA in vitro: the polymerase chain reaction. *Cold Spring Harbor symposia on quantitative biology* 51 Pt 1, 263-273.

Murphy, M.P., Echtay, K.S., Blaikie, F.H., Asin-Cayuela, J., Cocheme, H.M., Green, K., Buckingham, J.A., Taylor, E.R., Hurrell, F., and Hughes, G., et al. (2003). Superoxide activates uncoupling proteins by generating carbon-centered radicals and initiating lipid peroxidation: studies using a mitochondria-targeted spin trap derived from alpha-phenyl-N-tert-butyl nitron. *The Journal of biological chemistry* 278, 48534-48545.

8 LITERATURE

Naumann, M., Nieters, A., Hatada, E.N., and Scheidereit, C. (1993). NF-kappa B precursor p100 inhibits nuclear translocation and DNA binding of NF-kappa B/rel-factors. *Oncogene* 8, 2275-2281.

Nelson, K.C., Carlson, J.L., Newman, M.L., Sternberg, P., Jones, D.P., Kavanagh, T.J., Diaz, D., Cai, J., and Wu, M. (1999). Effect of dietary inducer dimethylfumarate on glutathione in cultured human retinal pigment epithelial cells. *Investigative ophthalmology & visual science* 40, 1927-1935.

Nibbering, P.H., Thio, B., Zomerdijk, T.P.L., Bezemer, A.C., Beijersbergen, R.L., and van Furth, R. (1993). Effects of Monomethylfumarate on Human Granulocytes. *Journal of Investigative Dermatology* 101, 37-42.

Ockenfels, H.M., Schultewolter, T., Ockenfels, G., Funk, R., and Goos, M. (1998). The antipsoriatic agent dimethylfumarate immunomodulates T-cell cytokine secretion and inhibits cytokines of the psoriatic cytokine network. *The British journal of dermatology* 139, 390-395.

Oh-Hora, M., Yamashita, M., Hogan, P.G., Sharma, S., Lamperti, E., Chung, W., Prakriya, M., Feske, S., and Rao, A. (2008). Dual functions for the endoplasmic reticulum calcium sensors STIM1 and STIM2 in T cell activation and tolerance. *Nature immunology* 9, 432-443.

Ohl, K., Tenbrock, K., and Kipp, M. (2016). Oxidative stress in multiple sclerosis: Central and peripheral mode of action. *Experimental neurology* 277, 58-67.

Osborn, L., Kunkel, S., and Nabel, G.J. (1989). Tumor necrosis factor alpha and interleukin 1 stimulate the human immunodeficiency virus enhancer by activation of the nuclear factor kappa B. *Proceedings of the National Academy of Sciences of the United States of America* 86, 2336-2340.

Ou, W.J., Cameron, P.H., Thomas, D.Y., and Bergeron, J.J. (1993). Association of folding intermediates of glycoproteins with calnexin during protein maturation. *Nature* 364, 771-776.

Palmgren, M.G., and Nissen, P. (2011). P-type ATPases. *Annual review of biophysics* 40, 243-266.

Park, C.Y., Hoover, P.J., Mullins, F.M., Bachhawat, P., Covington, E.D., Raunser, S., Walz, T., Garcia, K.C., Dolmetsch, R.E., and Lewis, R.S. (2009). STIM1 clusters and activates CRAC channels via direct binding of a cytosolic domain to Orai1. *Cell* 136, 876-890.

Parslow, T.G., and Granner, D.K. (1982). Chromatin changes accompany immunoglobulin kappa gene activation: a potential control region within the gene. *Nature* 299, 449-451.

8 LITERATURE

- Pedersen, P.L., and Carafoli, E. (1987). Ion motive ATPases. I. Ubiquity, properties, and significance to cell function. *Trends in Biochemical Sciences* 12, 146-150.
- Peier, A.M., Reeve, A.J., Andersson, D.A., Moqrich, A., Earley, T.J., Hergarden, A.C., Story, G.M., Colley, S., Hogenesch, J.B., and McIntyre, P., et al. (2002). A heat-sensitive TRP channel expressed in keratinocytes. *Science (New York, N.Y.)* 296, 2046-2049.
- Peng, H., Guerau-de-Arellano, M., Mehta, V.B., Yang, Y., Huss, D.J., Papenfuss, T.L., Lovett-Racke, A.E., and Racke, M.K. (2012). Dimethyl fumarate inhibits dendritic cell maturation via nuclear factor κ B (NF- κ B) and extracellular signal-regulated kinase 1 and 2 (ERK1/2) and mitogen stress-activated kinase 1 (MSK1) signaling. *The Journal of biological chemistry* 287, 28017-28026.
- Perkins, N.D. (2007). Integrating cell-signalling pathways with NF-kappaB and IKK function. *Nature reviews. Molecular cell biology* 8, 49-62.
- Pesta, D., and Gnaiger, E. (2012). High-resolution respirometry: OXPHOS protocols for human cells and permeabilized fibers from small biopsies of human muscle. *Methods in molecular biology (Clifton, N.J.)* 810, 25-58.
- Phaniendra, A., Jestadi, D.B., and Periyasamy, L. (2015). Free radicals: properties, sources, targets, and their implication in various diseases. *Indian journal of clinical biochemistry : IJCB* 30, 11-26.
- Pozzan, T., Rizzuto, R., Volpe, P., and Meldolesi, J. (1994). Molecular and cellular physiology of intracellular calcium stores. *Physiological reviews* 74, 595-636.
- Prakriya, M., Feske, S., Gwack, Y., Srikanth, S., Rao, A., and Hogan, P.G. (2006). Orai1 is an essential pore subunit of the CRAC channel. *Nature* 443, 230-233.
- Prins, D., Groenendyk, J., Touret, N., and Michalak, M. (2011). Modulation of STIM1 and capacitative Ca²⁺ entry by the endoplasmic reticulum luminal oxidoreductase ERp57. *EMBO reports* 12, 1182-1188.
- Puck, T.T., Cieciura, S.J., and Robinson, A. (1958). GENETICS OF SOMATIC MAMMALIAN CELLS : III. LONG-TERM CULTIVATION OF EUPLOID CELLS FROM HUMAN AND ANIMAL SUBJECTS. *The Journal of Experimental Medicine* 108, 945-956.
- Rahman, I., Kode, A., and Biswas, S.K. (2006). Assay for quantitative determination of glutathione and glutathione disulfide levels using enzymatic recycling method. *Nature protocols* 1, 3159-3165.

8 LITERATURE

Roos, J., DiGregorio, P.J., Yeromin, A.V., Ohlsen, K., Lioudyno, M., Zhang, S., Safrina, O., Kozak, J.A., Wagner, S.L., and Cahalan, M.D., et al. (2005). STIM1, an essential and conserved component of store-operated Ca²⁺ channel function. *The Journal of cell biology* *169*, 435-445.

Rossi, A.E., and Dirksen, R.T. (2006). Sarcoplasmic reticulum: the dynamic calcium governor of muscle. *Muscle & nerve* *33*, 715-731.

Saraste, M. (1999). Oxidative phosphorylation at the fin de siècle. *Science (New York, N.Y.)* *283*, 1488-1493.

Satoh, T., Okamoto, S.-i., Cui, J., Watanabe, Y., Furuta, K., Suzuki, M., Tohyama, K., and Lipton, S.A. (2006). Activation of the Keap1/Nrf2 pathway for neuroprotection by electrophilic correction of electrophilic phase II inducers. *Proceedings of the National Academy of Sciences of the United States of America* *103*, 768-773.

Scarborough, G.A. (1999). Structure and function of the P-type ATPases. *Current Opinion in Cell Biology* *11*, 517-522.

Schägger, H., and Jagow, G. von (1991). Blue native electrophoresis for isolation of membrane protein complexes in enzymatically active form. *Analytical biochemistry* *199*, 223-231.

Schieven, G.L., Kirihaara, J.M., Myers, D.E., Ledbetter, J.A., and Uckun, F.M. (1993). Reactive oxygen intermediates activate NF-kappa B in a tyrosine kinase-dependent mechanism and in combination with vanadate activate the p56lck and p59fyn tyrosine kinases in human lymphocytes. *Blood* *82*, 1212-1220.

Schilling, S., Goelz, S., Linker, R., Luehder, F., and Gold, R. (2006). Fumaric acid esters are effective in chronic experimental autoimmune encephalomyelitis and suppress macrophage infiltration. *Clinical and experimental immunology* *145*, 101-107.

Schmidt, M.M., and Dringen, R. (2010). Fumaric acid diesters deprive cultured primary astrocytes rapidly of glutathione. *Neurochemistry international* *57*, 460-467.

Schmidt, T.J., Ak, M., and Mrowietz, U. (2007). Reactivity of dimethyl fumarate and methylhydrogen fumarate towards glutathione and N-acetyl-L-cysteine--preparation of S-substituted thiosuccinic acid esters. *Bioorganic & medicinal chemistry* *15*, 333-342.

Schultz, B.E., and Chan, S.I. (2001). Structures and proton-pumping strategies of mitochondrial respiratory enzymes. *Annual review of biophysics and biomolecular structure* *30*, 23-65.

8 LITERATURE

- Schulze-Topphoff, U., Varrin-Doyer, M., Pekarek, K., Spencer, C.M., Shetty, A., Sagan, S.A., Cree, B.A.C., Sobel, R.A., Wipke, B.T., and Steinman, L., et al. (2016). Dimethyl fumarate treatment induces adaptive and innate immune modulation independent of Nrf2. *Proceedings of the National Academy of Sciences of the United States of America* *113*, 4777-4782.
- Schweckendiek, W. (1959). Heilung von Psoriasis vulgaris. *Medizinische Monatschrift* *13*, 103-104.
- Sebök, B., Bonnekoh, B., Geisel, J., and Mahrle, G. (1994). Antiproliferative and cytotoxic profiles of antipsoriatic fumaric acid derivatives in keratinocyte cultures. *European Journal of Pharmacology: Environmental Toxicology and Pharmacology* *270*, 79-87.
- Sefton, B.M., and Taddie, J.A. (1994). Role of tyrosine kinases in lymphocyte activation. *Current opinion in immunology* *6*, 372-379.
- Seidel, P., Merfort, I., Tamm, M., and Roth, M. (2010). Inhibition of NF- κ B and AP-1 by dimethylfumarate correlates with down-regulated IL-6 secretion and proliferation in human lung fibroblasts. *Swiss medical weekly* *140*, w13132.
- Serfling, E., Berberich-Siebelt, F., Avots, A., Chuvpilo, S., Klein-Hessling, S., Jha, M.K., Kondo, E., Pagel, P., Schulze-Luehrmann, J., and Palmetshofer, A. (2004). NFAT and NF-kappaB factors-the distant relatives. *The international journal of biochemistry & cell biology* *36*, 1166-1170.
- Shaw, J.P., Utz, P.J., Durand, D.B., Toole, J.J., Emmel, E.A., and Crabtree, G.R. (1988). Identification of a putative regulator of early T cell activation genes. *Science (New York, N.Y.)* *241*, 202-205.
- Shaw, K.T., Ho, A.M., Raghavan, A., Kim, J., Jain, J., Park, J., Sharma, S., Rao, A., and Hogan, P.G. (1995). Immunosuppressive drugs prevent a rapid dephosphorylation of transcription factor NFAT1 in stimulated immune cells. *Proceedings of the National Academy of Sciences of the United States of America* *92*, 11205-11209.
- Siekevitz, P. (1957). Powerhouse of the Cell. *Sci Am* *197*, 131-144.
- Sies, H. (1985). *Oxidative Stress* (Burlington: Elsevier Science).
- Sies, H. (1993). Strategies of antioxidant defense. *European journal of biochemistry* *215*, 213-219.
- Smith, M.D., Calabresi, P.A., and Bhargava, P. (2018). Dimethyl fumarate treatment alters NK cell function in multiple sclerosis. *European journal of immunology* *48*, 380-383.

8 LITERATURE

- Smith, P.K., Krohn, R.I., Hermanson, G.T., Mallia, A.K., Gartner, F.H., Provenzano, M.D., Fujimoto, E.K., Goeke, N.M., Olson, B.J., and Klenk, D.C. (1985). Measurement of protein using bicinchoninic acid. *Analytical biochemistry* *150*, 76-85.
- Soboloff, J., Rothberg, B.S., Madesh, M., and Gill, D.L. (2012). STIM proteins: dynamic calcium signal transducers. *Nature reviews. Molecular cell biology* *13*, 549-565.
- Soboloff, J., Spassova, M.A., Tang, X.D., Hewavitharana, T., Xu, W., and Gill, D.L. (2006). Orai1 and STIM reconstitute store-operated calcium channel function. *The Journal of biological chemistry* *281*, 20661-20665.
- Spencer, C.M., Crabtree-Hartman, E.C., Lehmann-Horn, K., Cree, B.A.C., and Zamvil, S.S. (2015). Reduction of CD8(+) T lymphocytes in multiple sclerosis patients treated with dimethyl fumarate. *Neurology(R) neuroimmunology & neuroinflammation* *2*, e76.
- Spencer, S.R., Wilczak, C.A., and Talalay, P. (1990). Induction of glutathione transferases and NAD(P)H:quinone reductase by fumaric acid derivatives in rodent cells and tissues. *Cancer research* *50*, 7871-7875.
- Stewart, A.A., Ingebritsen, T.S., Manalan, A., Klee, C.B., and Cohen, P. (1982). Discovery of a Ca²⁺- and calmodulin-dependent protein phosphatase: probable identity with calcineurin (CaM-BP80). *FEBS letters* *137*, 80-84.
- Stokes, A., Wakano, C., Koblan-Huberson, M., Adra, C.N., Fleig, A., and Turner, H. (2006). TRPA1 is a substrate for de-ubiquitination by the tumor suppressor CYLD. *Cellular signalling* *18*, 1584-1594.
- Stoof, T.J., Flier, J., Sampat, S., Nieboer, C., Tensen, C.P., and Boorsma, D.M. (2001). The antipsoriatic drug dimethylfumarate strongly suppresses chemokine production in human keratinocytes and peripheral blood mononuclear cells. *The British journal of dermatology* *144*, 1114-1120.
- Story, G.M., Peier, A.M., Reeve, A.J., Eid, S.R., Mosbacher, J., Hricik, T.R., Earley, T.J., Hergarden, A.C., Andersson, D.A., and Hwang, S.W., et al. (2003). ANKTM1, a TRP-like Channel Expressed in Nociceptive Neurons, Is Activated by Cold Temperatures. *Cell* *112*, 819-829.
- Stranick, K.S., Zambas, D.N., Uss, A.S., Egan, R.W., Billah, M.M., and Umland, S.P. (1997). Identification of transcription factor binding sites important in the regulation of the human interleukin-5 gene. *The Journal of biological chemistry* *272*, 16453-16465.

8 LITERATURE

- Strotmann, R., Harteneck, C., Nunnenmacher, K., Schultz, G., and Plant, T.D. (2000). OTRPC4, a nonselective cation channel that confers sensitivity to extracellular osmolarity. *Nature cell biology* *2*, 695-702.
- Sun, R., Eriksson, S., and Wang, L. (2012). Oxidative stress induced S-glutathionylation and proteolytic degradation of mitochondrial thymidine kinase 2. *The Journal of biological chemistry* *287*, 24304-24312.
- Sun, S.-C. (2017). The non-canonical NF- κ B pathway in immunity and inflammation. *Nature reviews. Immunology* *17*, 545-558.
- Szabo, S.J., Gold, J.S., Murphy, T.L., and Murphy, K.M. (1993). Identification of cis-acting regulatory elements controlling interleukin-4 gene expression in T cells: roles for NF-Y and NF-ATc. *Molecular and cellular biology* *13*, 4793-4805.
- Tak, P.P., and Firestein, G.S. (2001). NF-kappaB: a key role in inflammatory diseases. *The Journal of clinical investigation* *107*, 7-11.
- Takahashi, N., Mizuno, Y., Kozai, D., Yamamoto, S., Kiyonaka, S., Shibata, T., Uchida, K., and Mori, Y. (2008). Molecular characterization of TRPA1 channel activation by cysteine-reactive inflammatory mediators. *Channels* *2*, 287-298.
- Takemura, H., Hughes, A.R., Thastrup, O., and Putney, J.W. (1989). Activation of calcium entry by the tumor promoter thapsigargin in parotid acinar cells. Evidence that an intracellular calcium pool and not an inositol phosphate regulates calcium fluxes at the plasma membrane. *The Journal of biological chemistry* *264*, 12266-12271.
- Tebay, L.E., Robertson, H., Durant, S.T., Vitale, S.R., Penning, T.M., Dinkova-Kostova, A.T., and Hayes, J.D. (2015). Mechanisms of activation of the transcription factor Nrf2 by redox stressors, nutrient cues, and energy status and the pathways through which it attenuates degenerative disease. *Free radical biology & medicine* *88*, 108-146.
- Thastrup, O., Cullen, P.J., Drøbak, B.K., Hanley, M.R., and Dawson, A.P. (1990). Thapsigargin, a tumor promoter, discharges intracellular Ca²⁺ stores by specific inhibition of the endoplasmic reticulum Ca²⁺(+)-ATPase. *Proceedings of the National Academy of Sciences of the United States of America* *87*, 2466-2470.
- Thio, H.B., Zomerdijk, T.P., Oudshoorn, C., Kempenaar, J., Nibbering, P.H., van der Schroeff, J.G., and Ponc, M. (1994). Fumaric acid derivatives evoke a transient increase in intracellular free calcium concentration and inhibit the proliferation of human keratinocytes. *The British journal of dermatology* *131*, 856-861.

8 LITERATURE

- Tong, X., Ying, J., Pimentel, D.R., Trucillo, M., Adachi, T., and Cohen, R.A. (2008). High glucose oxidizes SERCA cysteine-674 and prevents inhibition by nitric oxide of smooth muscle cell migration. *Journal of molecular and cellular cardiology* *44*, 361-369.
- Toyoshima, C., Nakasako, M., Nomura, H., and Ogawa, H. (2000). Crystal structure of the calcium pump of sarcoplasmic reticulum at 2.6 Å resolution. *Nature* *405*, 647-655.
- Treumer, F., Zhu, K., Gläser, R., and Mrowietz, U. (2003). Dimethylfumarate is a potent inducer of apoptosis in human T cells. *Journal of Investigative Dermatology* *121*, 1383-1388.
- Trushin, S.A., Pennington, K.N., Algeciras-Schimmich, A., and Paya, C.V. (1999). Protein kinase C and calcineurin synergize to activate I κ B kinase and NF- κ B in T lymphocytes. *The Journal of biological chemistry* *274*, 22923-22931.
- Vaeth, M., and Feske, S. (2018). NFAT control of immune function: New Frontiers for an Abiding Trooper. *F1000Research* *7*, 260.
- Valko, M., Leibfritz, D., Moncol, J., Cronin, M.T.D., Mazur, M., and Telser, J. (2007). Free radicals and antioxidants in normal physiological functions and human disease. *The international journal of biochemistry & cell biology* *39*, 44-84.
- van der Blik, A.M., Sedensky, M.M., and Morgan, P.G. (2017). Cell Biology of the Mitochondrion. *Genetics* *207*, 843-871.
- Vandermeeren, M., Janssens, S., Wouters, H., Borghmans, I., Borgers, M., Beyaert, R., and Geysen, J. (2001). Dimethylfumarate is an inhibitor of cytokine-induced nuclear translocation of NF- κ B1, but not RelA in normal human dermal fibroblast cells. *Journal of Investigative Dermatology* *116*, 124-130.
- Vasiliou, V., Ross, D., and Nebert, D.W. (2006). Update of the NAD(P)H:quinone oxidoreductase (NQO) gene family. *Human genomics* *2*, 329-335.
- Veal, E.A., Day, A.M., and Morgan, B.A. (2007). Hydrogen peroxide sensing and signaling. *Molecular cell* *26*, 1-14.
- Venkatachalam, K., and Montell, C. (2007). TRP channels. *Annual review of biochemistry* *76*, 387-417.
- Vig, M., and Kinet, J.-P. (2009). Calcium signaling in immune cells. *Nature immunology* *10*, 21-27.
- Wehrhahn, J., Kraft, R., Harteneck, C., and Hauschildt, S. (2010). Transient receptor potential melastatin 2 is required for lipopolysaccharide-induced cytokine production in human monocytes. *The Journal of Immunology* *184*, 2386-2393.

8 LITERATURE

Wheeler, M.L., and Defranco, A.L. (2012). Prolonged production of reactive oxygen species in response to B cell receptor stimulation promotes B cell activation and proliferation. *The Journal of Immunology* *189*, 4405-4416.

Williams, R.T., Manji, S.S., Parker, N.J., Hancock, M.S., van Stekelenburg, L., Eid, J.P., Senior, P.V., Kazenwadel, J.S., Shandala, T., and Saint, R., et al. (2001). Identification and characterization of the STIM (stromal interaction molecule) gene family: coding for a novel class of transmembrane proteins. *The Biochemical journal* *357*, 673-685.

Wilms, H., Sievers, J., Rickert, U., Rostami-Yazdi, M., Mrowietz, U., and Lucius, R. (2010). Dimethylfumarate inhibits microglial and astrocytic inflammation by suppressing the synthesis of nitric oxide, IL-1beta, TNF-alpha and IL-6 in an in-vitro model of brain inflammation. *Journal of neuroinflammation* *7*, 30.

Wu, K.D., Lee, W.S., Wey, J., Bungard, D., and Lytton, J. (1995). Localization and quantification of endoplasmic reticulum Ca(2+)-ATPase isoform transcripts. *The American journal of physiology* *269*, C775-84.

Wu, M.M., Buchanan, J., Luik, R.M., and Lewis, R.S. (2006). Ca²⁺ store depletion causes STIM1 to accumulate in ER regions closely associated with the plasma membrane. *The Journal of cell biology* *174*, 803-813.

Wu, Q., Wang, Q., Mao, G., Dowling, C.A., Lundy, S.K., and Mao-Draayer, Y. (2017). Dimethyl Fumarate Selectively Reduces Memory T Cells and Shifts the Balance between Th1/Th17 and Th2 in Multiple Sclerosis Patients. *The Journal of Immunology* *198*, 3069-3080.

Xu, Z., Zhang, F., Sun, F., Gu, K., Dong, S., and He, D. (2015). Dimethyl fumarate for multiple sclerosis. *The Cochrane database of systematic reviews*, CD011076.

Yarosz, E.L., and Chang, C.-H. (2018). The Role of Reactive Oxygen Species in Regulating T Cell-mediated Immunity and Disease. *Immune network* *18*, e14.

Yeung, Y.-G., and Stanley, E.R. (2009). A solution for stripping antibodies from polyvinylidene fluoride immunoblots for multiple reprobing. *Analytical biochemistry* *389*, 89-91.

Yoshida, H., Matsui, T., Yamamoto, A., Okada, T., and Mori, K. (2001). XBP1 mRNA is induced by ATF6 and spliced by IRE1 in response to ER stress to produce a highly active transcription factor. *Cell* *107*, 881-891.

Yu, F., Sun, L., Hubrack, S., Selvaraj, S., and Machaca, K. (2013). Intramolecular shielding maintains the ER Ca²⁺ sensor STIM1 in an inactive conformation. *Journal of cell science* *126*, 2401-2410.

8 LITERATURE

- Zaidi, A., and Michaelis, M.L. (1999). Effects of reactive oxygen species on brain synaptic plasma membrane Ca(2+)-ATPase. *Free radical biology & medicine* 27, 810-821.
- Zhang, S.L., Yeromin, A.V., Zhang, X.H.-F., Yu, Y., Safrina, O., Penna, A., Roos, J., Stauderman, K.A., and Cahalan, M.D. (2006). Genome-wide RNAi screen of Ca(2+) influx identifies genes that regulate Ca(2+) release-activated Ca(2+) channel activity. *Proceedings of the National Academy of Sciences of the United States of America* 103, 9357-9362.
- Zhao, D., Yang, J., Han, K., Liu, Q., Wang, H., Liu, Y., Huang, X., Zhang, L., and Li, Y. (2019). The unfolded protein response induced by Tembusu virus infection. *BMC veterinary research* 15, 34.
- Zhou, B., Cron, R.Q., Wu, B., Genin, A., Wang, Z., Liu, S., Robson, P., and Baldwin, H.S. (2002). Regulation of the murine Nfatc1 gene by NFATc2. *The Journal of biological chemistry* 277, 10704-10711.
- Zhu, J., Lu, X., Feng, Q., and Stathopoulos, P.B. (2018). A charge-sensing region in the stromal interaction molecule 1 luminal domain confers stabilization-mediated inhibition of SOCE in response to S-nitrosylation. *The Journal of biological chemistry* 293, 8900-8911.
- Zündorf, G., and Reiser, G. (2011). Calcium dysregulation and homeostasis of neural calcium in the molecular mechanisms of neurodegenerative diseases provide multiple targets for neuroprotection. *Antioxidants & redox signaling* 14, 1275-1288.

9 APPENDIX

ABBREVIATIONS

%	percent	CRAC	Ca ²⁺ release-activated Ca ²⁺
-/-	knockout	C-terminus	carboxy-terminus
°C	degree Celsius	cyt.	cytoplasm
∅	diameter	DAG	diacylglycerol
λ	wavelength	DAPI	4',6-diamidino-2-phenyl-indole
2-NBDG	2-(N-(7-nitrobenz-2-oxa-1,3-diazol-4-yl)amino)-2-deoxyglucose	DM	double mutant
7-AAD	7-Aminoactinomycin D	DMF	dimethyl fumarate
A	actuator domain	DMSO	dimethyl sulfoxide
A96	A967079	DNA	deoxyribonucleic acid
ADP	adenosine diphosphate	DNP	2,4-dinitrophenyl-hydrazine
AM	acetoxymethyl ester	dNTP	deoxynucleotide
Ama	antimycin A	DTNB	5,5'-dithiobis-(2-nitrobenzoic acid)
ATF6	activating transcription factor 6	DTT	dithiothreitol
ATP	adenosine triphosphate	e ⁻	electrons
BAPTA	1,2-bis(2-aminophenoxy)ethane-N,N,N',N'-tetraacetic acid	E.coli	Escherichia coli
BCA	bicinchoninic acid	EAE	experimental autoimmune encephalomyelitis
BCR	B cell receptor	EDTA	ethylenediaminetetraacetic acid
BIOGEE	biotinylated glutathione ethyl ester	EGTA	ethylene glycol-bis(2-aminoethyl ether)-N,N,N',N'-tetraacetic acid
BiP	binding immunoglobulin protein	Em	emission
BSA	bovine serum albumin	ER	endoplasmic reticulum
C	cysteine	ETS	electron transport system
Ca ²⁺	calcium	EV	empty vector
CAD	CRAC activation domain	Ex	excitation
CC	coiled-coil	F	fluorescence
CD	cluster of differentiation	FACS	fluorescence-activated cell sorting
cDNA	complementary DNA	FADH ₂	reduced flavin adenine dinucleotide
cEF	canonical EF-hand	FCCP	carbonyl cyanide 4-(trifluoromethoxy) phenyl-hydrazone
CHO	chinese hamster ovaries	FCS	fetal bovine/calf serum
CNS	central nervous system		
COS	CV-1 in Origin Simian-1		
cm	centimeter		
CO ₂	carbon dioxide		

9 APPENDIX

FFA	flufenamic acid	MFI	median or mean
Fluo-8	CalciFluor Fluo-8, AM		fluorescence intensity
GΩ	gigaohm	mg	milligram
g	gram	min	minute
GAPDH	glyceraldehyd 3-phosphate dehydrogenase	ml	milliliter
		mM	millimolar
GFP	green fluorescent protein	MMF	monomethyl fumarate
GPCR	G-protein-coupled receptors	mRNA	messenger RNA
GSH	glutathione	ms	millisecond
GSR	glutathione reductase	MS	multiple sclerosis
GSSG	glutathione disulfide	mV	millivolt
GTP	guanosine triphosphate	n	number
h	hour	N	nucleotide binding domain
H ₂ O ₂	hydrogen peroxide	Na ⁺	sodium
H ₂ O	water	NA	numerical aperture
HC	HC030031	ng	nanogram
hEF	hidden EF-hand	nm	nanomol
HBSS +/-	Hank's Balanced Salt Solution with calcium/magnesium	N-terminus	amino-terminus
		NADH	reduced nicotinamide
HDAC1	histone deacetylase 1		adenine dinucleotide
HPRT	hypoxanthine phosphor-ribosyltransferase	NADPH	reduced nicotinamide
			adenine dinucleotide
ICC	immunocytochemistry		phosphate
IFN-γ	interferon-gamma	NFAT	nuclear factor of activated
IκBα	NF-κB inhibitor alpha		T cells
IκB	NF-κB inhibitor	NF-κB	nuclear factor kappa-light-chain-enhancer of activated
IKK	IκB kinase		B cells
IL	interleukin		
Iono	ionomycin	ng	nanogram
IP3	inositol-1,4,5-tris-phosphate	NGS	normal goat serum
IP3R	inositol-1,4,5-tris-phosphate receptor	NIK	NF-κB-inducing kinase
		nm	nanometer
IRE1α	inositol-requiring enzyme 1α	NP-40	Nonidet P-40
IV	current-voltage	NQO1	NAD(P)H quinone oxido-reductase-1
KEAP1	kelch like-ECH-associated protein 1	Nrf2	nuclear factor erythroid
			2-related factor 2
kb	kilobase		
kDa	kilodalton	nuc.	nucleus
kg	kilogram	O ₂	oxygen
LaCl ₃	lanthanum(III) chloride	OD	optical density
LB	lysogeny broth	Omy	oligomycin
leak	leak respiration	OXPHOS	oxidative phosphorylation
MΩ	megaohm	P	phosphorylation domain
M	molar	p50 and p105	NF-κB1
MEF	mouse embryonic fibroblasts	p52 and p100	NF-κB2

9 APPENDIX

p65	RelA	SJL	Swiss Jim Lambert
pA	picoampere	SOCE	store-operated Ca ²⁺ entry
PBS	phosphate buffered saline	SP	signal peptide
PBS-T	phosphate buffered saline Tween®20	STIM1	stromal interaction molecule 1
PCR	polymerase chain reaction	TBS	tris-buffered saline
PERK	protein kinase RNA-like ER kinase	TBS-T	tris-buffered saline Tween®20
Pi	inorganic phosphate	TCR	T cell receptor
PIP2	phosphatidylinositol-4,5- bisphosphate	TG	thapsigargin
PKC	protein kinase C	Th	T helper
PLC	phospholipase C	TM	transmembrane domain
PMA	phorbol 12-myristate 13- acetate	TNB	5'-thio-2-nitrobenzoic acid
PMSF	phenylmethylsulphonyl fluoride	TNF- α	tumor necrosis factor-alpha
PMCA	plasma membrane Ca ²⁺ - ATPase	TRP	transient receptor potential
PS	proline and serine-rich region	TRPA1	transient receptor potential ankyrin 1
PVDF	polyvinylidene difluoride	TRPC	transient receptor potential canonical
qPCR	quantitative real-time polymerase chain reaction	TRPM	transient receptor potential melastatin
RIPA	radioimmunoprecipitation assay	TRPML	transient receptor potential mucolipin
RNA	ribonucleic acid	TRPN	transient receptor potential no mechanoreceptor potential C
ROS	reactive oxygen species	TRPP	transient receptor potential polycystin
Rot	rotenone	TRPV	transient receptor potential vanilloid
routine	routine respiration	U	units
ROX	residual oxygen consumption	UPR	unfolded protein response
rpm	revolutions per minute	UV	ultraviolet
RT	reverse transcriptase	V	volt
RuRed	ruthenium red	Veh	vehicle
RyR	ryanodine receptor	v/v	volume/volume
S	serine	WT	wildtype
SAM	sterile α -motif	w/v	weight/volume
SD	standard deviation	x	times
SDS	sodium dodecyl sulfate	XBP1	X box-binding protein 1
SDS-PAGE	sodium dodecyl sulfate polyacrylamide gel electrophoresis	x g	times gravity
sec	second	μ l	microliter
SERCA	sarco/endoplasmic reticulum Ca ²⁺ -ATPase	μ g	microgram
		μ M	micromolar

ACKNOWLEDGMENT

For data protection reasons the acknowledgment is not included in the online version.

DECLARATION

I, Ann-Kathrin Herrmann, hereby declare that I have conducted this present PhD thesis without inappropriate help by another person. I have not used other sources than stated. Moreover, I declare that this thesis has not been submitted for a higher degree to any other University or Institution.

Mainz, 20.05.2019

(Ann-Kathrin Herrmann)

CURRICULUM VITAE

For data protection reasons the curriculum vitae is not included in the online version.